Fermi National Accelerator Laboratory

FERMILAB-Conf-87/54
2021.000

Detecting *W/Z* Pairs and Higgs at High Energy pp Colliders: Main Experimental Issues*

George Alverson
Northeastern University, Boston, MA 02115

Hans-Uno Bengtsson
University of California, Los Angeles, Los Angeles, CA 90024

John Hauptman
Iowa State University/Ames Laboratory, Ames IA 50010

David Hedin
State University of New York at Stony Brook, Stony Brook, NY 11794

Maria Jose Herrero and Edward Wang
Lawrence Berkeley Laboratory, Berkeley, CA 94720

Stephan Linn and Christopher Young
SCRI and Florida State University, Tallahassee, FL 32306

Barrett Milliken
California Institute of Technology, Pasadena, CA 91125

Frank Paige and Serban Protopopescu
Brookhaven National Laboratory Upton, NY 11973

Aurore Savoy-Navarro†
CEN Saclay, Gif-sur-Yvette CEDEX, France

Torbjörn Sjöstrand
University of Lund, Lund, Sweden

Wesley Smith
Columbia University, New York, NY 10027

Yoshi Takaiwa and Aki Yamashita
University of Tsukuba, Ibaraki, Japan, and Fermi National Accelerator Laboratory, Batavia, IL 60510

March 1987

*To be published in the Proceedings of the 1986 Snowmass Summer Study on the Physics of the SSC, Snowmass, CO, June 23-July 11, 1986.
†Coordinator of the Working Group on "W/Z Pairs and Higgs at the SSC" with J. Gunion.

DETECTING W/Z PAIRS AND HIGGS AT HIGH ENERGY PP COLLIDERS: MAIN EXPERIMENTAL ISSUES

George Alverson, Northeastern University , Boston MA
Hans-Uno Bengtsson, UCLA, Los Angeles CA
John Hauptman, Iowa State University/Ames Laboratory, Ames IO
David Hedin, State University of New York, Stony Brook NY
Maria Jose Herrero and Edward Wang, Lawrence Berkeley Laboratory, Berkeley CA
Stephan Linn and Christopher Young, SCRI and Florida State University, Tallahassee FL
Barrett Milliken, California Institute of Technology, Pasadena CA
Frank Paige and Serban Protopopescu, BNL, Upton NY
Aurore Savoy-Navarro*, CEN Saclay, Gif-sur-Yvette CEDEX France
Torbjörn Sjöstrand, University of Lund, Lund Sweden
Wesley Smith, Columbia University, New York NY
Yoshi Takaiwa and Aki Yamashita, Tsukuba University/Fermilab, Batavia IL

To be published in
Proc. 1986 Snowmass Summer Study on the
Physics of the SSC
Snowmass, Colo., 23 June - 11 July 1986

---

* Coordinator of the Working Group on "W/Z Pairs and Higgs at the SSC" with J. Gunion.

DETECTING W/Z PAIRS AND HIGGS AT HIGH ENERGY PP COLLIDERS: MAIN EXPERIMENTAL ISSUES

George Alverson, Northeastern University, Boston MA
Hans-Uno Bengtsson, UCLA, Los Angeles CA
John Hauptman, Iowa State University/Ames Laboratory, Ames IA
David Hedin, State University of New York, Stony Brook NY
Maria Herrero and Edward Wang, Lawrence Berkeley Laboratory, Berkeley CA
Stephan Linn and Christopher Young, SCRI and Florida State University, Tallahassee FL
Barrett Milliken, California Institute of Technology, Pasadena CA
Frank Paige and Serban Protopopescu, BNL, Upton NY
Aurore Savoy-Navarro, CEN Saclay, Gif-sur-Yvette CEDEX France*
Torbjörn Sjöstrand, University of Lund, Lund Sweden
Wesley Smith, Columbia University, New York NY
Yoshi Takaiwa and Aki Yamashita, Tsukuba University/Fermilab, Batavia IL

Abstract

The main detection issues implied by the search for W and Z^0 pairs and Higgs in a high energy pp collider context are discussed here. It includes: precise electron identification, missing energy measurement, multilepton recognition, sophisticated jet pattern recognition, and pile-up. The study uses, as much as possible, a "realistic simulation of life."

Introduction

From an experimental point of view, the search for W or Z^0 pairs is a fundamental issue for *pp* colliders. It implies that a detector provides sufficient information enabling identification of W's and Z^0's in their various decay modes, namely:

$$W \to l\nu_l \ , \ Z^0 \to l\bar{l} \ , \text{ and } \nu_l\bar{\nu}_l$$

$$W \to q\bar{q} \ , \text{ and } Z^0 \to q\bar{q} \ ,$$

with $l = e, \mu, \tau...$ Recognition of polarization properties and invariant mass reconstruction of WW or Z^0Z^0 pairs are necessary in Higgs identification. In addition, the "usual pp environment" must be considered, especially at very high energy and very high luminosity (event pile-up problem).

We investigate various detection problems : electron identification with high resolution, missing energy measurement, multilepton recognition, sophisticated jet pattern recognition, and pile-up confusion. We confront these problems by exploring a variety of possible solutions and techniques and estimate corresponding detection efficiencies.

Our approach has been to first study these questions with a simulation using a near perfect detector. This is mainly done in the first report of our group and is described in section one of this paper[1]. This serves as a feasibility check of the "ideal" cases. If a technique looks promising after this initial test we then step further and study the question with a more "realistic" detector simulation. This is what we have done in this second report.

1.0 Realistic Simulations

For a more accurate reproduction of nature, a detector simulation used by the DØ collaboration for high statistics trigger studies is adapted for use here. DØ is a 4π

general purpose detector comprised of central tracking chambers with no magnetic field, a Uranium liquid-argon calorimeter, and a muon spectrometer employing magnetized iron and proportional drift tubes. The dimensions of DØ have been scaled to be appropriate for an SSC detector. The inner radius of the calorimeter is 200 cm and its half-length is 400 cm. The calorimeter is between 12 and 15 absorption lengths thick with a coverage out to 6 units of rapidity. It has a uniform segmentation of 0.05×0.05 in azimuth and rapidity. Electromagnetic and hadronic showers are simulated using a parameterization taken from test data on DØ prototypes. Some areas of the calorimeter have been deadened to simulate supports, cable pathways and a cryostat. A single cryostat design has been chosen with clam shell flanges at 90 degrees. This eliminates the large dead area that occurs when three cryostats are used. We assume resolutions of

$$\sigma/E = 0.01 + 0.20/\sqrt{E}$$

$$\sigma/E = 0.05 + 0.50/\sqrt{E}$$

for electrons and hadrons respectively. The relative response of electrons to pions is taken to be 1.1 and constant with energy. The beam interaction diamond is smeared with a Gaussian of width 20 cm. Fig. 1 shows an overview of the detector we call D1.

The simulation includes a transition radiation detector (TRD) with parameters identical to DØ. There are nine TRD chambers instead of three as in DØ. TRD information is used only to distinguish between zero, one or two ionizing tracks. Fig. 2 shows the total charge deposited in the TRD for single electrons and pions which rejects 50 percent of the pions while accepting 90 percent of all electrons. In our "trigger" we use the sum of the TRD channels corresponding to the "hit" calorimeter cells. This distribution is shown in Fig. 3 where one can see peaks corresponding to one or more particles. Because of these overlaps, the TRD is used only to detect the presence of a charged particle. The rejection factor of Fig. 2 would apply to isolated tracks only. Because we simulate only events that have high p_t electrons, it is not necessary to make stringent cuts with the TRD. The TRD would be useful in discriminating against the QCD background. We note that the efficiency and rejection of this device was the same for both 300 GeV and 800 GeV cases studied. The point where e's and π's have equal signals, corresponds to a p_t of about 500 GeV. The usefulness of this device for electron identification at small angles corresponds to a p_t approximately ten times lower. Therefore, a TRD of the DØ design would only be useful in the central rapidity region. A better set of TRD parameters could be found for SSC energies, even for forward detectors, if space permitted. It should be pointed out that segmentation of TRD's is very important. The effect of overlaps is seen by comparing the distributions of Figs. 2 and 3.

2.0 W and Z^0 Pairs in a "Realistic Detector"

The Pythia Monte-Carlo (V4.7) has been used to generate samples of signal and backgrounds for Higgs' of mass 300 GeV and 800 GeV produced by pp collisions at $\sqrt{s}$ = 40 TeV. One thousand events have been generated for each of the following processes:

$$\mathrm{pp} \rightarrow \mathrm{H^0} \rightarrow \mathrm{e}\nu_\mathrm{e}\ \mathrm{q\bar{q}} \tag{1}$$

$$\mathrm{pp} \rightarrow \mathrm{WW} \rightarrow \mathrm{e}\nu_\mathrm{e}\ \mathrm{q\bar{q}} \tag{2}$$

$$\mathrm{pp} \rightarrow \mathrm{W\ q\ or\ g} \rightarrow \mathrm{e}\nu_\mathrm{e}\ \mathrm{q\ or\ g} \tag{3}$$

$$pp \rightarrow WZ^0 \rightarrow e\nu_e\ q\bar{q} \quad (4)$$

$$pp \rightarrow Z^0Z^0 \rightarrow ee\nu_l\ \bar{\nu}_l \quad (5)$$

$$pp \rightarrow Z^0\ q \text{ or } g \rightarrow ee\ q \text{ or } g \quad (6)$$

$$pp \rightarrow qq \text{ or } gg \text{ or } qg \quad (7)$$

The continuum background processes were generated with 100 GeV wide windows in p_t centered on 150 GeV or 400 GeV where relevant. For the Z^0 pair modes, the decay neutrinos were ν_e , ν_μ or ν_τ. The generated events have been passed through the detector simulation described in Section 1 and then analyzed.

2.1 Identification of W-Pair Events

In Section 4.4 of our first report[1] to these proceedings, a trigger strategy is defined to identify such events, using an "idealized 4π detector". Now, we use the D1 simulation, to define a more realistic way to trigger on W-pairs. We also estimate the experimentally achievable resolution for the main parameters of these processes, and the efficiency of each stage of the detection as well as an overall efficiency.

A realistic W-pair trigger is defined according to the following steps. For each event:

- Search for all clusters in the electromagnetic part of the calorimeter within a range in rapidity $\eta \leq 4$ and with $E_t > 10$ GeV using a clustering radius of 0.5 units.
- Require that at least 95 percent of the energy be contained in the first 40 radiation lengths of the calorimeter. This is to ensure the "electron-character" of the cluster.
- Require the isolation of the cluster to be larger than 95 percent. (See Fig 4 caption for definition of isolation).
- Require the cluster radius be less than 0.1 (See Fig 5).
- Ask for the matching of the e.m. cluster with an associated track , with more than 400 KeV of ionization, in the TRD (See Fig 3). It should be noted that most of these criteria are biased toward accepting electrons in the central rapidity region. A "cleaner" sample of events is obtained with a cut at three units of rapidity with a corresponding reduction of acceptance.

The remaining electron candidates which pass all these cuts are then sorted into a list decreasing in p_t for use in signals with more than one electron. The electron candidate with the highest p_t is used to reconstruct the W.

The longitudinal component of the momentum of the neutrino (i.e. the component along the beam axis) is not well defined in pp collisions because large amounts of energy escape detection at small angles. The missing-p_t is used to infer the existence of a neutrino and to reconstruct the $e\nu$-system decaying from the W. A cut on missing-p_t at 10 GeV is almost 100 percent efficient for processes with a $W \rightarrow l\nu$.

The four-momentum of the electron and the two components of the missing momentum along with the W-mass constraint yield a quadratic equation in longitudinal neutrino momentum:

$$m_W^2 = (E_\nu + E_e)^2 - (\vec{P}_\nu + \vec{P}_e)^2$$

There are two possible solutions; we use the solution which yields the smallest value for p_z (this is correct 60 percent of the time).

Assuming an object with the W-mass completely constrains the kinematics, so the W-momentum is determined. The transverse mass of the $e\nu$-system is shown in Fig. 6. The resolution of both the electron and the missing-p_t are shown in Figs. 7 and 8

respectively; they are equal to 3.4 percent and 20 percent respectively. We list in Table 1 the efficiency $\epsilon_{e\nu}$ for identifying the $e\nu$-system as defined above. All processes where a W has been produced which decays leptonically, give a value of about 60 percent for $\epsilon_{e\nu}$. The Higgs' process gives a slightly higher value of 70 percent.

Now we analyze the 2-jet part of the event. We define a strategy to recognize the second W by using constraints from the first W. It follows various steps:

- First, we find all the clusters with E_t greater than 10 GeV , using now the full depth information from the calorimeter and a larger cluster radius (i.e. of one unit instead of 0.5 unit for the e.m. cluster)
- Find the cluster (jet1) with the highest E_t in the opposite hemisphere from the leptonically decaying W.
- Make all possible combinations of jet1 with all other clusters in the opposite hemisphere. Keep the cluster (jet2) which combines with jet1 to have an invariant mass closest to m_W. The efficiency after this stage (ϵ_{jj}) is given in Table 1.
- A cut is then made in physical mass at 120 GeV. The remaining events constitute an event sample which can then be subjected to a more sophisticated analysis as will be described below. The efficiency after this cut (ϵ_{WW}) which constitues the final trigger efficiency for each process considered is listed in Table 1.

TABLE 1

Efficiencies at successive stages of analysis for a 300 GeV Higgs decaying to WW and corresponding backgrounds. Background processes were simulated only for the p_t interval 100-200 GeV.

Process	σ (pb)	$\epsilon_{e\nu}$	ϵ_{jj}	ϵ_{WW}
$pp \rightarrow H^0 \rightarrow e\nu\ q\bar{q}$	2.0	.70	.61	.30
$pp \rightarrow WW \rightarrow e\nu\ q\bar{q}$	1.9	.61	.49	.30
$pp \rightarrow W\ q(g) \rightarrow e\nu\ q(g)$	$4.9\ 10^2$	.67	.55	.12
$pp \rightarrow WZ^0 \rightarrow e\nu\ q\bar{q}$	$4.1\ 10^{-1}$	.62	.50	.33
$pp \rightarrow qq$ or gg or qg	$1.2\ 10^5$	.01	.001	.0003

This "trigger" efficiency is about 30 percent for events with two W's. For events produced by $pp \rightarrow W + (q \text{ or } g)$ where the parton recoil jet fakes the other W, the efficiency is about 12 percent. This study attempted to optimize the acceptance of the trigger for a low mass Higgs (300 GeV) at the SSC; therefore, low thresholds have been used. Setting low thresholds when starting to run an experiment at the SSC will be mandatory to allow us to explore the entire mass-range[1]. We believe the effect of higher thresholds would have a multiplicative effect on all efficiencies quoted. Such a study has not been done yet.

We define mass resolution (σ_m/m), where (σ_m) is the standard deviation from a Gaussian fit, after cuts and including the natural width. This value is 21 percent for the hadronically decaying W and 21 percent for the reconstructed Higgs mass. The two distributions are shown in Figs. 10 and 11 respectively. For comparison with the $W \rightarrow e\nu$ case we also display the transverse mass of the jet-jet system in Fig. 9.

For the 300 GeV case we attempted to estimate the effect of these cuts on the background from ordinary QCD jets. A sample of 5000 events with p_t between 100 and 200 GeV was simulated on a Cyber-205 supercomputer. The Isajet Monte

Carlo was used to generate these events. Some trivial vectorization of the code was performed but the simulation and analysis were essentially the same. The results from this study are included in Table 1. While the number of surviving events is small, the cross-section is several orders of magnitude larger. It should be emphasized that the E_t and missing-p_t cuts were un-realistically low; future trigger studies must optimize cuts to reduce this background.

The results of the 800 GeV Higgs simulation are given in Table 2. It was necessary to change the clustering radius used in the jet finding algorithm from 1.0 unit to 0.5 units. A clustering radius of 1.0 unit quite often lumps both jets from the hadronically decaying W into one jet. This illustrates an important point: Jets at the SSC will cover a very broad range of p_t; therefore, they will vary considerably in shape. The method employed by "seed and accrete" jet-finders has parameters that must be "hand tuned" to give good results. We recommend that any future studies use a true clustering algorithm. To make the results easily comparable, we did not change any of the other parameters. The same threshold values were kept to compare the low- and high-mass cases with the same imposed conditions. However, we forsee at this refined stage to have filters for both low- and high-mass ranges. Clearly the set of cuts will have to be tuned in a different way in both cases to optimize the search for each type of object. The result was that the 800 GeV events with two W's passed the cuts 10 percent more often than the 300 GeV events. Events with a single W passed the cuts 30 percent more often. We speculate that this was due to the higher multiplicity of spectator jets that could conspire to have the W-mass. The mass resolution of the di-jet system improves to the 11 percent in the 800 GeV case while the Higgs' mass resolution remains about the same (20 percent) for $m_H = 800$ GeV. These distributions are shown in Figs. 12 and 13 respectively.

In conclusion, for both Higgs' masses considered, the mass resolution was about 20 percent. For the 300 GeV case, the ratio of the background from pp $\rightarrow$ W + (q or g) to the signal(S/B) from Higgs or continuum W-pair production was in both cases about 0.01. For the high-mass case, this ratio was 0.05 for an 800 GeV Higgs and 0.01 for the corresponding continuum.

TABLE 2

Efficiencies at successive stages of analysis for a 800 GeV Higgs decaying to WW and corresponding backgrounds. Background processes were simulated only for the p_t interval 200-300 GeV.

Process	σ (pb)	$\epsilon_{e\nu}$	ϵ_{jj}	ϵ_{WW}
$pp \rightarrow H^0 \rightarrow e\nu\, q\bar{q}$	.19	.79	.56	.32
$pp \rightarrow WW \rightarrow e\nu\, q\bar{q}$	.04	.75	.62	.44
$pp \rightarrow W\, q(g) \rightarrow e\nu\, q(g)$	5.4	.71	.58	.24

2.2 Identification of Z^0 Pairs

Identification of Z^0 pair events, where one of the Z^0 decays into charged leptons and the other one into neutrinos is in some sense much easier than W pair events. The only important background is from pp $\rightarrow$ Z^0 + jets where missing energy can be artificially produced by mis-measured jets. What matters here is energy lost in cracks or dead regions of the apparatus. Table 3 contains the results of this study. The double electron efficiency is about 43 percent; this is slightly better than the square of

the single electron efficiency which is due to correlations. The mass resolution of the $Z^0 \rightarrow ee$ system is 2.7 percent as can be seen in Fig. 14. The missing-p_t distributions for the signal and scaled background are displayed in Fig. 15. A cut in missing p_t at about 50 GeV retains about 97 percent of the detected electron pairs while rejecting 88 percent of the single-Z^0 background. The mass of the Higgs' can be determined in the same way that the W mass was determined at Sp$\overline{\text{p}}$S collider. A fit can be made to the transverse mass distribution. The residual transverse mass distribution is shown in Fig. 16; when fit to a Gaussian this gives a transverse mass resolution of 11 GeV.

TABLE 3

Efficiencies of different cuts for $H \rightarrow ZZ$ and its backgrounds. Backgrounds were simulated over limited p_t ranges: 100-200 GeV and 200-300 GeV for 300 and 800 GeV signals respectively.

Process	σ (pb)	ϵ_{ee}	ϵ_{P_t}	Mass
$pp \rightarrow Z^0Z^0 \rightarrow ee\nu\,\overline{\nu}$	$4\ 10^{-2}$	.43	.97	300
$pp \rightarrow Z^0\ q(g) \rightarrow ee\ q(g)$	$6.6\ 10^{1}$	.48	.12	300
$pp \rightarrow H^0 \rightarrow ee + \nu\overline{\nu}$	$1.0\ 10^{-2}$	.38	.92	800
$pp \rightarrow Z^0Z^0 \rightarrow ee + \nu\overline{\nu}$	$8.1\ 10^{-4}$	.40	.99	800
$pp \rightarrow Z^0\ q(g) \rightarrow ee\ q(g)$	$7.2\ 10^{-1}$	.43	.25	800

3.0 Recognition of W Hadronic Decays

Most of the physics which will be studied at the SSC imply new particles which decay into $q\overline{q}$ or $qq\overline{q}$ (plus additional neutrinos). This is the case for new heavy quarks, new heavy leptons, and supersymmetric particles. In this section we concentrate on pattern recognition of jets.

Differentiating events from the process of Eq.1 from the ones produced by the standard backgrounds of Eqs. 2-3 where the W decays into leptonic mode or where the W is radiated from the quark or the gluon is the major difficulty.

We present here the results of an analysis[2] which uses fine-grained calorimetry to discriminate between different energy deposition patterns characteristic of the quark-anti-quark decay of a W boson and the fragmentation products of a single parton (quark or gluon).

3.1. Fine-Grained Calorimetry

This study is done using a tower geometry calorimeter, with: $d\eta = d\phi = 0.01$ for the electromagnetic front section and $d\eta = d\phi = 0.02$ for the hadronic back section. The energy resolution was $\sigma/E = 0.15$ for the e.m. part ,and $\sigma/E = 0.50$ for the hadronic part. The polar angle covered by the calorimeter extends down to 2.0 degrees. It is assumed that the hadronic and electromagnetic sections of the calorimeter are constructed of similar or identical materials, so that fluctuations in longitudinal shower development do not introduce fluctuations in measured response due to different sampling techniques in the two calorimeters. In addition, a channel-to-channel miscalibration of 1.5 percent *rms* was introduced. Systematic miscalibrations, however, are not introduced and the response of the calorimeters to electrons and hadrons (the e/h ratio) has been taken to be 1. Muons are assigned an rms energy uncertainty of 11 percent, independent of energy. Thus, we assume a detector system

with good calorimetry, good muon reconstruction and no magnetic field. A magnetic field would, in fact, degrade the resolution of the detector assumed here since the energies measured in the towers would have to be "moved back to where they belong" by solving the problem of apportioning the energy measured in the calorimeter towers among the momenta of the tracks reconstructed in a tracking system. A tracking system in a high track density environment, may fall short of 100 percent efficiency, possibly by several percent. Consequently, track mis-assignments result in erroneous four vector assignments to towers. If for simplicity we think of these errors as just degrading the tower granularity, then a degradation from a granularity of 0.01 to 0.10 leads to a substantial degradation of the mass resolution of the system[3]. Every tower channel with energy exceeding 0.1 GeV is saved as part of the event record. The calorimeter event record consists of the energy absorbed by each tower, the rapidity and the azimuthal coordinates of the center of each tower.

3.2 Definition of Parameters Characterizing the Event Structure

We measure **depositions of energy** with a calorimeter. Therefore, we can study their magnitude and their shape. The first characteristic of a two quark system, such as the one provided by the hadronic decay of the W, is its invariant mass. It is calculated from the tower energies by summing over all the towers included in the W-cluster. Then $m_{jj} = \sqrt{E^2 - P^2}$ where

$$\mathrm{E} = \sum \mathrm{E_k},$$

$$\mathrm{P_x} = \sum \mathrm{E_k} \sin\theta_\mathrm{k} \cos\phi_\mathrm{k},$$

$$\mathrm{P_y} = \sum \mathrm{E_k} \sin\theta_\mathrm{k} \sin\phi_\mathrm{k},$$

$$\mathrm{P_z} = \sum \mathrm{E_k} \cos\theta_\mathrm{k}$$

and θ_k and ϕ_k are the polar angles of the k-th cell.

The mass distributions for the hadronic W decays and single partons are shown in Fig 17. The low mass region for W decays is populated by events with missing neutrinos and missing particles that travel down the beam hole. The high mass region for W decays is due to mis-reconstruction and confusion with fragments from beam jets.

The conclusion from this figure is that the parameter m_{jj} alone is not enough to distinguish the signal from the QCD background. Other properties must be exploited.

The W-"blob" can be characterized in another way by parameterizing its "shape". Usually the event is represented in the calorimetry by a so-called Lego-plot (E_t represented in the plane (η, ϕ). Here, we have chosen to project the energy of each calorimeter cell included in the W-system onto the thrust axis (t) of the event in the 2-dimensional(η, ϕ) plane of the calorimeter.

The t-axis is found by maximizing the quantity:

$$T = 2 \times \sum \vec{e_k} \cdot \vec{t} / \sum e_k$$

where each calorimeter tower is one element of the sum, and $\vec{e_k}$ is the 2-dimensional vector in (η, ϕ), pointing from the centroid of the energy pattern to the k-th calorimeter

tower. The average of these components of the energy pattern which are parallel and perpendicular to the t-axis are calculated as:

$$E_{\parallel} = 1/E \sum \vec{e_k} \cdot \vec{t}$$

$$E_{\perp} = 1/E \sum \vec{e_k} \times \vec{t}$$

where the sum is done over all the cells belonging to the W-"blob" and E is the scalar total energy in the system. The ratio $E_{\perp}/E_{\parallel}$ measures the "elongation" of the jet system and is quite different for W's and QCD jets as seen in Fig 18. We defined the variable S as the distance in rapidity and azimuth from the centroid of the energy pattern scaled by the energy of the system over the mass of the W. Therefore, S is energy independent and furthermore, for a symmetric W-decay, decay products from the fragmentation of the two quarks will appear as a peak at S = +1 and S = −1. The calorimeter energy measured relative to the S-axis for a W+jet event is shown in Fig 19. A three peak structure appears clearly, where one peak is due to the QCD jet of recoil and the two other peaks represent the W-system. The corresponding Lego-plot of this event shown in Fig 20. Figure 21 shows the case of a symmetric W decay. The general case is not as simple because the energy pattern of hadronic decays of W's may differ significantly as is shown in Fig 22.

Two effects which strongly influence the energy pattern of a W-system are gluon bremsstrahlung and the angle between the two emitted quarks. Gluons may be radiated by both initial and final state partons. Pythia and Isajet Monte Carlo's take this effect into account. In Figs. 23 and 24 show how the Monte-Carlo reproduces this effect. Fig. 23 shows an event generated by Pythia for the process:

$$pp \rightarrow W \rightarrow W\ H^0.$$

The W decays into $c\bar{s}$ and the H^0 with a mass of 100 GeV decays into $\tau^+\tau^-$, at $\sqrt{s} = 10\ TeV$; this event has then be submitted to a full simulation in the CDF detector. As pointed out in this picture, the c-quark (corresponding to a cluster with E_t of 36 GeV) emits a radiated gluon (corresponding to a cluster with E_t of 40 GeV). Both clusters are so nearby that the cluster algorithm in the CDF detector merges them. Another picture of such an effect is shown in Fig. 24 where an event has been generated by the Pythia Monte-Carlo, for the process : $pp \rightarrow WW$ at $\sqrt{s} = 40\ TeV$. The W^- decays into $e\nu$ and W^+ decays into $c\bar{s}+4g$. The c-quark cluster (corresponding to 58 GeV of E_t) is accompanied by a cluster of emitted gluons of 28 GeV of E_t; the $\bar{s}$-quark cluster corresponding itself to 20 GeV of E_t has an additional 47 GeV of E_t due to radiated gluons. The additional amount of transverse energy due to these emitted gluons is in both cases quite substantial. Fig. 24 shows together with the LEGO plot of the $(c\bar{s})$ system (Fig 24a), the "distortion" due to this radiation of gluons appearing also in the energy pattern of the $(c\bar{s})$ system (Fig 24b).

In the case of a QCD single parton jet, radiated gluon jets can also mimic a two jet topology. Moreover, depending on the quark decay angle, this energy pattern may have a very similar shape. This energy pattern in S is shown in Fig. 25, for 3 regions of the quark decay cosine in the W-center of mass. The corresponding contour plot $(1/E\ dE/dSdcos\theta^*)$ is shown in Fig. 26. The cosine of the quark decay angle is calculated as:

$$\cos\theta^* = \beta_W \times (P_{l1} - P_{l2})/(P_{l1} + P_{l2})$$

where P_{l1} and P_{l2} are the summed tower energies along the W line-of-flight in the lab, for positive and negative s, respectively. This assumes that kinematically, W-decay is just like π^0 decay, that is, the decay of a heavy object to light mass objects. The resolution in cosine is shown in Fig 27, which displays the difference between the reconstructed cosine and the true (Pythia) cosine for a large sample of W-decays. This resolution is about 0.1 unit in cosine, but there are non-Gaussian tails extending out to a full 1 unit, presumably due to mis-reconstructions. We take this cosine as another distinguishing characteristic between W decays and partons. The distribution of this cosine for W-decays and partons is shown in Fig. 28, in which the partons fragmentations often simulates a highly asymmetric W-decay and therefore populates the region near the cosine of +1. Indeed, a highly asymmetric decay in which one quark from the W takes away most of the momentum is essentially a single parton system, and, as such, is not distinguishable from a primary single parton. Therefore, to improve the discrimination, we apply a combined cut: we cut both on cosine and the chi-squared of the shape ($\chi^2_{\mathbf{shape}}$). This variable is calculated using the mean of the 1/E dE/dS distribution (for $S > 0$ and $S < 0$ respectively)and the *rms* fluctuations about these means. The variables $S+_{\mathbf{rms}}$ and $S-_{\mathbf{rms}}$ are calculated as the rms width of the energy deposition for positive and negative s respectively. The ratio of these quantities is shown in Fig. 29 for W-decays and single jets Fig. 30 shows the $\chi^2_{\mathbf{shape}}$ distributions ,integrated over all $\cos\theta^*$ for W's and single jets The combined discrimination of a cosine cut is very effective since partons often resemble the S-axis distribution in Fig 20, that is, a single structure whose cosine is usually calculated to be near +1, and hence the chi-squared calculation compares this parton jet with the W-shape for a cosine near +1, and of course finds fairly good agreement and a small chi-squared. A cut in cosine 0.6 or 0.8, eliminates these partons and those remaining preferentially have poor chi-squareds.

Finally we also use another characteristic[4] which is the ratio of the transverse momentum of the lower energy W-decay quark to the W+jet invariant mass, all in the W+jet frame; this quantity named $\mathbf{R_{min}}$ is plotted in Fig 31 for W-decays and partons .

The parameter $\cos\theta^*$ is also used to show a very important property of the W decay depending if they come from the H^0 decay or not - the **polarization** effect. W's with transverse polarization will give a $1+\cos^2\theta^*$ distribution whereas W's with longitudinal polarization will have $\sin^2\theta$ angular distribution.

All the above parameters directly derived from quantities measured in the calorimeter are then used to overcome the various backgrounds.

3.3 ($W \to q\bar{q}$) jet pattern versus single jet patterns

The rate for QCD jet production will exceed that for W production by a factor of 100 (or more) as indicated in Table 1. In Fig 32 the mass distribution of W and single parton jets are displayed together. No W-signal is clearly discernable in this figure. As successive cuts are applied, the resulting mass distributions for W-decays and single jets are shown separately in Fig 33a-e. It corresponds to the following set of conditions: $\mathbf{R_{min}} > 0.38$, $\chi^2_{\mathbf{shape}} < 1.5$, $\cos\theta^* < .60$, $E_\perp/E_\parallel < .25$, and $s^+_{\mathbf{rms}}/s^-_{\mathbf{rms}} < 2.0$. After these five cuts, the single parton distribution is reduced to such a level that the W decay signal competes with this background at a signal-to- noise level of about 1-to-1. A subsequent mass cut, in the mass region of the W from 80 to 88 GeV, at these values leaves in the total sample: 1438 W decays out of the 20667 originally generated; so 7% W-efficiency and 9 single jets versus 1619 W-decays, so a 160 ± 53 rejection factor.

The rejection factor is the ratio of the number of W's which survive the series of 5 cuts (previously explained) to the number of jets which pass the same series of cuts. By varying the values of these several cuts and combining samples from different cuts, a curve of W-efficiency versus rejection against single jets may be obtained as is shown in Fig 34. To vary the cuts, we just vary all five cuts by 20% of their values for 5 step up and 5 step down. The "nominal" value corresponds to the list of cuts previously mentioned for the (W+jet) sample with $p_t > 0.3$ GeV/c. The result we obtain now, is about a factor of 3 worse than that obtained previously[5] and may be ascribed to a more realistic event simulation, including the presence of initial state gluon radiation.

It should be noted that while the errors on the W-efficiency are very small, the ones on the rejection factor may be quite large as they should go like the square root of the number of jets left. For instance, the number quoted for the case (W+jet) with $p_t > 0.3$ TeV/c has an error on the rejection factor of 160 ± 53.

If the process is repeated for a sample of (W+jet) events with $p_t > 0.15$ TeV/c ,which would correspond to a m_H^0 of the order of 300 GeV, by applying the same set of cuts as those which were optimized for the (W+jets) events with $p_t > .3$ TeV/c, a rather poor rejection factor of 45 is obtained for a W-efficiency of 10.8%. This reiterates that recognizing $WW \rightarrow e\nu q\bar{q}$ at a rather low mass range ,of the order of 300 GeV, should be harder than working at a higher mass range. On the other hand, certainly more work on the pattern recognition among the calorimeter cells may improve the results. Futhermore, an optimization of the cuts for the worse case ,low mass, could also give better results in the higher mass case. However, at this stage, one may overcome the background due to standard QCD jet and so distinguish ($W \rightarrow q\bar{q}$) jets from the single parton jets by using the rather sophisticated analysis that we have just described.

3.4 $W \rightarrow q\bar{q}$ versus 2 Parton Jets

A background which has an even higher rate than the previous one (about 10 times higher, according to the estimates reported in Section 3 of reference 1), is:

$$q\bar{q} \text{ or } qg \rightarrow q\bar{q} \text{ or } qg + W$$

where the W is radiated by one of the final partons. The question now is: Does the sophisticated analysis proposed above still give a good separation of the ($W \rightarrow q\bar{q}$) signal from this background? To answer this point, we "forget" about the previous analysis and try to define independently a set of 5 "best" cuts for the (W + 2 jets) sample. To do this study we generate a sample of events (W + 2 jets), where the 2 jets are required to have an invariant mass centered around the W mass within a rather large window (40 to 200 GeV). The p_t^W is imposed to be larger than 0.3 TeV/c. A set of new cuts corresponding to: $R_{min} > 0.38$, $\chi^2_{shape} < 20$, $\cos\theta^2 < .70$, $E_\perp/E_\parallel < .60$, and $s^+_{rms}/s^-_{rms} < 2.4$. gives the optimum results in this case: an efficiency for W's of about 10 percent and a rejection factor of 6 only; by far not sufficient enough. Moreover, as in real life, events are mixed together, we will have to apply the same set of cuts to all data. By applying the series of cuts described in Fig. 33 to the sample of events (W + 2 jets) with $p_t > 0.3$ TeV/c or 0.15 TeV/c respectively, we obtained very poor W-efficiencies (1.4 percent and 3.3 percent respectively) and not high enough rejection factors (64 and 46 respectively)(See corresponding efficiencies in Fig. 34).

Though we think we know how to differentiate a ($W \rightarrow q\bar{q}$) system from that of a single parton jet by paying the price of both a high-resolution, fine-grained calorimeter and sophisticated filtering of data, it will be even harder to win when dealing with a two parton jets system.

3.5 Resolving $W \to q\bar{q}$ from $Z^0 \to q\bar{q}$

The effect of varying the granularity of a calorimeter is also studied. The measure used is the ability to separate the $W \to q\bar{q}$ system from a $Z^0 \to q\bar{q}$ system. A sample of WZ^0 continuum events is generated using Pythia, with $p_t(W, Z^0) > 0.3$ TeV. The invariant mass is calculated for three granularities and is shown in Figure 35. The hadronic granularity is, as usual, twice as large as the e.m. These figures evidently show that to resolve W's from Z^0's when considering their hadronic decays will require as finely grained a calorimeter as possible.

3.6 Some Characteristic Plots of $H^0 \to WW$

Finally, we want to display here some of the relevant distributions that are obtained using the various parameters we have previously defined to enhance the properties of the hadronic decays of W's from H^0 decays (namely, polarization).

The first plot (Fig 36) shows the distribution of $\cos\theta^*$ which, as expected, has a $\sin^2\theta$ behaviour (longitudinal polarization). Fig. 37 shows the plot of $E_\perp/E_{||}$ which measures the "elongation" of the $q\bar{q}$ system coming from the hadronic decay of one of the W's. Some examples of 1/S dE/dS spectra are given in Fig. 38; these show mostly a well-ballanced two peak structure because the jets are well separated.

In conclusion, it is certainly very hard to recognize hadronic decays of IVB's in a pp collider environment.[6] This is due to the QCD backgrounds which have large rates and produce both single parton and 2-parton jets which are sometimes very difficult to distinguish from the W or Z 2-quark decay. Furthermore, to distinguish W's from Z's when they both decay hadronically is also very difficult. The reconstructed invariant mass of the corresponding jets is not good enough to solve the problem. Therefore, we have defined a set of parameters which takes advantage of all the information that we may extract from a fine-grained calorimeter; they allow us to describe the structure of the events, their main properties and in particular their energy pattern. These quantities allow the discrimination between W decays and single parton jets with a reasonably good efficiency (of the order of 10% for a S/B rejection rate of the order or larger than 100); this is sufficient at least for the high mass case to overcome this background. Looking at the di-jet system is more difficult and it is not completely solved even using this sophisticated approach as both the efficiencies and the rejection factor are too low to give a S/B ratio of 1.

4.0 Electron recognition

The identification of high p_t electrons is a main issue in many different aspects of this study; it concerns in particular, the signature of W pairs, where one of the W decays leptonically into $e\nu_e$ (that we have studied in details, in various parts of this report), or the Z^0 pairs, where one of the Z's decays into a pair of electrons; it is also essential when considering the reaction: $H^0 \to WW + t\bar{t}$ (with m_{H^0}=300 GeV, dominantly produced through $t\bar{t}$ fusion), where the $t\bar{t}$ is produced in the forward direction and one of the top decays semileptonically emitting a relatively high p_t electron. We will study this case in details in section 6. Tagging electrons is also important when searching for possible charged Higgs, according to the process: $H^\pm \to \tau\nu_\tau$. Identifying the τ in pp colliders[7] means that we have an efficient way to separate pions from electrons ("hadronicity"). Moreover, the work we have done so far, to try to extract the hadronic decay of W's (or Z^0's) from the ordinary QCD jets, pushes us to look for purely leptonic decays or "enriched leptonic" signatures of W pairs and Z pairs events. Even if they provide lower rates, the signatures are cleaner and simpler if the detector has good enough

lepton identification and measurement. All the various cases we have listed now show that it is really mandatory to have a detector able to recognize high p_t electrons.

First by high p_t electrons, we mean electrons which have passed the trigger threshold. As defined earlier, the electron threshold for W pairs has been set at 25 GeV in E_t. This implies a transverse momentum threshold around 15 to 20 GeV/c in p_t. A minimal threshold is around 10 GeV/c in p_t. Typically we will have to consider here a very wide range in p_t which may extend from 10 GeV to greater than or of the order of 500 GeV, to correspond with Higgs' which may have a mass from 300 GeV to 1 TeV. Therefore, the technique we have used so far to detect e's, namely using a fine grained calorimeter plus TRD's, may be not able to allow the detection of electrons over this complete p_t range. We know, for instance, that TRD's may have limitations.[8] So, as an alternative, or complementary to that, one may study how the detection of electrons is improved by introducing a tracking device plus a magnetic field into the scenario.

A magnetic field has been demonstrated to be an essential tool in the case of the UA1 detector for the study of $W \rightarrow e\nu_e$ decays or $W \rightarrow \tau\nu_\tau$ decays or for the search of semileptonic decays of heavy flavors. Such a device together with a B-field (provided it can work in an SSC environment), will allow precise measurements of the spatial coordinates and momentum of an electron. Matching this information with the one provided by a fine-grained calorimeter separated into 2 sections: e.m and hadronic, each one segmented in depth, allow a good determination of all the characteristics of the electron and a good separation of e/π.

Concerning the problem of high p_t electron detection, we have an ambitious series of questions that we would like to answer:

i) How well can a tracking device plus a magnetic field identify high p_t electrons?
ii) What B-field: solenoidal or dipole?
iii) How to match tracking plus B-field plus calorimetry?
iv) How does pile-up confuse the e-recognition?
v) How does a tracking device plus magnetic field compare with TRD's?

Many of these topics have been covered by the electron identification group whose results are contained in these proceedings.

We have used the GEANT 3 package attached to a simple tracking device to do a detailed event-by-event study. The central tracking region parameters are defined as follow: a beam pipe radius of 2 cm, a coil inner radius of 235 cm and a coil outer radius of 280 cm. The tracking chamber has an inner radius of 2 cm and an outer radius of 235 cm. The half length of the central tracking region is equal to 240 cm. The size of the magnetic field in the central region is 1.5 Tesla. Both solenoidal and dipole field have been tried. Two types of events are visualized: $H^0 \rightarrow WW$ as produced by Pythia with Higgs masses of 300 GeV and 800 GeV and with one W decaying hadronically and the other leptonically. Transverse and lateral views (with respect to the beam axis) of these events are shown. They contain the information provided by the tracking device in a B-field: i.e. charged tracks. Figure 39 gives a set of views of all charged tracks for a Higgs of 300 GeV with an electron going very forward with a solenoidal field (39a,b) or a dipole (39c,d). Another $H \rightarrow WW$ event with a mass of 800 GeV is shown with a solenoidal field in Fig. 39(e,f); in this case the electron is quite central. The same events and displays are shown in Fig 40 but only displaying the charged tracks which have a momentum greater than 1 GeV.

These pictures show that the events we are interested in are reasonably populated and one may even distinguish the electron track (dashed line) from the other charged

tracks in the event. We now try to "isolate" this electron by drawing a cone in $\Delta R = \sqrt{(\Delta y^2 + \Delta \phi^2)}$ of 0.1. We display only the tracks which have a momentum larger than 1 GeV and which are contained in this ΔR cone. We see that such an isolation criteria may be achieved in the tracking device (see figure 41).

The heavy GEANT 3 machinery allows us to make such a detailed study event by event. Displaying events is a very important tool when starting this type of search; it allows us to understand the type of events we have to look for and to get a "first feeling" as to how they look.

Our next tasks (not yet achieved) are to see how pile-up disturbs the tracking and how to match the calorimeter information to that from the tracking plus B-field. We have made a first pass attempt to "visualize" the pile-up problem. We have used the simple display program presented in section 3 of our first report.[1] By superimposing a pile-up of 5 minimum bias events plus a low p_t event ($p_t^{jet} < 50$ GeV) onto a $H \rightarrow ZZ$ event (mass of 800 GeV) with each Z decaying into 2 electrons, we get the display of all charged tracks seen in Fig 42. If we now compare this display to the same event without pile-up (Fig 43), we may evaluate the amount of confusion that pile-up introduces into a tracking device. By showing only the tracks with $p_t > 1$ GeV (Fig 44), the display is, of course, much cleaner and it starts to be plausible to distinguish the electrons (dashed lines) even in such a congested situation. However, what we may already conclude is that high p_t isolated tracks seem to be resolvable in such a device with either a dipole or solenoidal field, provided of course the track does not disappear in a dead region or in the beam pipe. Furthermore, one has to demonstrate that tracking (and what tracking) can work in a SSC environment (i.e. lots of R&D...). We think it is worthwhile to pursue our work trying to answer the questions we have asked and certainly to actively participate to the developments of such devices.

5.0 Leptonic Signatures

We have mainly discussed, up to now, the detection of electrons. This does not mean that we completely disregard the detection of muons. On the contrary! The two next sections will deal with muon and multilepton signatures.

5.1 Muon Detection

The muon-identification depends primarily on good 4π coverage by the muon detector; it may include in particular the possibility to detect muons of a few GeV's in p_t in the very forward direction (i.e. from 1 to 5 degrees) compared with the beam axis and also very high p_t muons (up to O(1 TeV)) in the central region covering the angular aperture from 5 degrees to 90 degrees. Apart from good muon identification (which again means separation from hadrons), we also want a good measurement of the muon momentum as well as its sign and also to take advantage that muons may be more easily identified inside jets (so that strict isolation criteria are not required here, in principle) and that triggering on them will be more straightforward. These items are all discussed in detail in the Muon Detector Group report.[9] However, as they pointed out, at the SSC we enter a new domain in which radiative processes become a major energy loss mechanism for muons. The muon group has studied in particular how the muon measurement may be dramatically affected by catastrophic energy loss or generation of soft e.m. showers which accompany the muon and can generate many tracks obscuring the muon-track. The processes will reduce the muon detection efficiency by around 10-20% provided there are multiple muon detection layers. We will not take this into account, for the time being, of these problems and we will assume for the purpose of this

study that we have a 4π muon magnetic spectrometer able to detect and measure the properties of muons having a momentum from few GeV's (>4 Gev/c) up to 1 TeV/c. This muon detector is also assumed to have an angular acceptance which goes from 2 degrees to 90 degrees with respect to the beam axis. Using this, we will ask how the detection and measurement of such leptons may help us in extracting the signals we are interested in.

5.2 Multi-leptonic Signatures

We have studied so far:

$$H^0 \rightarrow WW \rightarrow e\nu_e q\bar{q}$$

$$H^0 \rightarrow Z^0Z^0 \rightarrow l^{\pm}l^{\pm}\nu\bar{\nu}$$

But we may also look at:

$$WW \rightarrow l^{\pm}\nu_l l^{\pm}\nu_l \quad (9)$$

$$WW \rightarrow l^{\pm}\nu_l t\bar{b} \text{ (where } t \rightarrow bl\nu) \quad (10)$$

$$Z^0Z^0 \rightarrow 4 \text{ leptons} \quad (11)$$

These channels, even if giving lower rates, may have as an advantage the requirement of leptonic signatures which may be more powerful than "jetty" signatures. Also, for the W-pair case, in order to reject single-W background events, cuts have to be imposed which depend on the W polarization. These cuts also reject W-pair continuum events. For the time being we have only studied the last two of these cases.

5.2.1 Study of the WW continuum

Two dilepton/dimuon channels (9 and 10) exist which might be used to detect the continuum. Both of these channels have 2 isolated muons but the two accompanying neutrinos will complicate their reconstruction. The branching ratios of reactions 9 and 10 for the muon channels are .0064 and .0032 and would give the number of events seen in Table 4 for an integrated luminosity of 10^{40}. If electron channels were included then these rates would be four times larger.

TABLE 4

Integrated W-pair to two muon rates For a 1 Year Run.

M_{WW} Range	$WW \rightarrow \mu\nu + \mu\nu$ No. events	$WW \rightarrow \mu\nu + t\bar{b}$ with $t \rightarrow b\mu\nu$ No. events
200-300 GeV	1500	750
300-400 GeV	400	200
400-500 GeV	100	50
500-600 GeV	40	20

This section looks at reaction 10 using an idealized analysis and attempts to reconstruct W-pairs from two muon plus jets events. Backgrounds and trigger rates from single W's and QCD jets are also considered.

Events are generated using Isajet 5.20. One W is forced to decay via $W \rightarrow \mu\nu$ with the other $W \rightarrow t\bar{b}$ and then the t-quark forced to decay to a muon (a top mass of 45 GeV was used). Other jets are treated normally. In this analysis, muons are assumed

to be perfectly identified. Jets are treated at the parton level (i.e. no clustering) except that any which decay, or have their daughters decay, into a muon with $p_t > 4$ GeV and $\theta_\mu > 3^0$ veto the event. Finally, the missing p_t is calculated using a perfect detector with $|\eta| < 5$.

For this analysis, 2000 W-pair events were generated with $100 < p_{tW} < 110$. This gave a M_{WW} spectrum centered around 350 GeV. Also, 100K single-W plus jet background events were generated in the same p_t range. Some of the cuts described below should be scaled (in a yet to be determined manner) by p_{tW}. QCD jets are only important at the trigger level and are generated with p_t from 5 to 1000 GeV/c (see the report of the Muon group in this proceedings).

The analysis chains for the W-pair signal and both single-W and QCD backgrounds are shown in Table 5. The first series of requirements is that there exist 2 isolated, oppositely charged muons. For purposes of this analysis, the higher p_t muon is assumed to come from the $W \rightarrow \mu\nu$ decay (which is true about 75% of the time) and will be referred to as μ_1 with μ_2 assumed to come from the top decay. The tight isolation cuts, $E_T < 15$ GeV in $\Delta R < .4$, on μ_2 rejects all non-t-quark decays (see figure 45).

TABLE 5

W-Pair analysis chain for the signal, and the two background channels (W + jet) and QCD. Shown are the acceptances (ϵ), the background to signal ratio (B/S) and, for QCD jets, the rate in Hz.

$WW \rightarrow \mu\nu + \mu\nu bb$		W + jet		QCD jets	
Cuts	ϵ	ϵ	B/S	Rate	B/S
2 muons $\theta_\mu > 3^o$ $p_{t\mu} > 4$ GeV opposite charge	.86	.019	220	1000	2×10^7
μ_1 Isolated ($E_t < 35$ GeV)	.83	.017	200	5	8×10^4
μ_2 Isolated ($E_t < 15$ GeV)	.69	.006	90	.02	400
$\theta_\mu > 4$ $p_{t\mu 1} > 30$ GeV $p_{t\mu 2} > 10$ GeV	.38	.0027	70	.001	20
$p_{t1} - p_{t2} > 20$	.27	.0019	70	.0006	12
$35 < M_T < 140$	.23	.0013	60	.0002	4
2 jets near μ_2	.10	.0003	30		
$55 < M(\mu_2 jj) < 80$	.051	.00007	15		
$\lvert P_{tW1} - P_{tW2} \rvert < 20$	.022	.00001	5		

Though muons are identifiable down to below 5 GeV/c, a $p_{t\mu 2} > 10$ GeV/c cut was chosen to reduce the single W plus jet rate. Also, $p_{t\mu 1} - p_{t\mu 2} > 20$ was required. This increased the fraction of time that the muon assignment was correct to 90%. Other ways of muon assigning were tried. Choosing the muon whose $M_T(\mu p_{tmiss})$ was closest to M_W did not improve upon just using the larger p_t selection. If the muon which had the largest hadronic activity (E_T in $\Delta R < 1$) around it was assigned to the t-quark, this was correct 67% of the time independent of the p_t selection. Also, for $|p_{t1} - p_{t2}| < 20$, the

correct choice was about 50% more likely to pass all the reconstruction cuts described below. For now, only the simple $p_{t1} - p_{t2} > 20$ requirement was used. This gives a clean selection but with an acceptance reduction.

For these dimuon events, the measured missing p_t seen in figure 46 is dominated by the two neutrinos. The direct neutrino has an average p_t of 60 while that from the t-quark decay is 25. In this analysis, all the missing p_t is assumed to be due to the neutrino from the direct W decay. Then the effect of the second neutrino dominates any measurement errors on missing p_t. More complete analyses utilizing all the kinematic constaints to determine the two neutrino vectors would, of course, depend upon the missing p_t resolution.

The most direct effect of the second neutrino is the broadening of the $M_T(\mu_1 p_{tmiss})$ distribution seen in figure 47a. While worse then the Jacobian peak normally seen in W-decay, the presence of a W is still clearly indicated. Figure 47b shows the M_T distribution of the "wrong" muon (μ_2) in the W-pair event. Cuts on M_T between 35 and 140 GeV were imposed to insure a $W \rightarrow \mu\nu$ decay in the event.

The events of interest (reaction 10) will have 2 b-jets in the final state. For now, a "jet-finding" algorithm consisted of looking at the parton level for jets with $p_{tj} > 15$ GeV/c and $\theta_j > 5^0$. This selection gave an average of 2.7 jets for the signal events. Next the jets had to be related to μ_2. This was done by requiring that $\cos\theta_{\mu_1 j} > .2$ and that $.3 < \Delta R_{\mu_1 j} < 4.0$. For now, only events with exactly 2 jets were kept (an additional 50% had more than 2 jets). About 65% of these signal 2-jet events had correctly found the 2 b-jets while only 25% of the background events had 2 b-jets. The number and distribution of jets "unrelated" to μ_2 was similar for the signal and background events.

Next, the invariant mass of μ_2 and the two jets were made (with the jets ordered so that $p_{t1} > p_{t2}$) and loose cuts made. Then, in order to select events from W decay. the mass of the μ_2 and the two jets (seen in figure 48) was required to be between 55 and 80 GeV. At this point, 80% of the signal events had 2 b-jets compared to only 14% (1 of 7) of the background events with almost all the extra jets being gluons.

The last step in this analysis was to look at the residual p_t vector of the system. This was defined as $|\mathbf{p_{tW1}} - \mathbf{p_{tW2}}|$ with W_1 composed of μ_1 and the missing p_t and W_2 from μ_2 and the two related jets. This residual p_t is shown in figure 49 before and after the $M_{\mu_2 j_1 j_2}$ cut. The signal peaks at low values with the background being decidedly not at low values. Currently, the statistics of the background are poor but it looks as if the noise to signal ratio is about 5 below 20 GeV/c and could be determined by extrapolating from the higher bins.

If these results are then applied to a year of running, the W-pair signal will consist of 20 events above a background level of 100 events (80 above 400 if we can include the electron channels). If it were possible to reject half the events which didn't have 2 b-jets (either by tagging the b-jets themselves or by tagging gluon jets) then the signal would be a 3σ effect (6σ with electron channels).

In conclusion, it seems possible to reconstruct the W-pair continuum using the decay chain in reaction 10. The simplified (and unoptimized) analysis presented here still has a large background rate but tightening up the cuts reduced the acceptance below detection limits. If the acceptance could be increased (by other means of assigning the muon or by being able to handle more than 2 jet events) then tighter cuts could be imposed. Also, the differentiation of b-jets from gluon jets would be a valuable tool in this analysis. Finally, this analysis should be done using a simulation of the detector response especially in the pattern recognition of the jets.

5.2.2 Study of the 4 lepton signature

The signature of $H^0 \rightarrow Z^0 Z^0$ where the two Z's decay into charged leptons provide a unique way to recognize Higgs' if they exist. Such events are called "gold plated". The recognition of such a signal mainly depends on the efficiency of the detector to tag the 4 leptons. It can be done almost at the 1st level trigger provided the detector is good enough.

A study[10] has been done calculating the probability that 4, 3, 2 and 1 muon transitted the detector volume, for a series of maximum pseudorapidity cuts from 1 to 6.5 (corresponds to a maximum angle coverage of 0.2 degree). The two following reactions have been looked at: $H^0 \rightarrow ZZ \rightarrow$ 4 leptons for 300 GeV and 800 GeV Higgs masses (where we have shown the plot with a minimum mass of 200 GeV; a minimum mass of 20 GeV gave identical results) and $q\bar{q} \rightarrow ZZ \rightarrow$ 4 *leptons* with requirements on the minimum p_t of 0, 100, 300 and 500 GeV. The corresponding curves giving the geometric acceptance for 4, 3, 2 and 1 muon as functions of the minimum angle of coverage is plotted in Fig 50 for the continuum and Fig 51 for the signal. The worse case gives of the order of 30% geometrical acceptance.

Therefore one may assume that provided a good 4π coverage, the detection of 4 leptons should be quite good. Now the problem arises in distinguishing the H^0 signal from the Z-pair continuum. It will require to pair the muons to reconstruct the best Z^0 masses and then to use the reconstructed Z-momenta to reconstruct the H^0 mass. Z-pairs from Higgs decays can be differentiated from the continuum both by their polarization[11] and by their mass bump (provided the mass isn't too high). As pointed out by the muon group, the momentum resolution of muons in an SSC enviroment will be limited to about 10% with broad tails due to energy loss. Also, tracks will be lost due to catastrophic energy loss. The effect of this on Higgs' reconstruction has not yet been studied.

In conclusion the geometrical acceptance to recognize 4 leptons (in particular 4 muons) cannot drop the signal by more than roughly a factor of 3, provided a good 4π-coverage. However, to extract the signal of the so-called gold plated sample out of the continuum may require more brain and work on our side and perhaps more money: a large piece of magnetized iron may not be enough (see the L3 project).

6 "A la recherche d'un lepton perdu"

We paraphrase Proust[12] to point out the importance of detecting relatively low p_t leptons (O(10GeV) or so). For intermediate mass Higgs' (mass about 300 GeV), the dominant mechanism of production goes through $t\bar{t}$ fusion. Therefore, in the final state together with the H^0 are produced t and $\bar{t}$ quarks which go in the forward direction. The same fact also occurs in the production of an intermediate mass charged Higgs which is mainly produced by $t\bar{b}$ fusion giving in the final state: $H^{\pm} t\bar{b}$. In these cases, as remarked by F.Paige, a lepton with $p_t > 10$ GeV/c is emitted in the forward direction coming from the semi-leptonic decay of the top.

We have studied what additional rejection factor may be gained, against the background, when tagging this lepton in these two scenarios. To do so, we have worked with 2 samples of events; a sample generated with Isajet according to the diagram shown in Fig. 52 which represents the W-pair continuum. By applying the condition $100 < p_{tW} < 200$ GeV, this is equivalent to the production of a Higgs with a mass of about 300 GeV produced according to the diagram in Fig. 53. The second sample is the background to this process represented by (W+jet) events where $100 < p_{tW} < 200$ GeV.

We reconstruct the first W (W1, i.e. the W decaying leptonically) by applying the same analysis as the one developed in section 2; namely we look for the highest E_t electron in the event and assign it to W1 (this is correct a fair fraction of the time; see Subsection 4.3 of reference 1). We veto this electron and look in the "opposite hemisphere" to W1, to reconstruct the second W, W2, which decays hadronically. We reconstruct the $q\bar{q}$ system by taking the 2 highest E_t jets in the "opposite hemisphere". If the $q\bar{q}$ system is made of $c\bar{c}$ or $b\bar{b}$ jets, they may also produce leptons by decaying semileptonically. To veto this possible lepton, we open a cone in ΔR of 1.0 around the axis of the $q\bar{q}$ system (or the axis of the highest E_t jet of this system) and veto the lepton inside this cone, if any.

We then look for the highest p_t lepton, with $p_t > 10$ GeV, outside this ΔR region and require in addition that $\eta > 2.5$ (to ensure the forward direction). Additional isolation cuts for the electrons are required in order to try to increase somewhat the background rejection. The result of this analysis applied to the W continuum gives that 30% of the events pass these cuts whereas only 1.5% of the (W+jet) events pass. This gives a rejection factor of roughly 10 to 20 gained by tagging this additional lepton.

We may remark that the analysis developed here has been directly applied to M.C. generated events (plus the idealized 4π detector simulation) of each type separatly, so that we have been able to check at each step the reliability of the criteria we impose. Therefore, this has to be taken more as a scheme of analysis which in our case allows us to evaluate the additional rejection factor which may be gained. However, it is clear that, in real life, one will have to develop more sophisticated filters to "isolate" this very precious lepton.

7.0 Pile-up

We are well aware that pile-up may disturb us in many different ways. It has been shown[13], for instance, how pile-up may perturb the measurement of the missing energy which is one of the main aspects of the signatures we are dealing with. What we have been mostly worried about in this study is the particular (but very important) question of how much pile-up confuses the electron identification and its momentum measurement. We have not yet gone very far in trying to answer this point; this is mainly due to technical problems (implementing GEANT3 plus correct pile-up generator) and lack of time; so the results we are presenting here are very preliminary.

First let us show some pictures (Lego plots) representing Higgs events with and without pile-up. In this case, the pile-up we have assumed is very "soft", i.e. it is just a superposition of 5 low p_t events (by low we mean events with $p_t < 10$ GeV, so minimum bias events). The highest E_t cluster in this case has just 10 GeV (Fig 54). Now, if we superimpose this pile-up onto a $H^0 \rightarrow WW$ event, with m_{H^0}=300 GeV (Fig 55), the highest E_t cluster in the event passes from 58.2 GeV to 59.3 GeV (Fig 56). The higher mass case was also simulated but the effect was not as noticable. Note that the cells in this simulation, a la D1, are 0.2x0.2.

Let us discuss now about the possible effect of pile-up on electron identification. As we have already seen in sections 2 and 4, a very important criteria to recognize high p_t electrons is to require an isolation of the electron candidate first in the calorimetry, then in a tracking device (to reinforce the first condition). So far, we have essentially tried to estimate how much pile-up may perturb the electron isolation in the calorimetry. This has been done by a rather rough simulation of what the pile-up could be. Namely, we have generated using Isajet a pile-up effect by superimposing onto the signal (which in this case is just a (W+jet) signal with $p_{tW} > 200$ GeV), a pile-up of events (minimum

bias plus low p_t jets) according to a Poisson distribution with pile-up rates given by: $L\sigma\Delta t$ where Δt =200 nsec. Our estimate of the effect is rather pessimistic as we have not considered here the possibility to sample Δt in less than 15 nsec to reproduce the electronic solution a la Radeka.[14]

Within these hypotheses, we have tried to compare the activity in the calorimeter cells surrounding the electron-cell inside a cone in ΔR of 0.3 and 0.7 respectively with and without such pile-up. The results we obtained are listed in Table 6; they should be taken with a lot of caution as we are certainly able to do better.

TABLE 6

Effect of pile-up on the "activity" around the electron-cell.

Parameters	Pile-up	No Pile-up
p_t(electron) (GeV/c)	124.	124.
No. leptons with p_t¿10 GeV/c	3	3
ΣE_t $\Delta R < 0.3$ (GeV)	4.6	0.72
ΣE_t $\Delta R < 0.7$ (GeV)	23.2	2.4
No. jets with E_t >20 GeV	22	3

The other concern we have is to see how pile-up may affect the tracking and, in particular, the measurement of high p_t leptons. Again we know, that for the electron, the isolation criteria is quite important. Certainly pile-up will have a double effect: introducing additional soft tracks and perturbing the digitization of the existing tracks (see section 5.4). This would result in sometimes making it very hard if not impossible to reconstruct the tracks.[15] This effect will be explored for the first time by the CDF experiment if the Tevatron gets an upgrade in luminosity as foreseen for 1992.

Pile-up is a touchy and subtle prolem which has therefore to be carefully studied in order to be correctly appreciated. We are developing the tools to do so. Also it is something that we don't have real life experience with (apart from the prehistorical ISR case). We will start to understand it and hopefully learn to live with when existing colliders and their associated experiments begin working with higher luminosities. It is by experimenting with real high luminosity conditions that we will be able to face it or at least be able to estimate it. Poisson distributed simulations have only the merit to make us aware that something may disturb us.

8.0 CONCLUSION

In this paper, we have mainly concentrated on a "realistic" study of the process:

$$H^0 \rightarrow WW \rightarrow e\nu_e + q\bar{q} \tag{12}$$

and

$$H^0 \rightarrow ZZ \rightarrow \nu\bar{\nu} + l^+l^- \tag{13}$$

for two possible Higgs masses of 300 GeV (low mass for the SSC) and 800 GeV (high mass i.e. good mass range for the SSC). "Realistic" means that we have submitted the generated events to a simulation of an apparatus which contains some facts of "real life" such as deadened areas, cracks, realistic parameters for electron and hadron identification, etc. We have studied how this may affect the quantities that we have

to measure (electron and missing energy resolution, jet structure of the event...)and also how it may bias the strategy developed in the first report to select the data. We summarize the main results of this work with the following remarks.

REMARK 1:

Process (12) gives a total rate of about 25 times more events compared to process (13) (from results quoted in Table 3.1 of Report 1). HOWEVER, once the complete filtering procedure is applied to extract the signal from the background, this relative difference drops quite significantly. The main background in the case of $H \rightarrow WW$ is due to the QCD process: $pp \rightarrow qq, qg \; or \; gg$ where one of the final parton emits a W. Once we apply the filtering strategy described in Section 2 to extract the W-pair signal out of this background and of the W+jet background, we obtain an estimate of the ratio of the signal to each of these backgrounds: S(WW)/B(W+jet) and S(WW)/B(QCD). We quote in Table 7 the corresponding numbers for each Higgs mass after each step of selection. It is interesting to note that in the case of a low mass Higgs, the W+jet background is 10 times lower than the QCD background and that in the case of the 800 GeV Higgs, they only differ by a factor of 4. Also, the relative (W+jet) background decreases by a factor 30 when going from 300 to 800 GeV mass, whereas the QCD background diminishes only by a factor of order 10 between these 2 ranges. From the selection of WW data reported in Section 2, we learn that the total efficiency of real W-pair events is of the order of 30% for both masses, whereas the efficiency of the (W+jet) background is only of the order 10% with the QCD background being about 1%. This last number differs from the number quoted in Table 1. This is due to the fact that in there, the analysis has been done only using simple QCD 2 jets events (so without implementing in some way the W-radiation). Therefore, to get a more realistic estimation of the ϵ(WW) for this background we assume here $\epsilon(e\nu)$ of about 40% (as usual for a leptonic decay of W) instead of the 1% quoted in Table 1 and then we multiply ϵ(WW) by this factor. Thus, after this WW selection, we finally stay with about 2.8×10^4 W-pair events and both backgrounds are now at the same level (i.e. S/B = 1% for each background). Next we applied the refined analysis of Section 3 to differentiate $W \rightarrow q\bar{q}$ from single or 2 parton QCD jets and found roughly an extra rejection factor of order 50 (in the low mass case) for single parton jet (from W+jet events) but only a rejection factor of order 10 for the 2 parton jets. Moreover, this is gained at the price of reducing the efficiency to only 1 to 3% for the W-pair sample. Therefore, we may expect to get a total of about 800 W-pair events (out of the initial 93000) once all selection criteria are applied and a ratio S(WW)/B(W+jet) of the order 1 and S(WW)/B(QCD) of about 0.2 to 1 (at best). The situation is a little bit different in the case of a high mass Higgs. Although the statistics are initially 20 times lower than for the low mass case, the corresponding backgrounds are also much lower (see Table 7). The situation becomes still more favorable because it is also easier to reduce these backgrounds. By applying the same selection procedures as before, we get for both backgrounds a ratio S/B of the order of 5 while losing relatively fewer signal events (7 to 10% efficiency for analysis of Section 3 compared to the 1 or 3% in the low mass case).

This low mass W-pair signal may be improved by applying a more realistic cut on E_t^{miss}. We have applied here only a cut of 10 GeV. If, for instance, we apply a cut of about 40 to 50 GeV, it is clear that the QCD background will be decreased thereby reaching a S/B of order 1. Moreover, by playing the requirement on longitudinal versus transversal polarization, the interesting signal will also be enhanced.

At this stage of our work we may conclude that we expect to get a few hundred W-pairs with S/B of the order 1 for the low Higgs mass region (for a SSC integrated luminosity of 10^{40}cm^{-2}), and about 100 such events for an 800 GeV Higgs, but with a much cleaner signal (S/B = 5). Obtaining these will widely use the resources provided by a realistic 4π fine-grained calorimeter together with a set of TRD's to identify electrons.

TABLE 7

Evolution of W-pair signal (Higgs and continuum) and the signal to background ratio (S/B) when applying the various filtering steps.

		$m_H = 300$			$m_H = 800$	
Filter step	No. of events	S/B (W+jet)	S/B (QCD)	No. of events	S/B (W+jet)	S/B (QCD)
0	93000	$6.5\ 10^{-3}$	$6.5\ 10^{-4}$	5000	0.02	$5\ 10^{-3}$
1	25000	0.01	0.02	1500	0.05	.1 to .5
2	800	1	0.2 to 1	100	5	1 to 5

Filter step 0 corresponds to the total number of expected events for this process, without applying any filter; filter step 1 corresponds to applying the selection criteria described in Section 2; filter step 2 is obtained after the analysis of Section 3.

REMARK 2:

In contrast with the previous case, the process (13), although it gives much lower rates, provides at the end a much cleaner signature. This is due to the fact that the main characteristics of these events are 2 high p_t leptons and a fair amount of missing energy. Therefore the main background, due to (Z+jet) production, will be easily overcome by applying simply an appropriate cut on the missing energy. We have summarized in Table 8 the result of the simple selection procedure extensively discussed in Section 2. We want to point out that we expect to find a clear signal $H^0 \rightarrow ZZ$ if the Higgs mass is around 300 GeV, by simply using this process. If the Higgs mass is high, the statistics starts to be low and Z-pair signal will be mostly used to reinforce what will be first delivered by the reaction $H \rightarrow WW$.

The numbers IN TABLE 8 refer to Z decay mode to electron and muon, and the three neutrino flavors. It is assumed that muon efficiencies are equal to electron efficiencies. It should finally be remarked that the statistics for the background was small for both low and high mass cases so that its shape and normalization were not well determined. Establishing the low mass Higgs via this channel is, at this point, inconclusive. A more careful study needs to be undertaken with a much larger (x10 or x100) set of events.

TABLE 8

Evolution of the Z-pair signal (Higgs and continuum) and the signal to background ratio S(ZZ)/B(Z+jet) when applying the various E_{tmiss} cuts maximizing (S/B) and significance (number of signal events/error in background).

	m_H = 300 GeV		m_H = 800 GeV	
E_{tmiss} Cut (GeV)	Number of events	S/B (Z+jet)	Number of events	S/B (Z+jet)
no cuts	2500	1.2×10^{-3}	200	5×10^{-3}
> 100	2120	.02	-	-
> 350	-	-	104	.5

REMARK 3:

The results presented in remarks 1 and 2 encourage us to investigate other types of "clean" signatures, namely the LEPTONIC ones. Leptons are objects which seem to be easier to measure than jetty structures in events produced by very high energy pp colliders. Therefore, we have investigated the kind of accuracy we need to identify and measure electrons (Section 4) and we have tried to search for additional possible leptons to better tag, in particular, low mass objects which are dominantly produced by $t\bar{t}$ or $t\bar{b}$ fusion which then produces an additional forward lepton. This lepton may be detected with a roughly 30% efficiency, gaining an additional rejection factor of 10 for the background (Section 6). These various facts lead us to the conclusion that our detector has to be able to detect and measure at the same time relatively low p_t electrons (few tens of GeV's) as well as very high p_t electrons (several hundreds of GeV). This clearly means that several techniques will have to be used to detect electrons. We have in particular studied a little bit how a tracking device will identify single high p_t e's in such a congested environment; how it may "isolate" such tracks. The "first impression" we get is not completely hopeless once we admit, of course, that a tracking device can work in a B-field in a high energy, high luminosity pp scenario.

Also more specific LEPTONIC signatures have been looked at such as: $WW \rightarrow \mu\nu_\mu + t\bar{b}$ (t decaying semi-leptonically) or $ZZ \rightarrow 4$ leptons. Even though these studies are still preliminary, they all show that the apparatus will have to detect electrons and muons in a very accurate way and over a wide p_t range.

REMARK 4:

Finally, we have attempted to evaluate some of the effects due to pile-up. We have tried to estimate the amount of confusion it can add to the tracking information and to the calorimetric information (Section 4 and 7).

We are therefore convinced at this stage, that if the neutral Higgs boson exists as expected in the standard model and has a mass within the range from 0.3 to 1 TeV, then after one year of good running conditions (i.e. 10^{40}cm^{-2} integrated luminosity) with a very high performance 4π detector, we should be able to discover this new signal at a very high energy pp collider such as the SSC. This statement implies also of course that the team of physicists who will run such an experiment not only will be quite lucky but also smart enough to design, construct and run "this very high performance 4π detector." They have maybe 10 years to do it...this is not so much...

Also we would encourage the pioneering teams running experiments at lower and "prehistorical" pp colliders such as the Tevatron to not be discouraged to pursue such a search; just the contrary. If the Higgs mass is from few tens of GeV up to about 80 GeV or so, provided the Tevatron gets enough luminosity ($5 \times 10^{31} \mathrm{cm}^{-2}\mathrm{s}^{-1}$), then it may have a unique chance to discover the Higgs. Clearly, if the Higgs is rather light (few Gev's to 30 or 40 GeV), our friends running experiments at the SLC and LEP e^+e^- colliders will certainly be in a privileged situation.

Apart from the existence of the Higgs, looking for very high mass W-pairs around the TeV range opens a new domain of high energy physics. We have tried to demonstrate by this work the fundamental role of a very high energy and very high luminosity pp collider in this respect.

One of us (ASN) would like to thank Fermilab and LBL for their kind hospitality and T. Gottshalk and L. Pondrom for their friendly support. This work was supported in part under U.S Department of Energy contracts DE-AS05-76ER03509, DE-FC05-85ER25000, W-7405-ENG-82, DE-AC02-80ER10699, and DE-AC03-76SF00098.

POSTSCRIPT: The Organization and Coordination of the W/Z/Higgs Experimental Working Group.

Our working group has been set-up during the UCLA Workshop, "Observable Standard Model Physics at the SSC: Monte Carlo Simulation and Detector Capabilities", held in January of 1986. J. Gunion and A. Savoy-Navarro have been charged to coordinate the theoretical and experimental aspects respectively. The first action taken has been to define, already at the UCLA meeting, the main orientations as well as the main goals to be achieved by this group. It was decided in particular to concentrate on a detailed study of two main processes, one characterized by mixed leptonic and hadronic signature: $H^0 \to WW(W \to e\nu_e \; and \; W \to q\bar{q})$; the other one a purely leptonic mode: $H^0 \to ZZ(Z \to l^+l^- \; and \; Z \to \nu\bar{\nu})$. Both processes have been studied for two possible mass ranges: 300 and 800 GeV. The main goal was first to develop the necessary tools to do this work, and then to define in a realistic way the detector needed to pursue such a search and to study its main performances and limitations.

Therefore the second step, from the UCLA meeting till the Snowmass Summer Study, has been to develop and implement these processes and their corresponding main backgrounds in two main generation facilities, Isajet and Pythia, for pp colliders. This has been done by the Monte Carlo's experts (F. Paige, H.U. Bengtsson and T. Sjöstrand) and a careful check has been pursued, by comparing the results they obtained with the theoretical expectations (J. Gunion) and also confronting the results each Monte-Carlo give when assuming a very simple simulation of an idealized 4π detector (A. Savoy-Navarro and Y. Takaiwa). At the same time a detailed analysis of the hadronic decay of the W's versus QCD background was developed (J. Hauptman) and the study of the low energy case, in particular the possibilities of the Tevatron with the CDF detector and of a 10 TeV pp collider, was done (A. Savoy-Navarro and Y. Takaiwa).

The last step has been achieved with an enlarged group of people both on the theoretical and experimental side. On one hand, the work done by J. Gunion and collaborators, described in the theoretical report of the W/Z/Higgs working group, has been largely dedicated, apart from refining the study on possible cuts to enhance the signal from its main background, to studying new channels and new Higgs as expected

beyond the Standard model. On the other hand, the "experimental team" formed at Snowmass, (see the name of contributors in the two Experimental reports in these proceedings), combined their efforts to develop the tools necessary to reproduce the "facts of real life", and also to pursue a complete analysis of the defined scenarios. This work has been done in good part at Snowmass, but it has been achieved in its final and refined form from August until December.

It is now interesting to point out some facts and some numbers about this work. The geographical dispersion of our experimental team is mainly characterized by the 5 main areas: Chicago (FNAL), California coast (LBL+SLAC), Florida (FSU), Paris (Saclay+CERN), Japan (KEK). Paris, which has been the coordination center, is situated at an 8 hour delay from Japan and is 9 hour in advance of California. The communication has been essentially maintained by extensively using Bitnet and Decnet mail. Results, plots, texts, comments, etc... were mainly transmitted this way. At an ultimate stage of the work, Telefax has also been used and in case of emergency (due to tight deadlines), information was sent through very express mail and telephone. The main present involvements of the most active people in this team are $p\bar{p}$ physics (UA1, CDF, D0 representatives) and some e^+e^- experts.

Apart from the development of the generation packages, a complete simulation and analysis framework have been developed by this team including also display packages. The main computing centers have been: FNAL (VAX cluster), Florida State University (Cyber 205), LBL (Vax 8600 and 782), and Ames (Vax 785). The summary of the computing expenses by our group is listed below. Globally speaking, about 800 hours of Vax 780 time has been used for our work and a minimum of 200K blocks disk space was constantly needed to run our jobs. Storage on magnetic tapes of generated as well as simulated data has been also extensively needed. We do not quote here the amount of computing time and disk space provided to us mainly by the FNAL Vax cluster during the Snowmass meeting itself.

This more or less summarizes the amount of fun and difficulties we encountered and faced in achieving this work.

COMPUTING USE SUMMARY

Computer center		Number of hours	Job Definition	Disk space (blocks)
FNAL	Vax Cluster	300	Mainly spent in Simulation and analysis	200K (500 evt)
		60	Generation of 100K $WW \rightarrow \mu\mu$ events	200K
		40	Analysis of 100K $WW \rightarrow \mu\mu$ events	
TOTAL		400 HOURS (VAX 780)		
LBL	Vax 8600	2	Generation of 7500 events keeping 2000	
		14	Simulation of 2000 evts	
		2	Analysis of 2000 evts	
TOTAL		70 HOURS (VAX 780)		
FSU	Cyber 205	10	Gen.+Sim.+Analysis of 5000 QCD evts	
AMES	Vax 785	27x5	Gen.+Sim. of 25K events x 5 times	Stored on tape 25K
		4x5	Analysis of 25K events x 5 times	evts/tape (6250bpi)
TOTAL		150 HOURS (VAX 780)		

References

[1] G. Alverson et al., "Experimental search for W/Z pairs and Higgs Bosons at very high energy hadron-hadron colliders", first Experimental Report of the W/Z/Higgs working group, these proceedings.

[2] This analysis procedure has been presented in its preliminary stage at the Madison Workshop on "Physics Simulations at High Energy", Madison, May 5-16, 1986. See the report of A. Savoy-Navarro, "Experimental searches for W-pairs and Higgs at a very high energy pp collider" and references therein.

[3] J. Hauptman et al., Proceedings of the Summer Study on the Design and Utilization of the Superconducting Super Collider, Snowmass, Colo., 1984.

[4] J. Gunion and M. Soldate have worked out a lot of cuts to apply on Higgs events produced by high energy pp collisions to be able to extract this signal from the main standard backgrounds. They have found a parameter that they called R_{min} (see Section 3) which is a very powerful way to increase the signal. See J.F. Gunion er al., "Theoretical Report of the W/Z/Higgs SSC Working Group" in these proceedings.

[5] E. Hernandez et al., Proceedings of the Summer Study on the Design and Utilization of the Superconducting Super Collider, Snowmass, Colo., 1984.

[6] M. Abud, R. Gatto and C.A. Savoy, Ann. Phys.**122**, 219 (1979).

[7] See reference 14 of Reference 1.

[8] For a discussion about the limitations of TRD's for measuring high momentum electron see the Report of the working group on Electron Identification, these proceedings.

[9] D. Carlsmith et al., "SSC Muon Detector Group Report", these poceedings.

[10] D. Carlsmith, D. Hedin, B. Milliken, "Leptonic Angular Acceptances", these proceedings.

[11] The importance of experimentally measuring the effects of W-polarization has been stressed several times in particular by M.J.Duncan and G.L. Kane,see for instance: M.J. Duncan, G.L. Kane, W.W. Repko, Phys. Rev. Lett, **55**, 773 (1985); M.J. Duncan, Physics Letters B, **179**, 394 (1986); G.L. Kane, "Physics and planning for future colliders", lectures at the 13th International Winter Meeting on Fundamantal Physics, Cuenca, Spain, April 1985.

[12] M. Proust, "A la recherche du temps perdu"; we have paraphrased here this title of a series of 8 autobiographic volumes which starts with "Du cote de chez Swann" and ends up with "Le temps retrouve".

[13] G. Alverson and J. Huston, these proceedings.

[14] V. Radeka, these proceedings.

[15] P. Berge, CDF Collaboration, private comunication to A. Savoy-Navarro.

Figures

Figure 1 Cut view of one quadrant of the D1 detector.

Figure 2 Single electron and pion dE/dx in the TRD.

Figure 3 Cluster dE/dx in the TRD.

Figure 4 Isolation defined as the ratio of cluster E_t to the E_t in a calorimeter trigger tower comprised of 9 cells (.15 × .15 units in area).

Figure 5 Cluster Radius defined as the energy-weighted *rms* of a cluster, in phase space units, for both electrons and jets.

Figure 6 Transverse mass of the $e\nu$ system (300 GeV Higgs).

Figure 7 Residual electron energy resolution defined as the fractional difference between incident and simulated energy (300 GeV Higgs).

Figure 8 Residual neutrino p_t-resolution defined as the fractional difference between the neutrino p_t and the missing-p_t of the event (300 GeV Higgs).

Figure 9 Transverse mass of the jet-jet system (300 GeV Higgs).

Figure 10 Mass of the jet-jet system (300 GeV Higgs).

Figure 11 Mass of the W-W system (300 GeV Higgs).

Figure 12 Mass of the jet-jet system (800 GeV Higgs)

Figure 13 Mass of the W-W system (800 GeV Higgs)

Figure 14 Mass of the e-e system for the process $pp \rightarrow Z^0Z^0$.

Figure 15 Missing p_t for the process pp $\rightarrow$ $Z^0Z^0$and Z^0 jet.

Figure 16 Residual transverse mass for the process $pp \rightarrow Z^0Z^0$.

Figure 17 Mass distribution for hadronic W decays(solid) and single partons(dashed). The two distributions have been normalized to the same number of events to show the shape of the jet-jet mass distribution of the hadonic decay of W's..

Figure 18 Distribution of $E_\perp/E_\parallel$ for W (solid) and QCD jets (dashed).

Figure 19 Energy projected on the thrust axis versus S of a (W+jet) event.

Figure 20 Lego plot of event displayed in Figure 19

Figure 21 Energy pattern along the S-axis of a symmetric W decay.

Figure 22 Energy pattern of various $W \rightarrow q\bar{q}$ systems from the process $pp \rightarrow WW$ where one of the W's decays hadronically.

Figure 23 The effect of gluon bremsstrahlung in an event: $pp \rightarrow W \rightarrow WH^0$ at $\sqrt{s}$ = 10 TeV, CDF simulation and Pythia Monte Carlo where $H^0 \rightarrow \tau^+\tau^-$ and $W \rightarrow c\bar{s}$ (with c-quark emitting a gluon).

Figure 24 Effect of gluon bremstrahlung on an event $pp \rightarrow Ww$ at $\sqrt{s} = 40\ TeV$ (where $W^+ \rightarrow c\bar{s}$ and $W^- \rightarrow e\nu$). a) LEGO plot view of the $W \rightarrow c\bar{s}$ b) Energy pattern of the $c\bar{s}$ system.

Figure 25 Energy pattern of $(W \rightarrow q\bar{q})$ for different $\cos\theta^*$ intervals

Figure 26 Contour plot of 1/E dE/dS vs $\cos\theta^*$

Figure 27 Residual $\cos\theta^*$ distribution

Figure 28 Distribution of $\cos\theta^*$ for $W \rightarrow q\bar{q}$(solid) and single jets(dashed)

Figure 29 Distribution of S^+/S^- for $W \rightarrow q\bar{q}$(solid) and single jets(dashed)

Figure 30 Distribution of Chi-squared shape for $W \rightarrow q\bar{q}$(solid) and single jets(dashed)

Figure 31 R_{min} for W (solid) and partons (dashed)

Figure 32 Invariant mass distributions of $(W \rightarrow q\bar{q})$ system compared to the jet mass due to QCD single partons. (True relative scale)

Figure 33 Effect of successive cuts on R_{min}, χ^2_{shape}, $\cos\theta^*$, $E_\perp/E_\parallel$, and S^+_{rms}/S^-_{rms} on W-mass (solid) and QCD single jets(dashed).

Figure 34 W-efficiency curve versus Rejection factor, after the set of cuts of Fig 33 for the sample (W + jets) with $p_t > 0.3$ TeV/c (solid) and for (W + 2 jet) sample with $p_t^W > 0.15$ TeV/c (dotted).

Figure 35a Invariant mass distributions for $W \rightarrow q\bar{q}$ (solid) and $Z^0 \rightarrow q\bar{q}$ (dashed) normalized to the same number of events, for a e.m. granularity of Δy=0.01 and $\Delta\phi$=0.01.

Figure 35b Invariant mass distributions for $W \rightarrow q\bar{q}$ (solid) and $Z^0 \rightarrow q\bar{q}$ (dashed) normalized to the same number of events, for a e.m. granularity of Δy=0.03 and $\Delta\phi$=0.03.

Figure 35c Invariant mass distributions for $W \rightarrow q\bar{q}$ (solid) and $Z^0 \rightarrow q\bar{q}$ (dashed) normalized to the same number of events, for a e.m. granularity of Δy=0.05 and $\Delta\phi$=0.05.

Figure 36 Distribution of $\cos\theta^*$ for $H \rightarrow WW$

Figure 37a Distribution of $E_\perp/E_\parallel$ for $H \rightarrow WW$

Figure 37b Distribution of $E_\perp/E_\parallel$ for $H \to WW$

Figure 38 Distributions of $1/SdE/dS$ for $pp \to H^0 \to WW$

Figure 39(a,b) Display of all charged tracks for a $H \to WW$ event with $m_H = 300$ GeV and $W \to e\nu$ and $W \to q\bar{q}$ in a solenoidal field. a) transverse view; b) lateral view. The electron is the dashed line.

Figure 39(c,d) Display of all charged tracks for a $H \to WW$ event with $m_H = 300$ GeV and $W \to e\nu$ and $W \to q\bar{q}$ in a dipole field. c) transverse view; d) lateral view.

Figure 39(e,f) Display of all charged tracks for a $H \to WW$ event with $m_H = 800$ GeV and $W \to e\nu$ and $W \to q\bar{q}$ in a solenoidal field. e) transverse view; f) lateral view. The electron is the dashed line.

Figure 40(a,b) Display of the charged tracks with $p > 1$ GeV for a $H \to WW$ event with $m_H = 300$ GeV and $W \to e\nu$ and $W \to q\bar{q}$ in a solenoidal field. a) transverse view; b) lateral view.

Figure 40(c,d) Display of the charged tracks with $p > 1$ GeV for a $H \to WW$ event with $m_H = 300$ GeV and $W \to e\nu$ and $W \to q\bar{q}$ in a dipole field. c) transverse view; d) lateral view.

Figure 40(e,f) Display of the charged tracks with $p > 1$ GeV for a $H \to WW$ event with $m_H = 800$ GeV and $W \to e\nu$ and $W \to q\bar{q}$ in a solenoidal field. e) transverse view; f) lateral view.

Figure 41(a,b) Isolation in a $\Delta R < 0.1$ cone around the electron for $H \to WW$ with mass of 300 GeV in a solenoidal field; a) transverse view; b) lateral view. Only tracks with momentums greater than 1 GeV are shown with the electron being the dashed line.

Figure 41(c,d) Isolation in a $\Delta R < 0.1$ cone around the electron for $H \to WW$ with mass of 300 GeV in a dipole field; c) transverse view; d) lateral view. Only tracks with momentums greater than 1 GeV are shown with the electron being the dashed line.

Figure 41(e,f) Isolation in a $\Delta R < 0.1$ cone around the electron for $H \to WW$ with mass of 800 GeV in a dipole field; e) transverse view; f) lateral view. Only tracks with momentums greater than 1 GeV are shown with the electron being the dashed line.

Figure 42: Effect of the pile-up of 5 minimum bias events plus a low p_t event onto a $H \to ZZ$ event (mass of 800 GeV) with each Z decaying to 2 electrons.

Figure 43: Same event as in Figure 42 but without the pile-up.

Figure 44: Same event as in Figure 42 but without the pile-up and applying a cut of $p_t^{track} > 1$ GeV on the displayed tracks.

Figure 45: E_T in a cone of $\Delta R < .4$ about the muon for W-pair events (solid line) and b) (W + jet) events.

Figure 46: Missing p_t for W-pair dimuon events.

Figure 47: The $M_T(\mu p_{tmiss})$ distributions for a) μ_1 and b) μ_2 (the "wrong" muon) in W-pair events.

Figure 48: The invariant mass of the $\mu_1 jet_1 jet_2$ system for W-pair events (solid line) and (W + jet) events (dashed line).

Figure 49: The residual p_t of the two W's (defined as the difference of the two p_{tW} vectors) before a) and after b) the $M_{\mu_2 j_1 j_2}$ cut for W-pair events (solid line) and (W + jet) events (dashed line).

Figure 50: Fraction of events accepted as a function of pseudorapidity coverage for a) $p_t > 0$, b) $p_t > 100$, c) $p_t > 300$, and d) $p_t > 500$.

Figure 51: Fraction of events accepted as a function of pseudorapiditycoverage for a) 300 GeV higgs and b) 800 GeV higgs.

Fig. 52: Feynman diagram for production of W pairs from continuum produced by $t\bar{b}$ fusion.

Fig 53: Feynman diagram for H° production through $t\bar{t}$ fusion.

Figure 54: Lego plot of 5 combined minimum bias events.

Figure 55: Lego plot of a 300 GeV $H \rightarrow WW$ event.

Figure 56: Same as Figure 55 but superimposing the pile-up due to 5 minimum bias events (Fig 54).

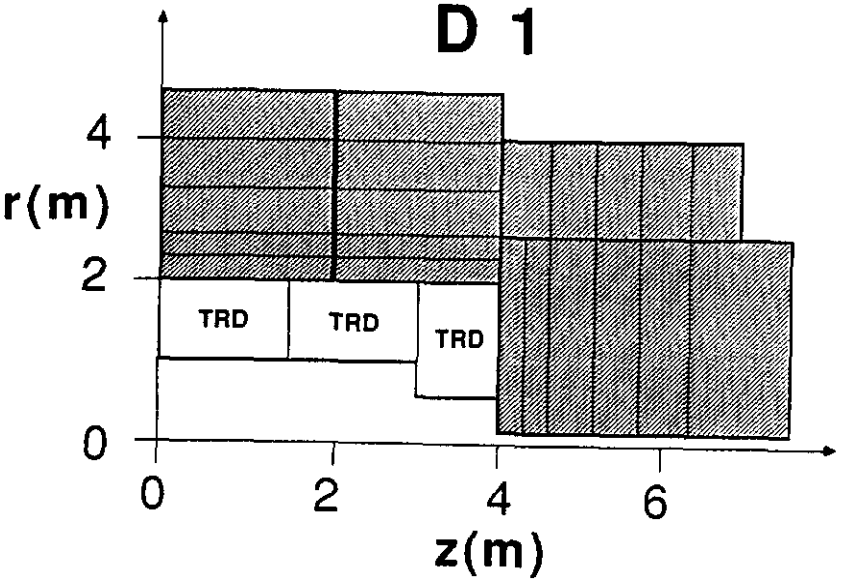

Figure 1

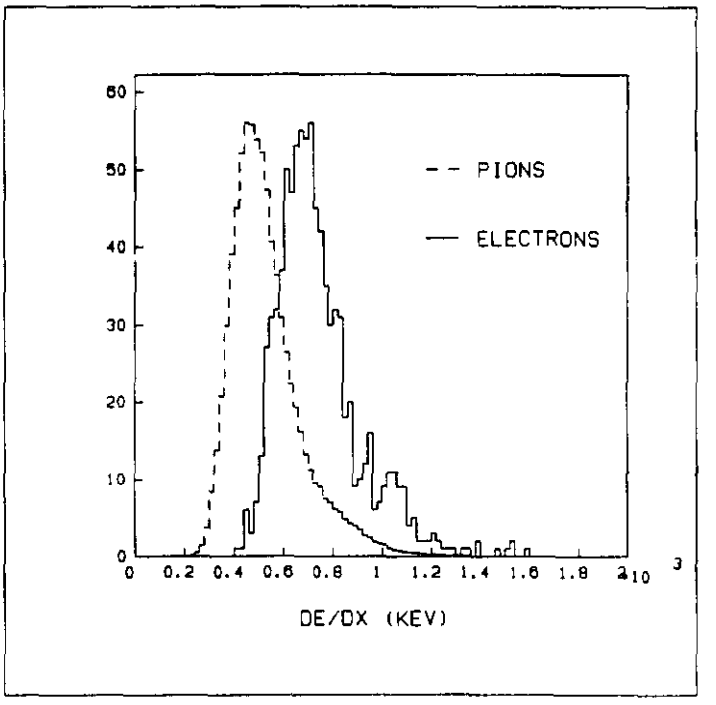

Figure 2

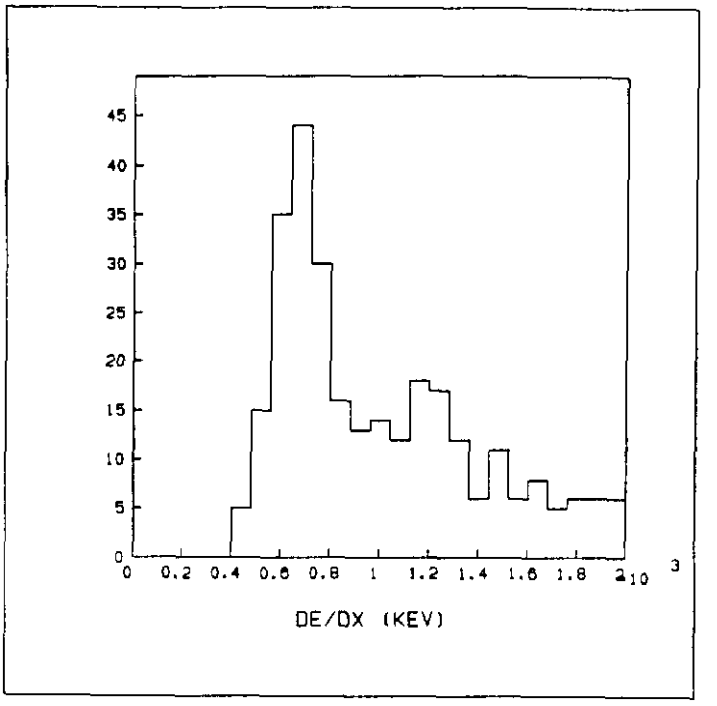

Figure 3

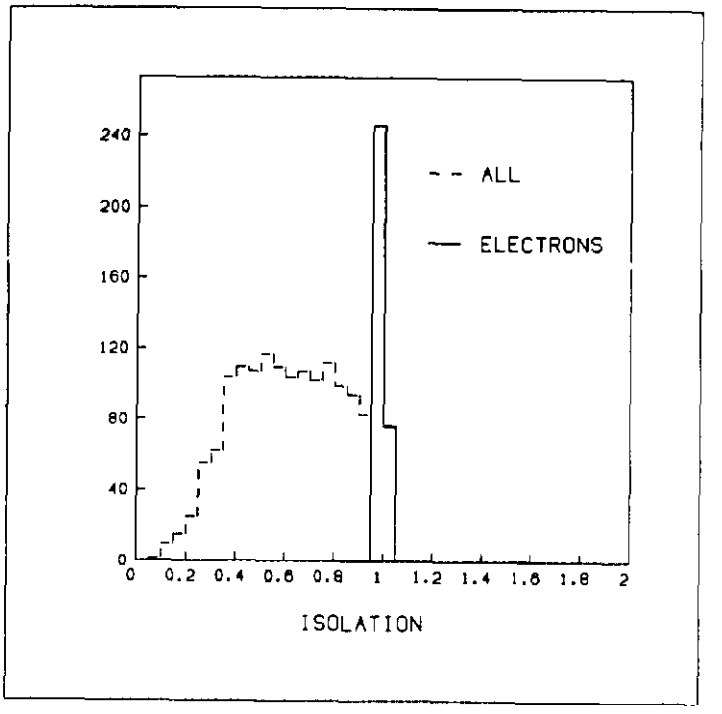

Figure 4

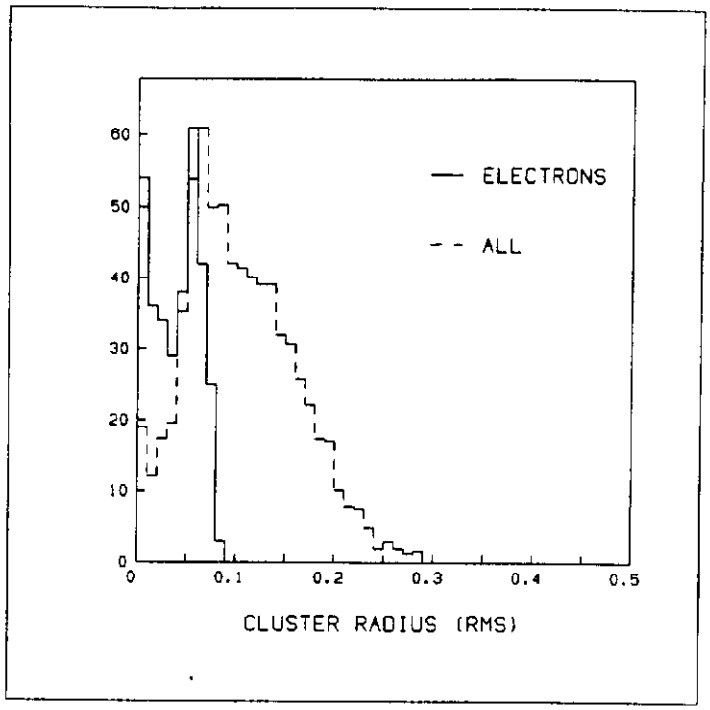

Figure 5

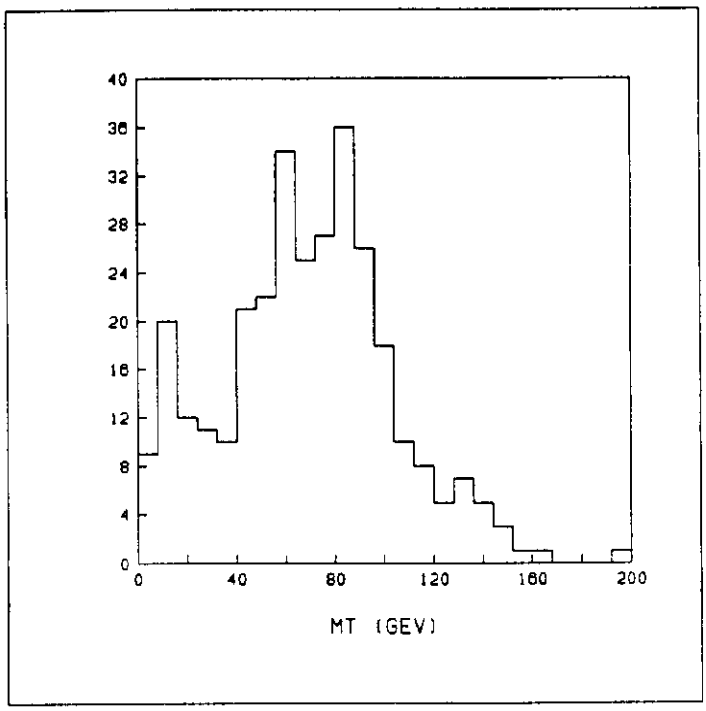

Figure 6

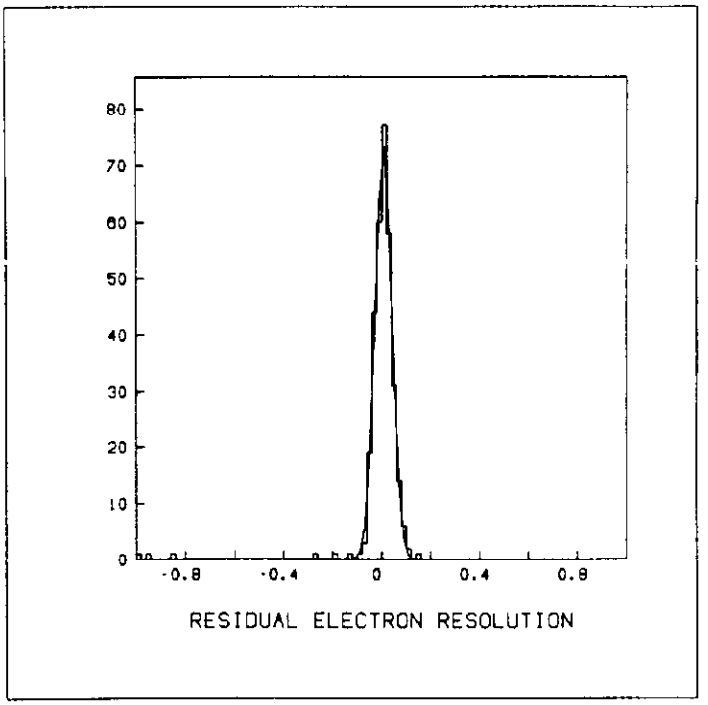

Figure 7

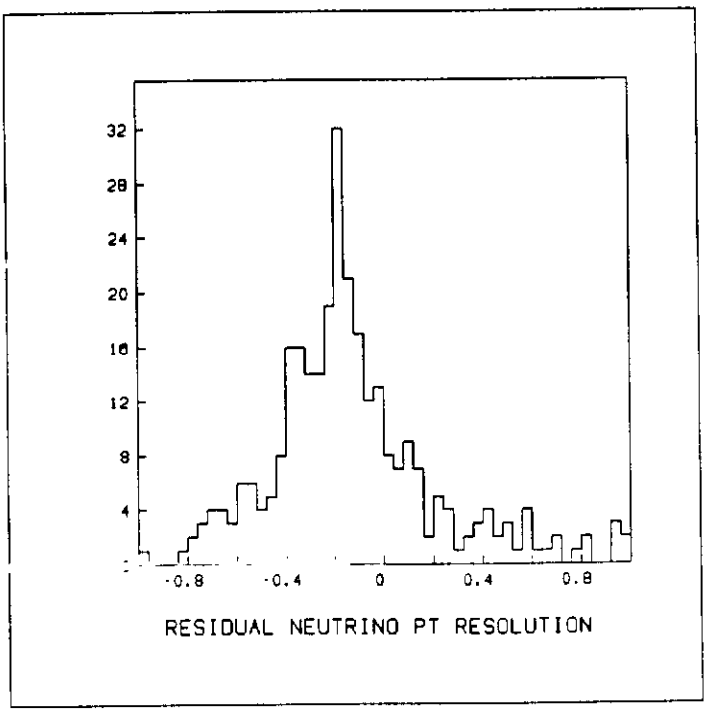

Figure 8

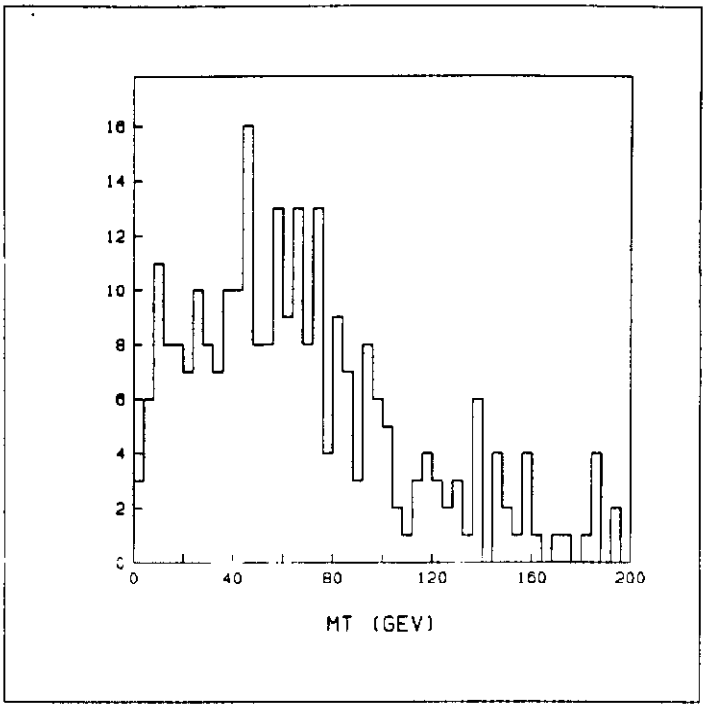

Figure 9

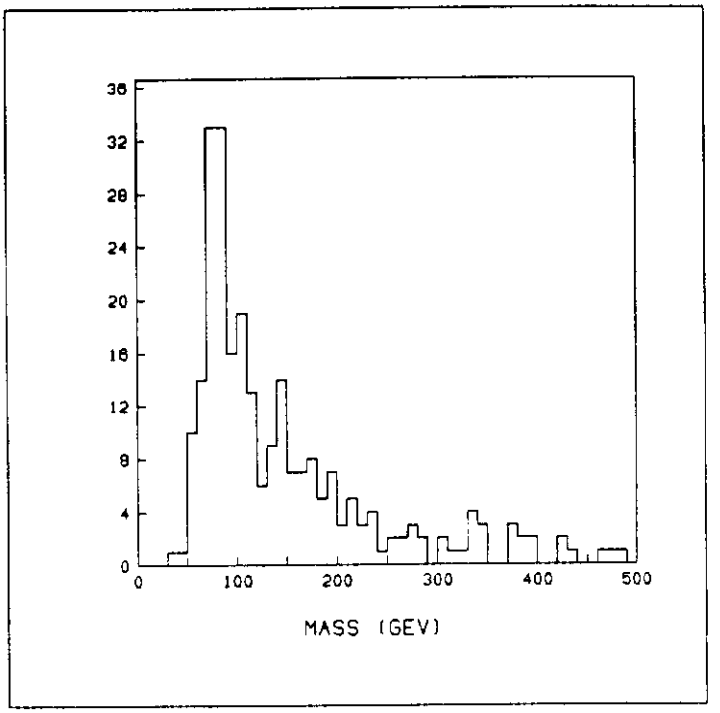

Figure 10

Figure 11

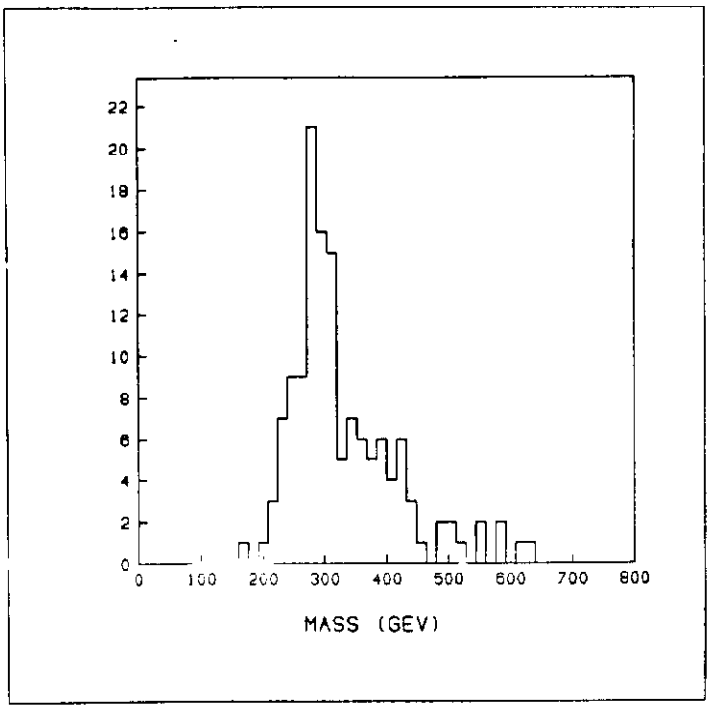

Figure 12

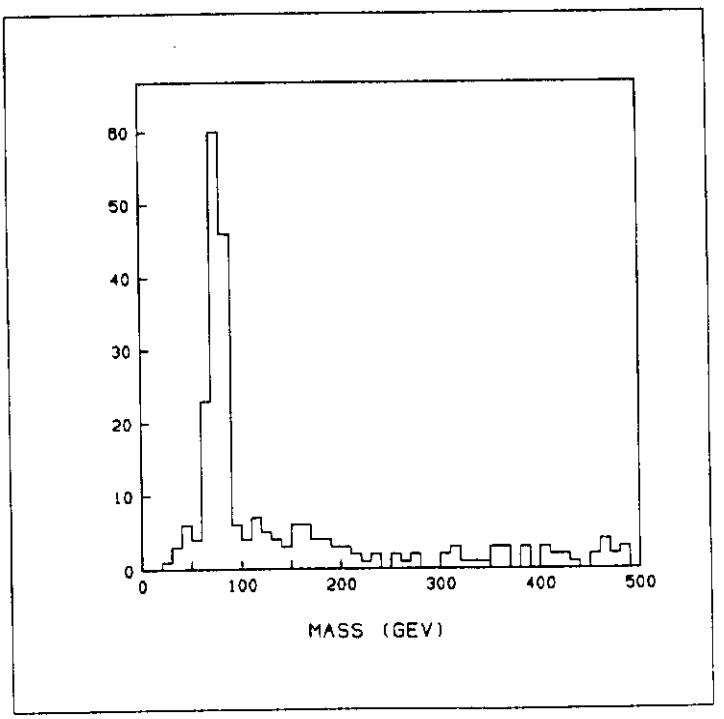

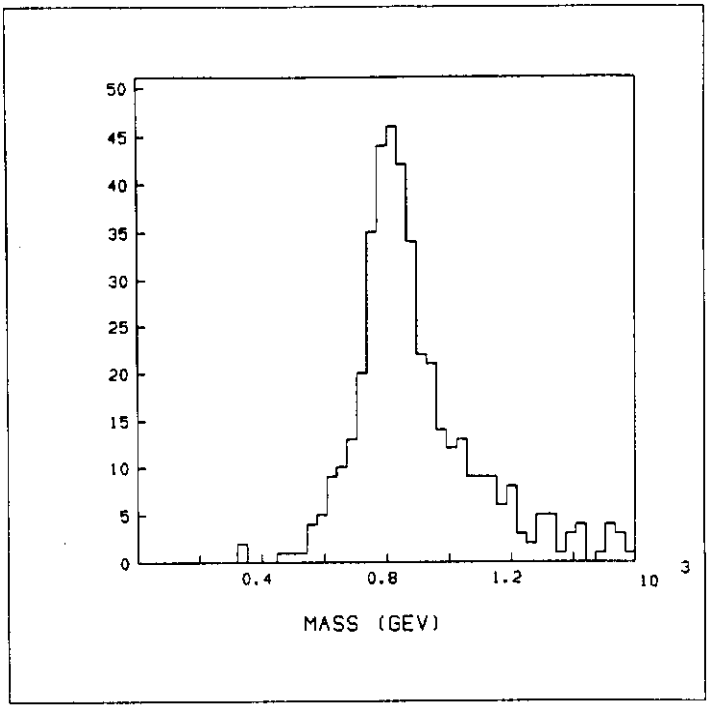

Figure 13

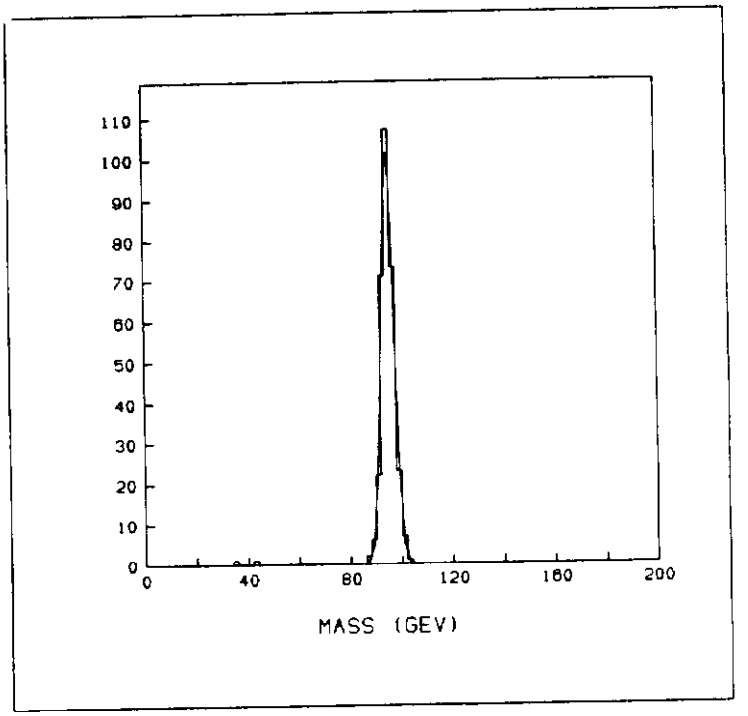

Figure 14

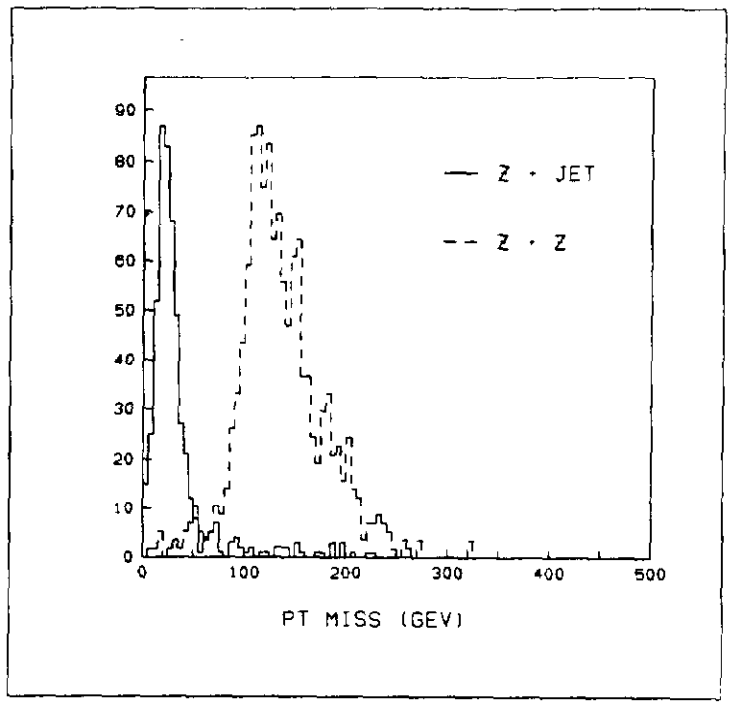

Figure 15

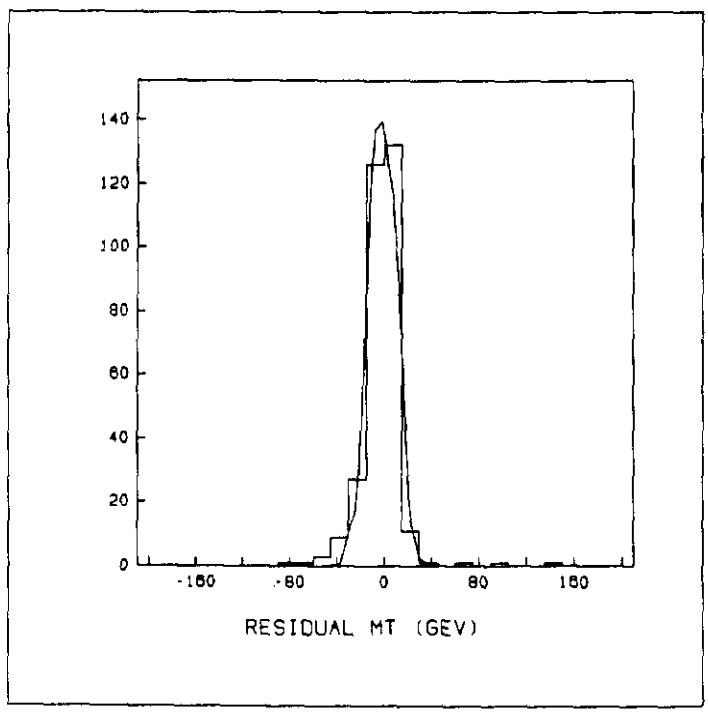

Figure 16

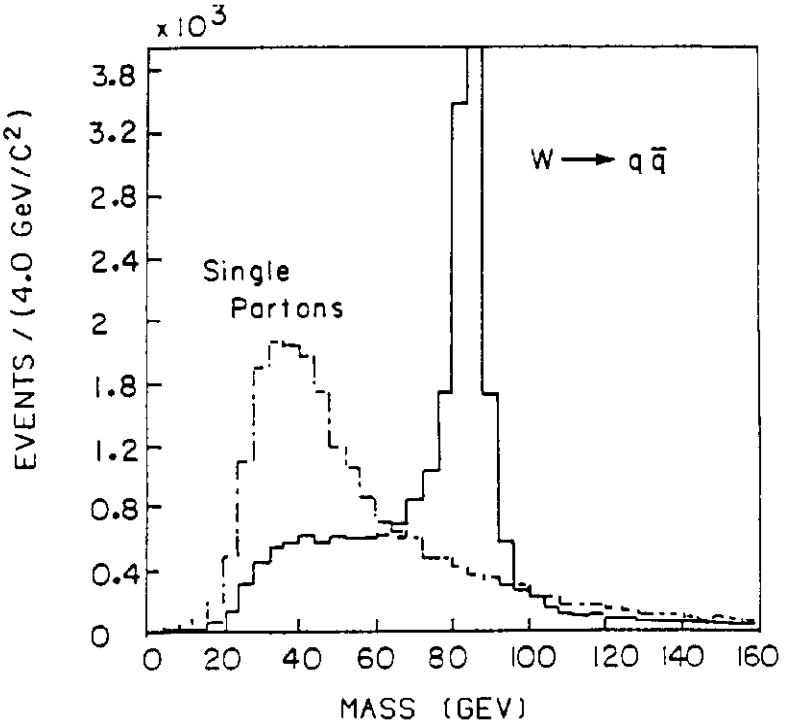

Figure 17

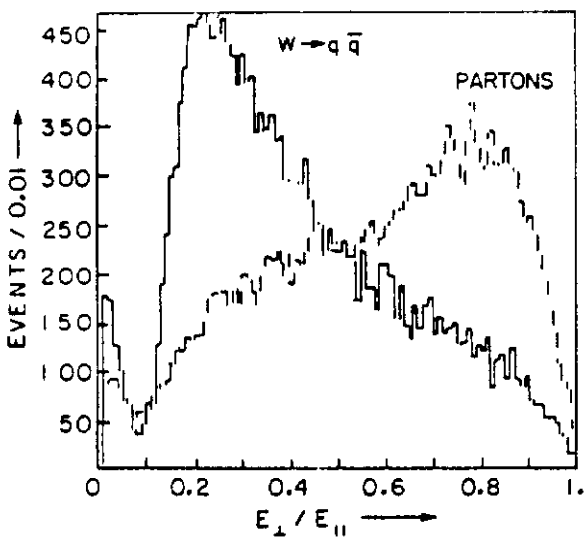

Figure 18

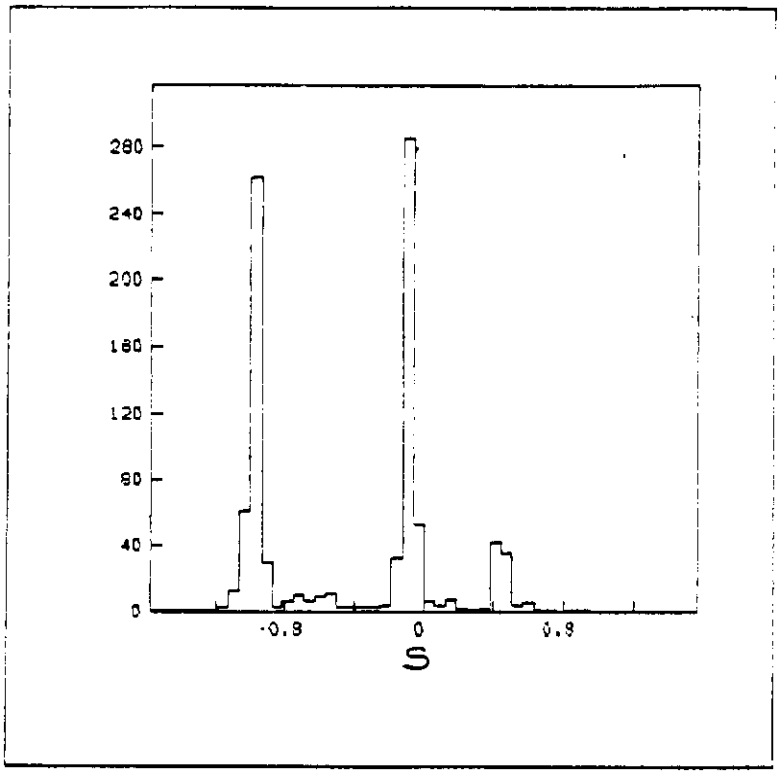

Figure 19

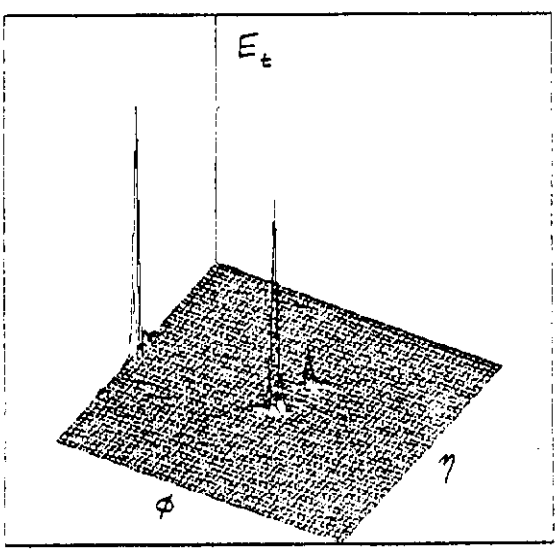

Figure 20

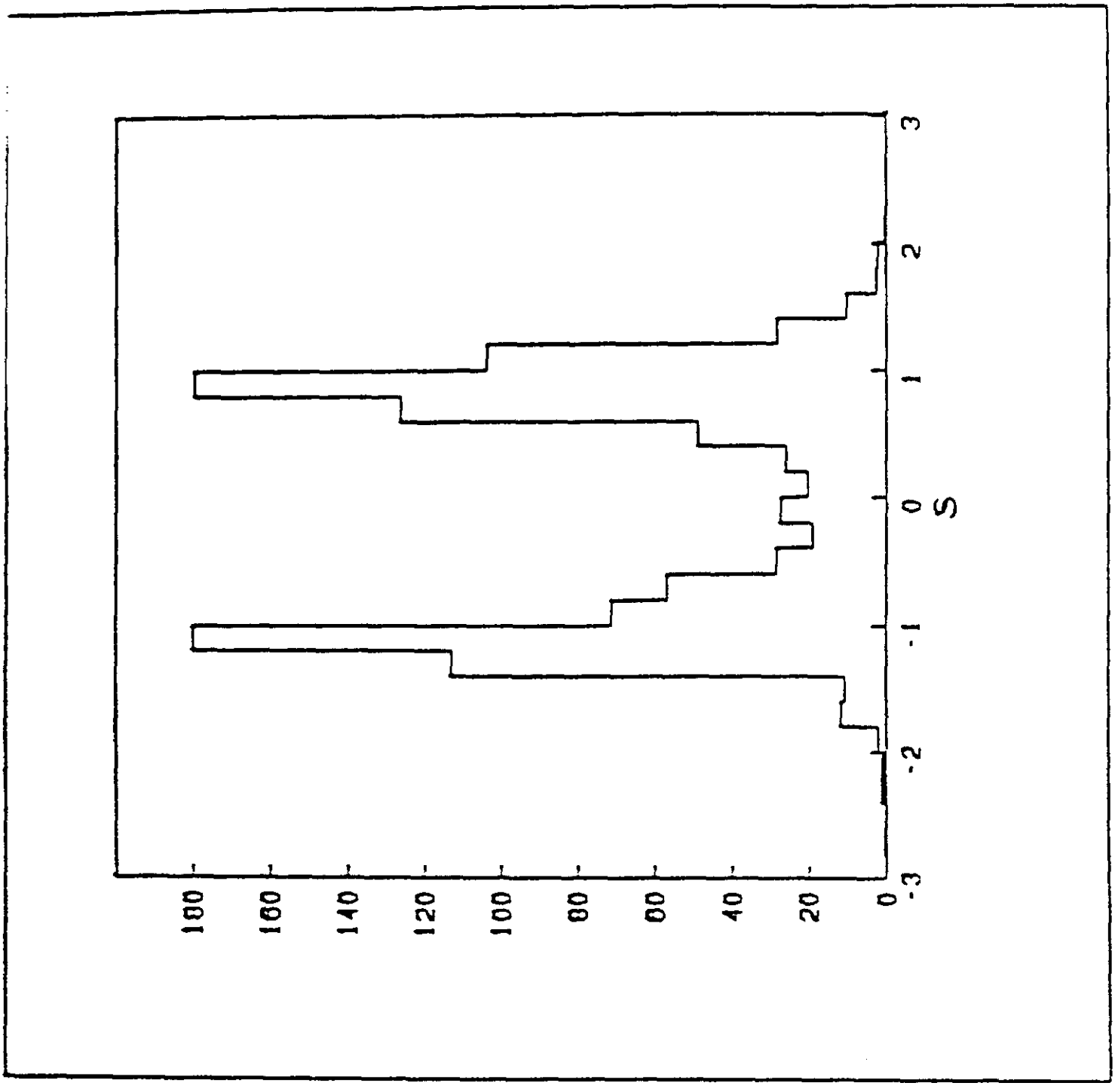

Figure 21

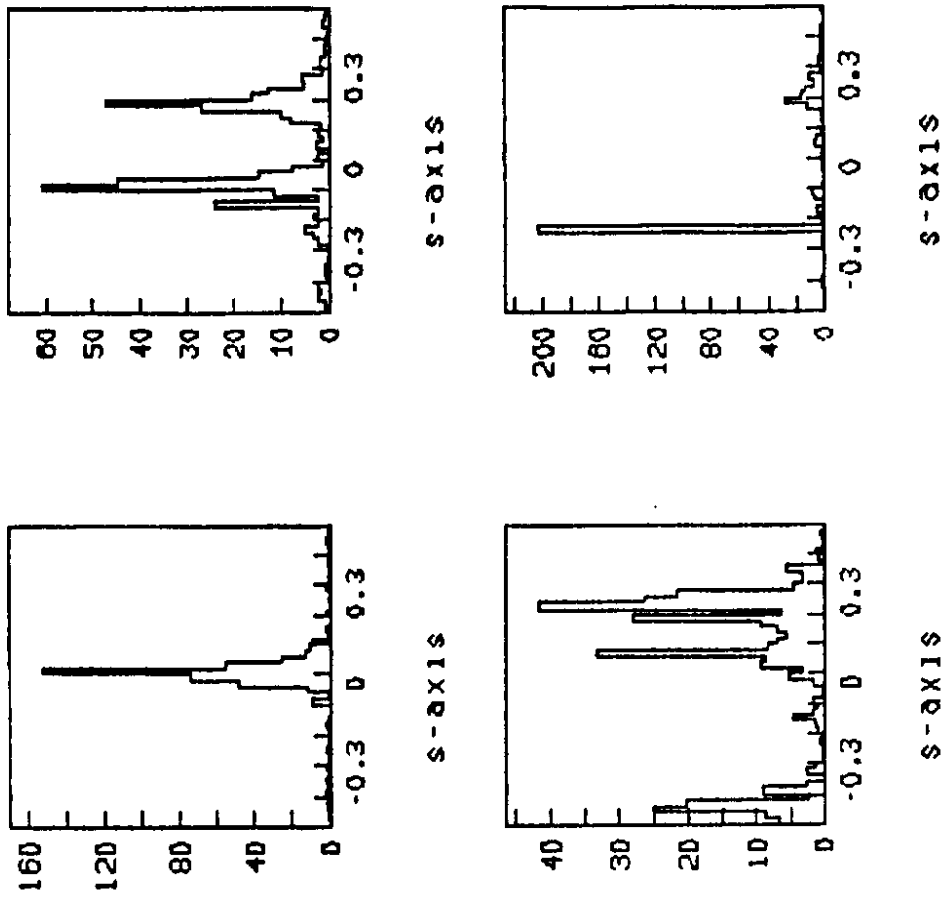
60
50
40
30
20
10
0
-0.3
0
0.3
s-axis
200
160
120
80
40
0
-0.3
0
0.3
s-axis
160
120
80
40
0
-0.3
0
0.3
s-axis
40
30
20
10
0
-0.3
0
0.3
s-axis

Figure 22

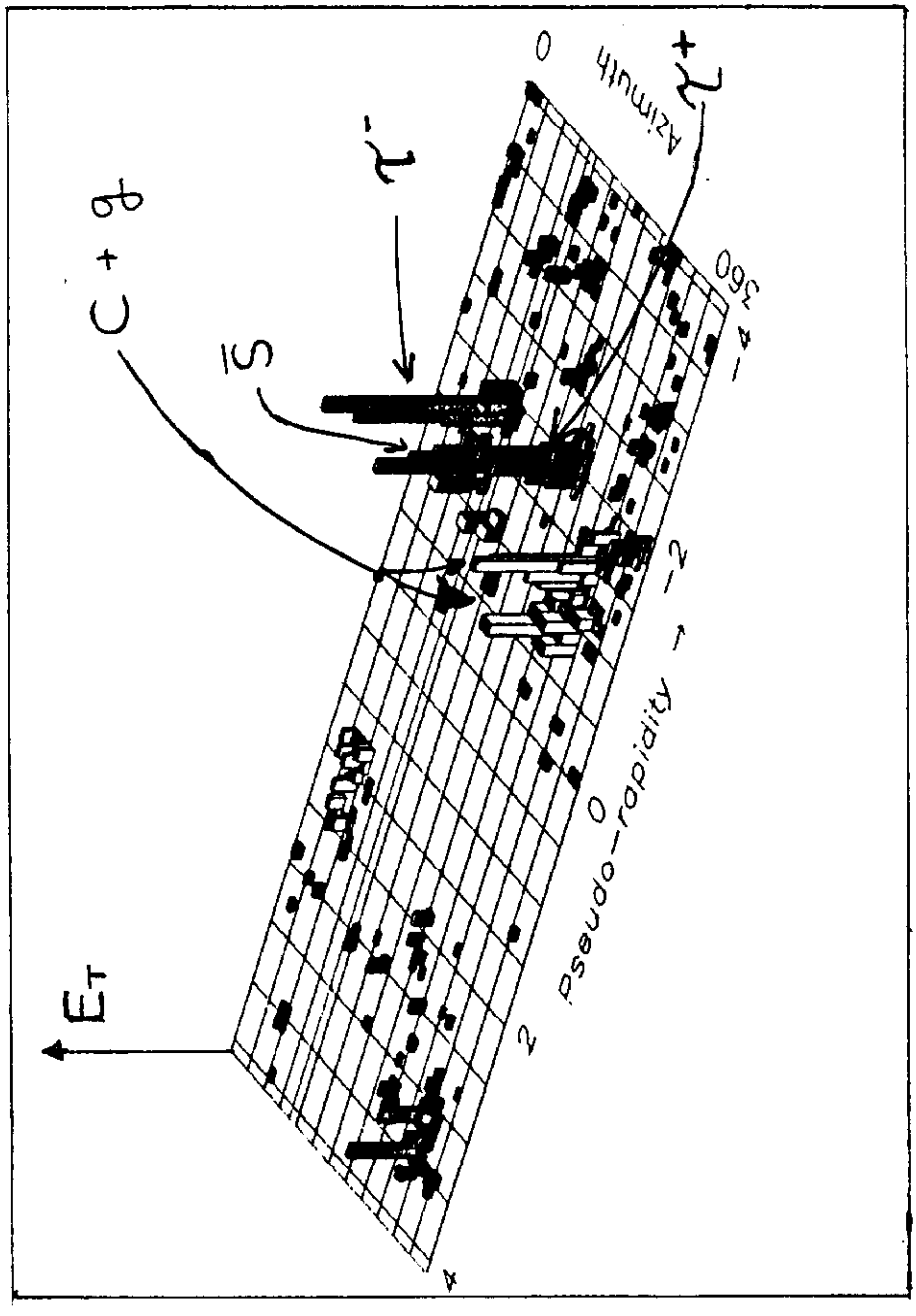

Figure 23

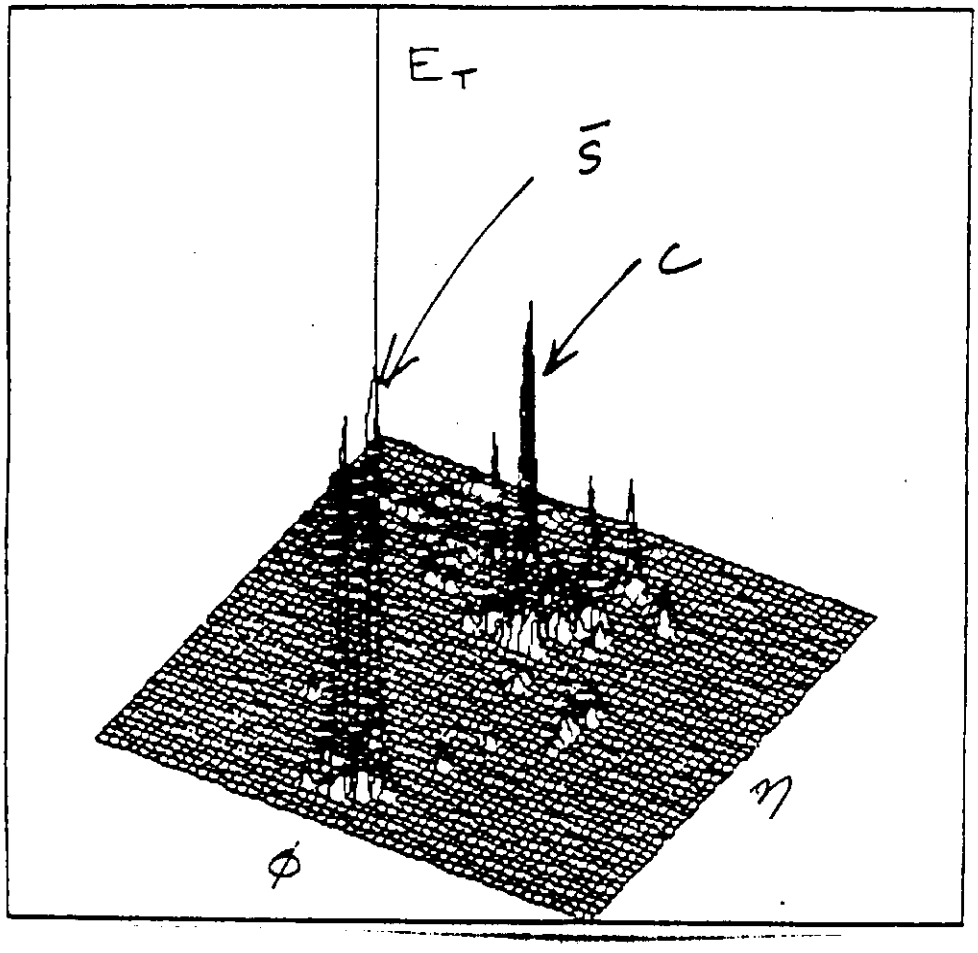

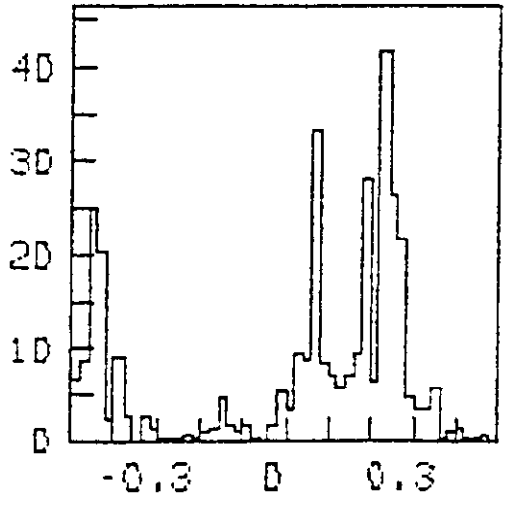

Figure 24

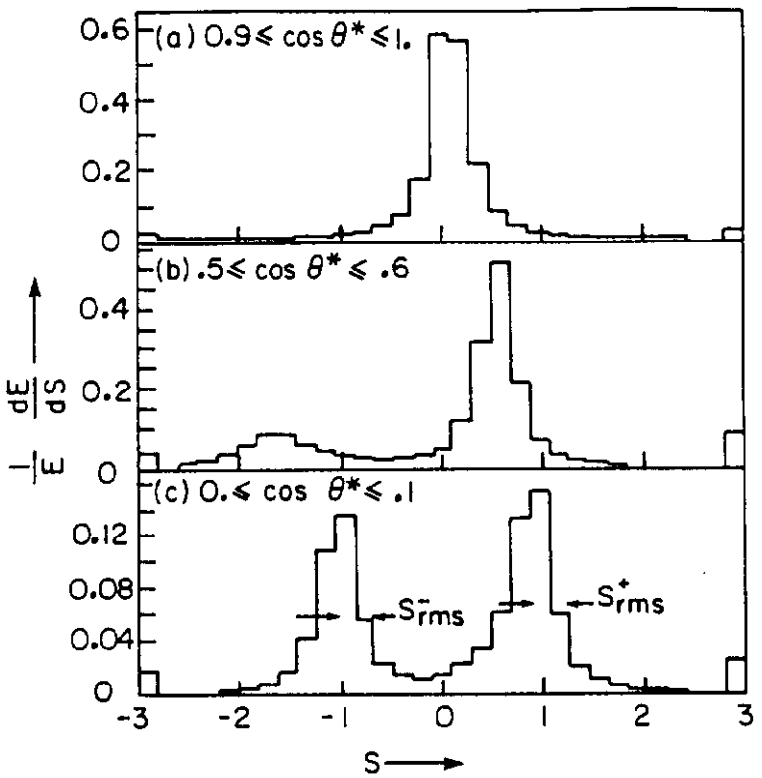

Figure 25

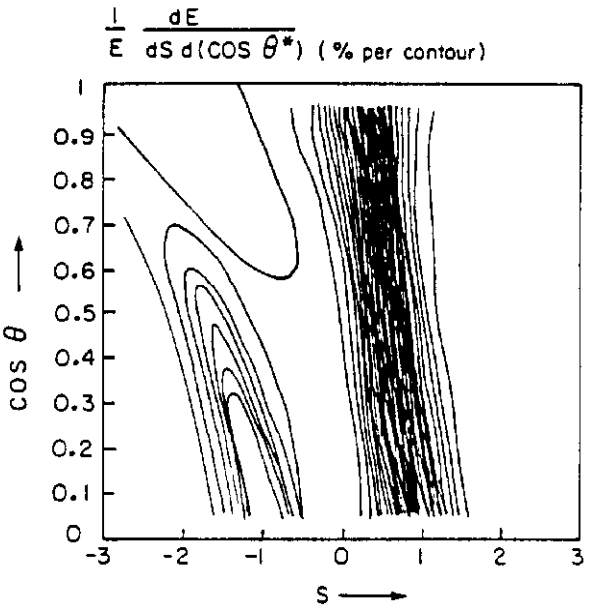

Figure 26

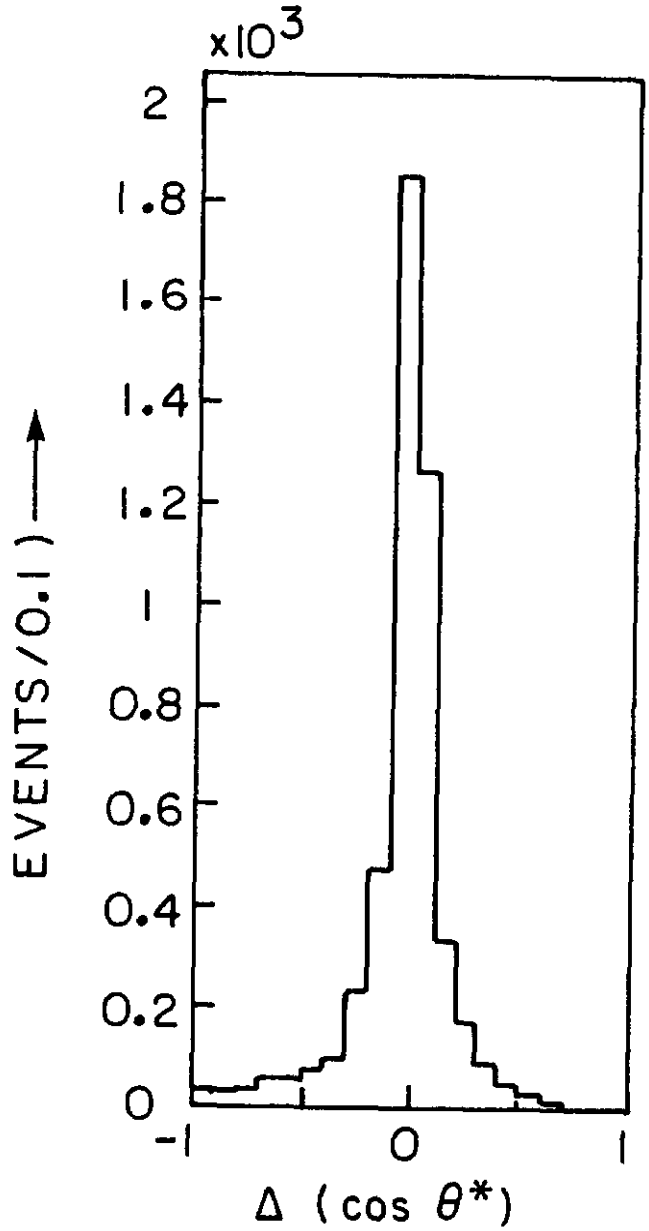

Figure 27

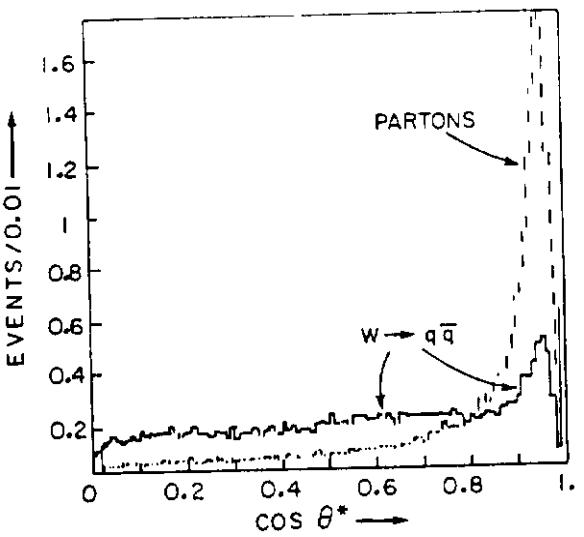

Figure 28

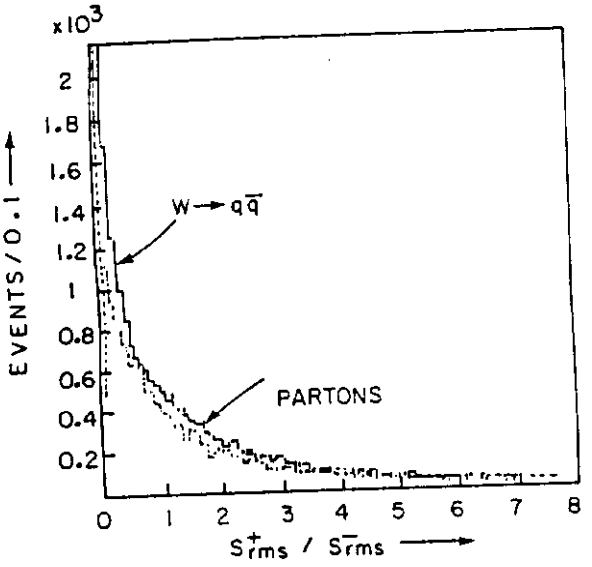

Figure 29

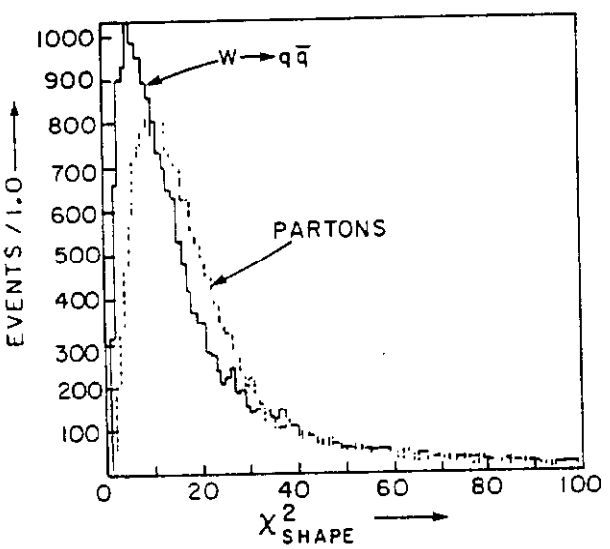

Figure 30

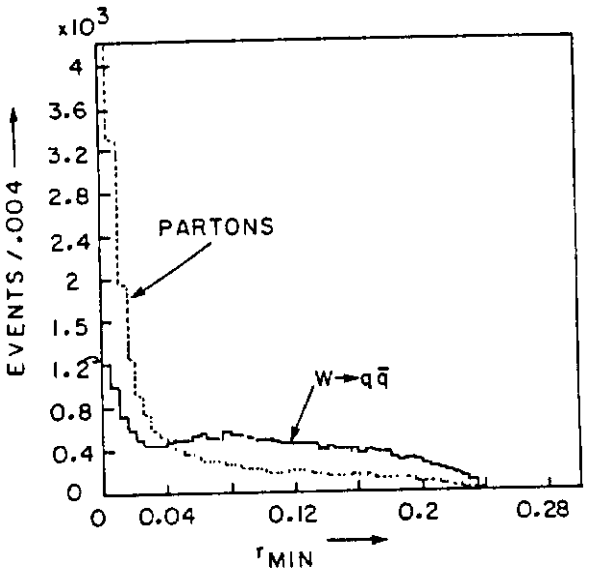

Figure 31

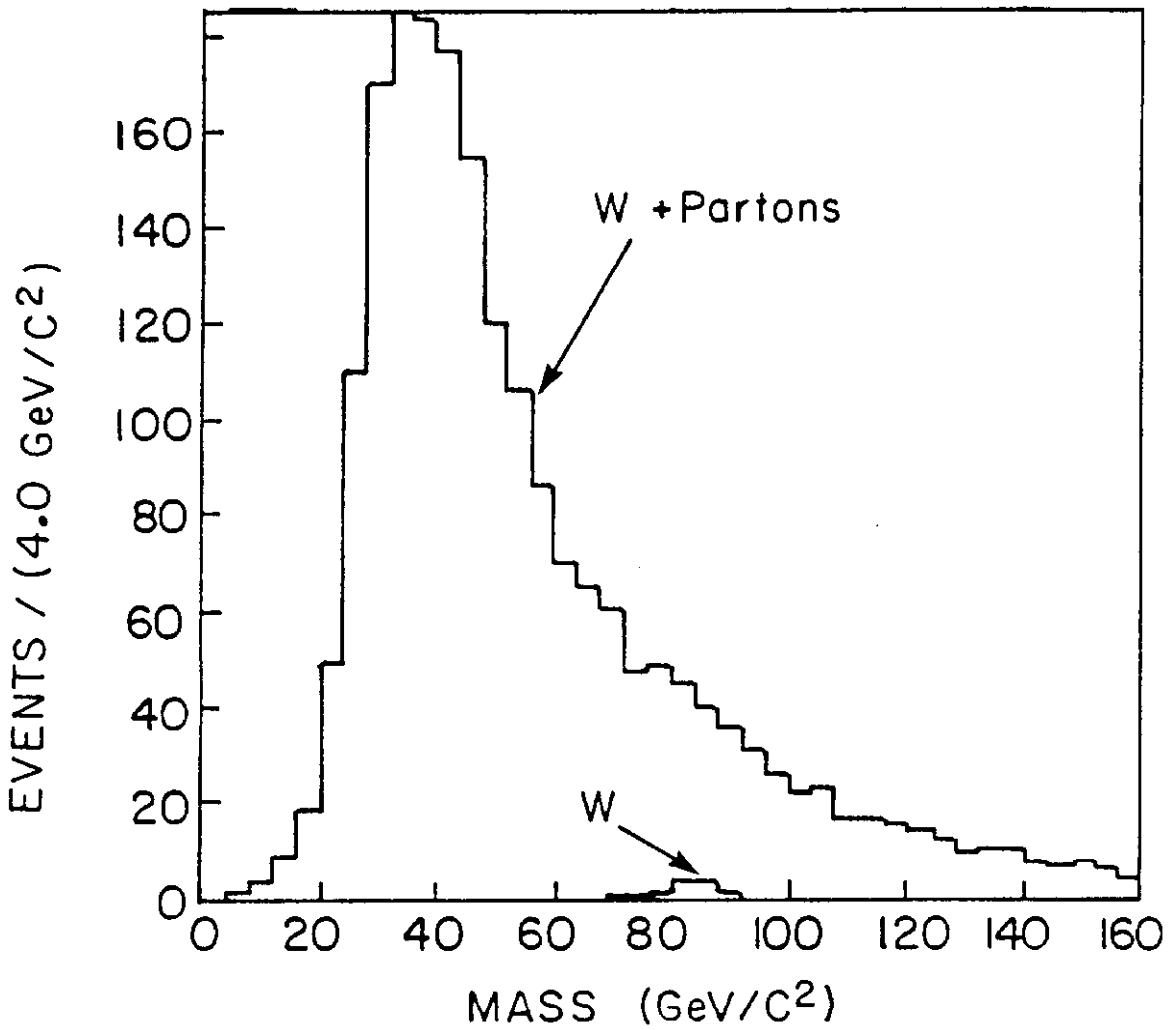
EVENTS / (4.0 GeV/C²)
0
20
40
60
80
100
120
140
160
W + Partons
W
0
20
40
60
80
100
120
140
160
MASS (GeV/C²)

Figure 32

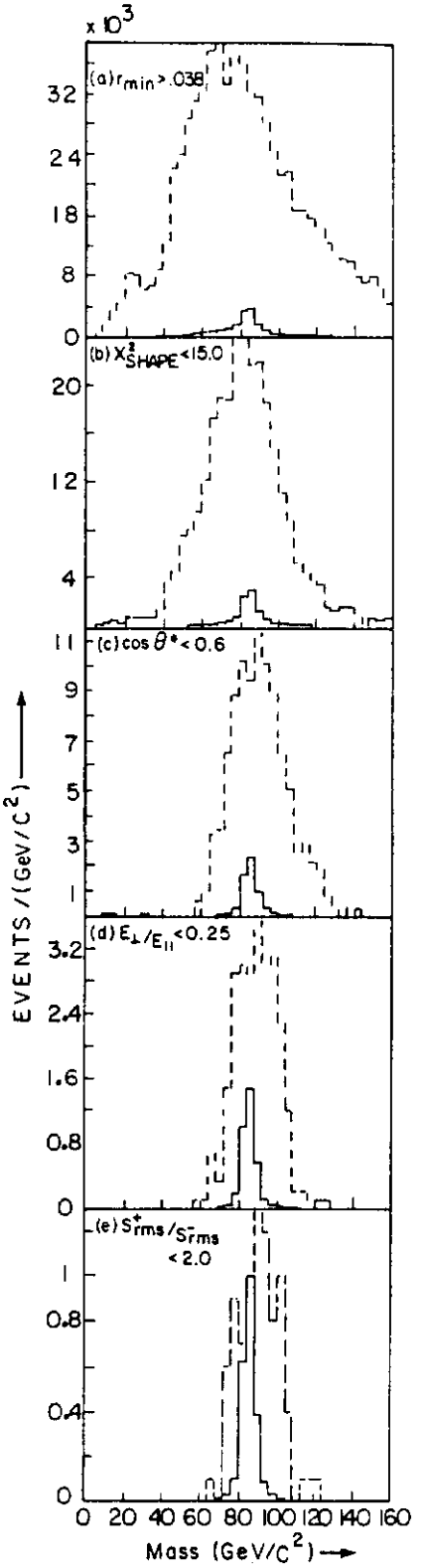
x 10^3
(a) r_min > .038
(b) X²_SHAPE < 15.0
(c) cos θ* < 0.6
(d) E⊥/E∥ < 0.25
(e) S⁺rms/S⁻rms < 2.0
EVENTS / (GeV/C²)
Mass (GeV/C²)
0 20 40 60 80 100 120 140 160

Figure 33

Figure 34

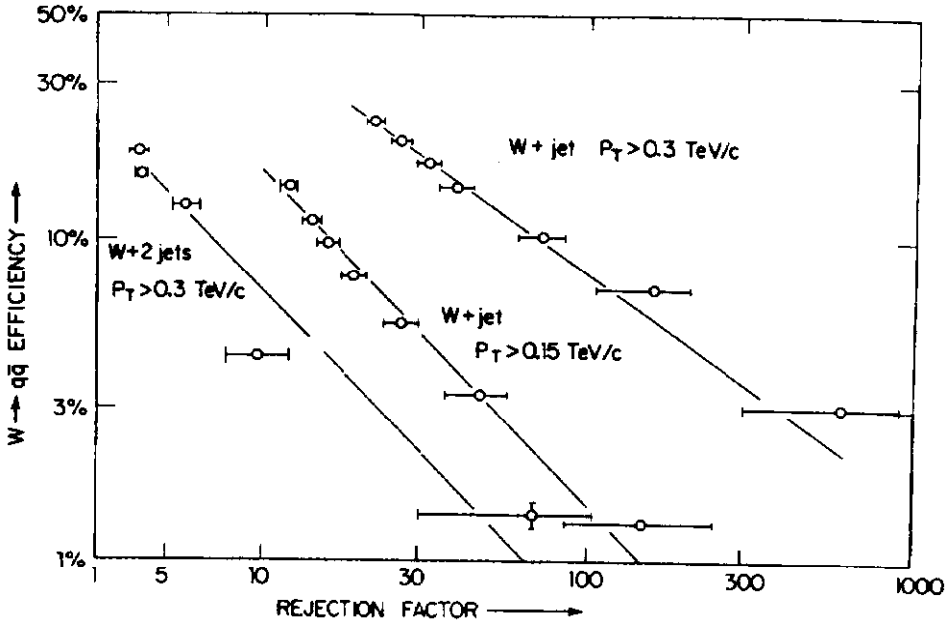

Figure 35 (a)

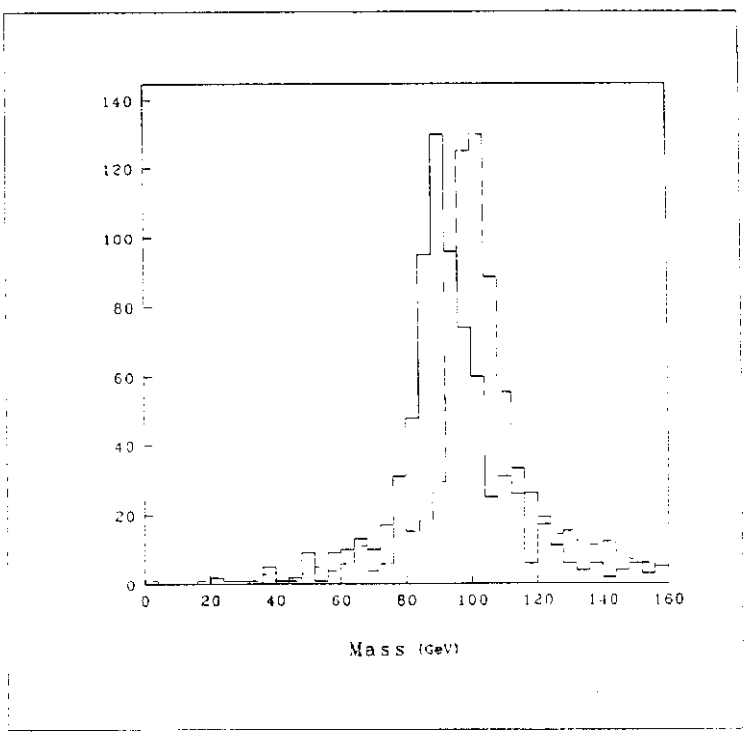

Figure 35 (b)

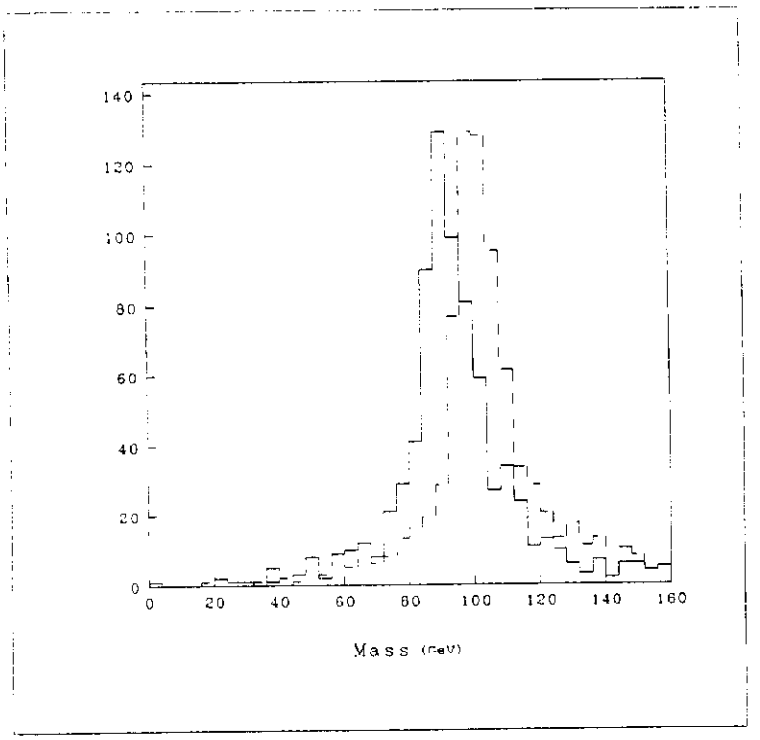

Figure 35 (c)

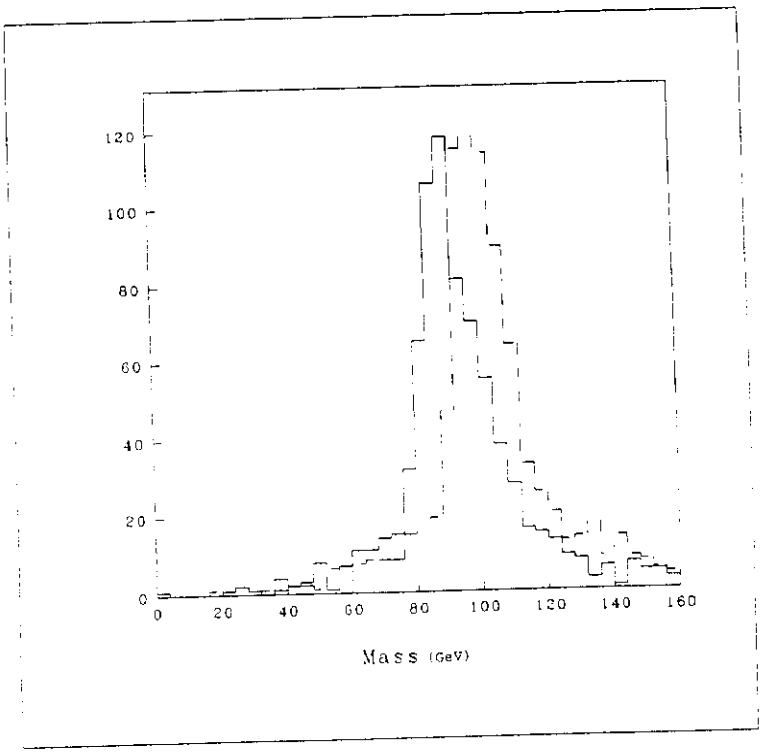

Figure 36

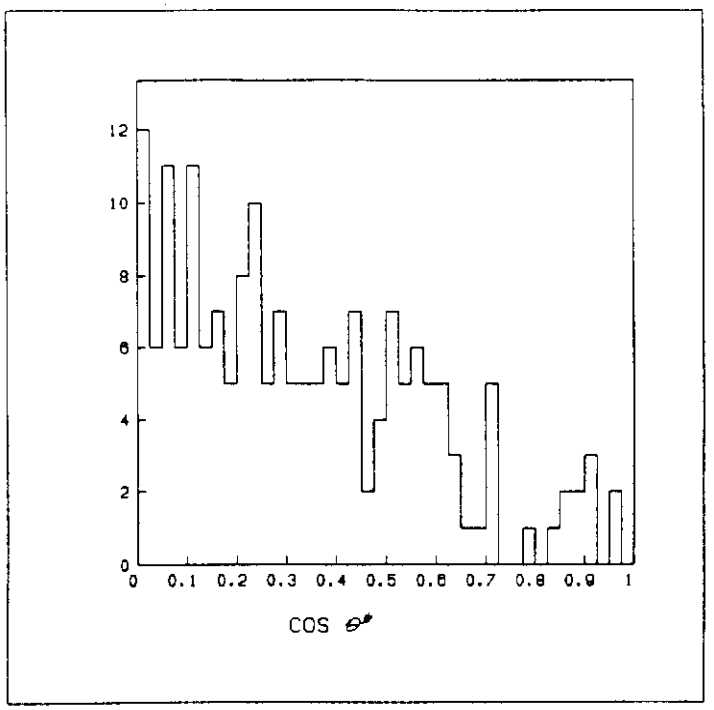

Figure 37

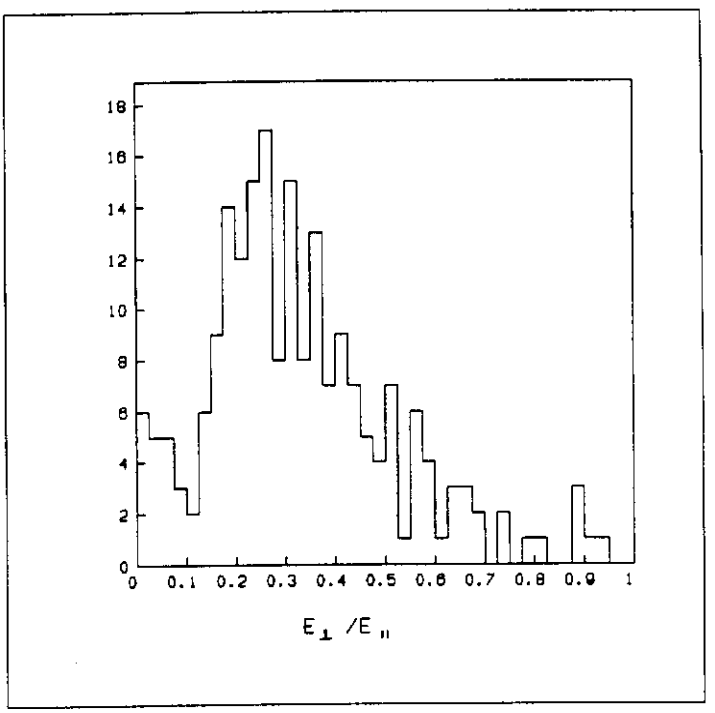

Figure 38 (a)

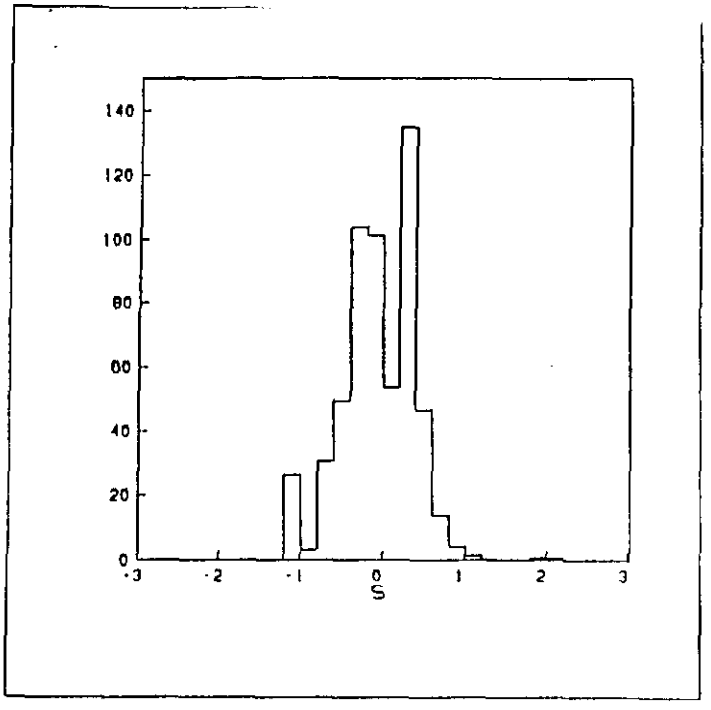

Figure 38 (b)

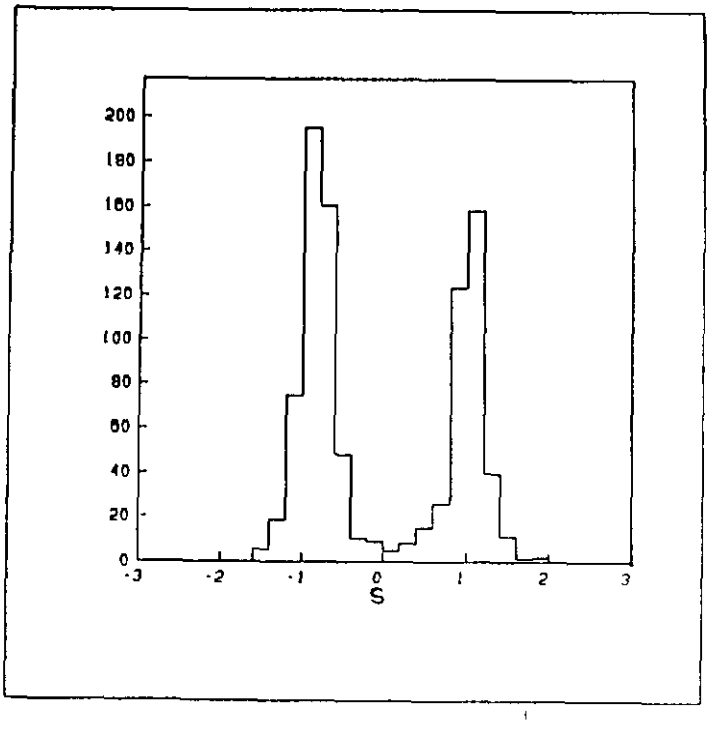

Figure 38 (c)

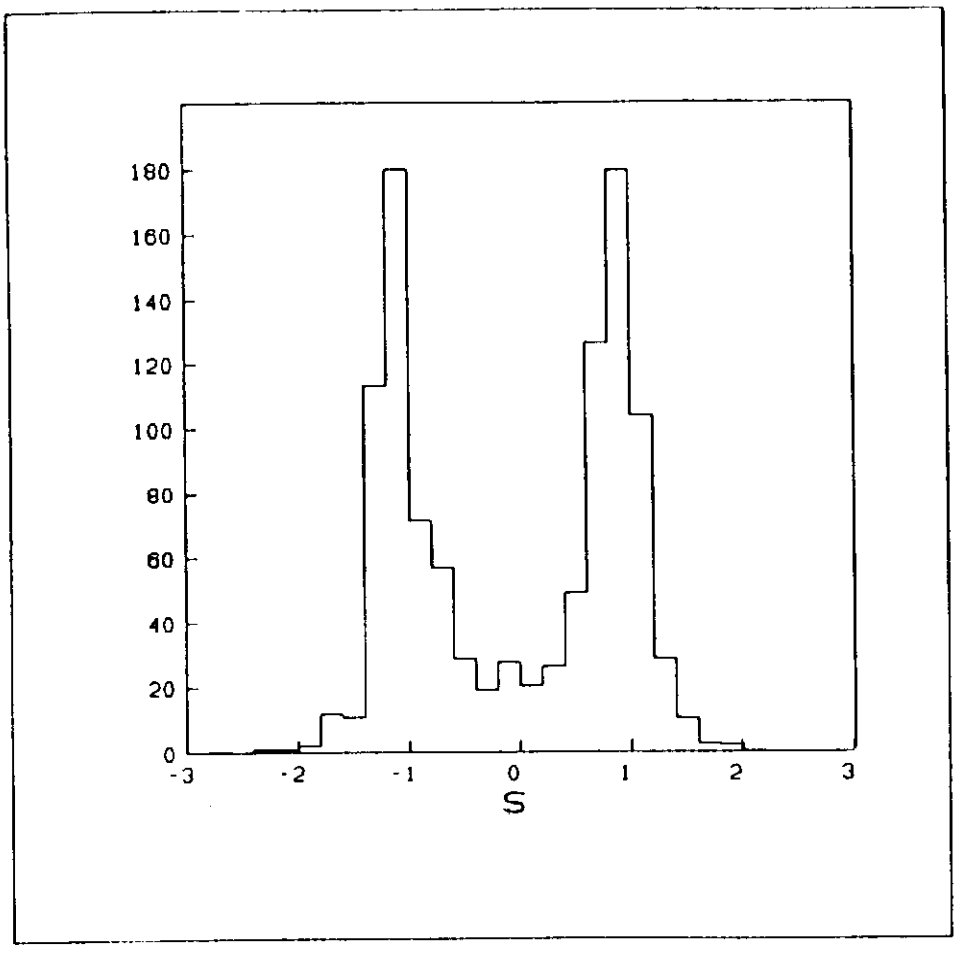

Figure 39 (a)

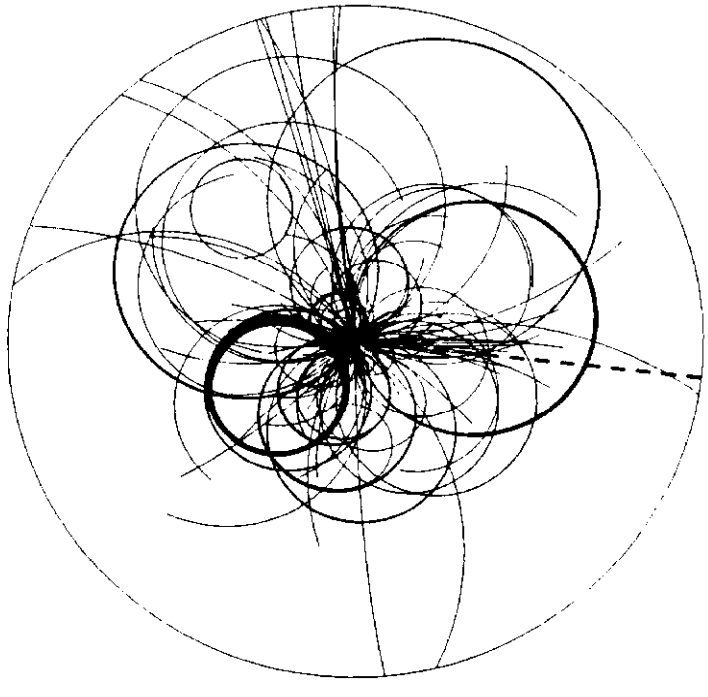

Figure 39 (b)

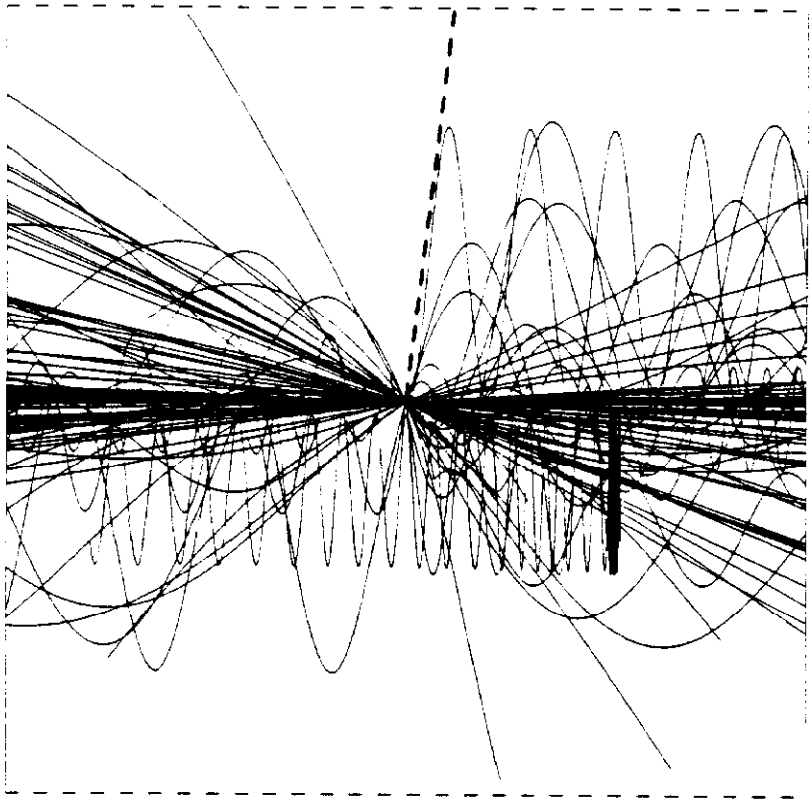

Figure 39 (c)

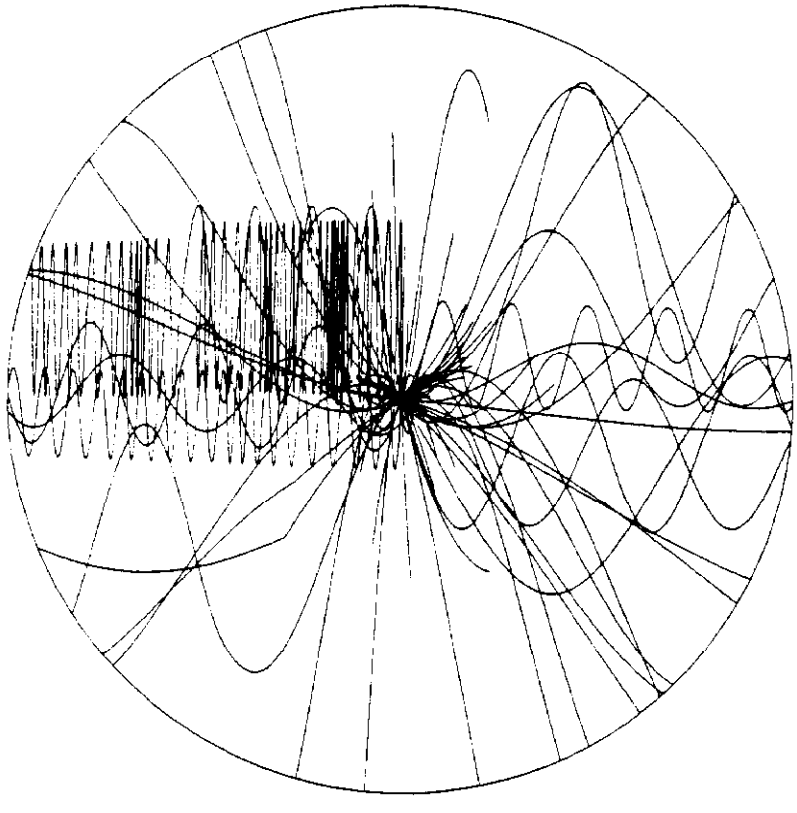

Figure 39 (d)

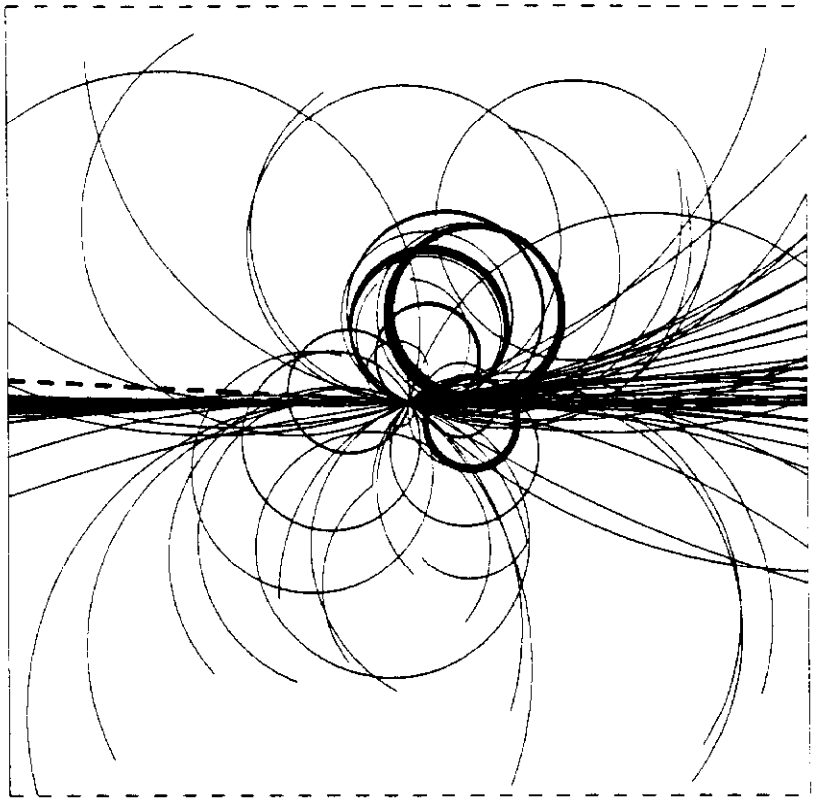

Figure 39 (e)

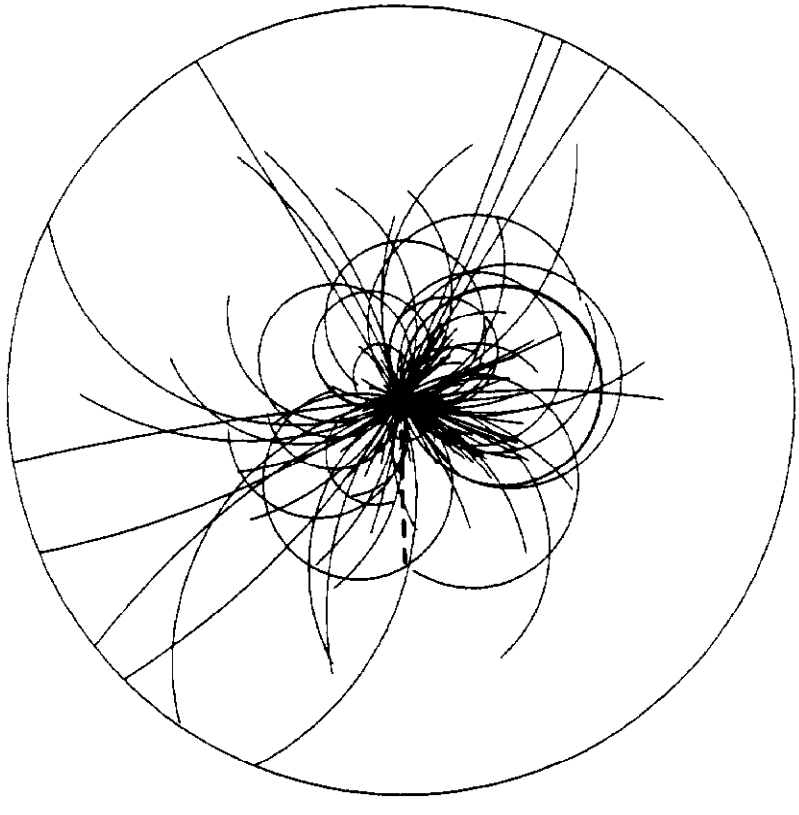

Figure 39 (f)

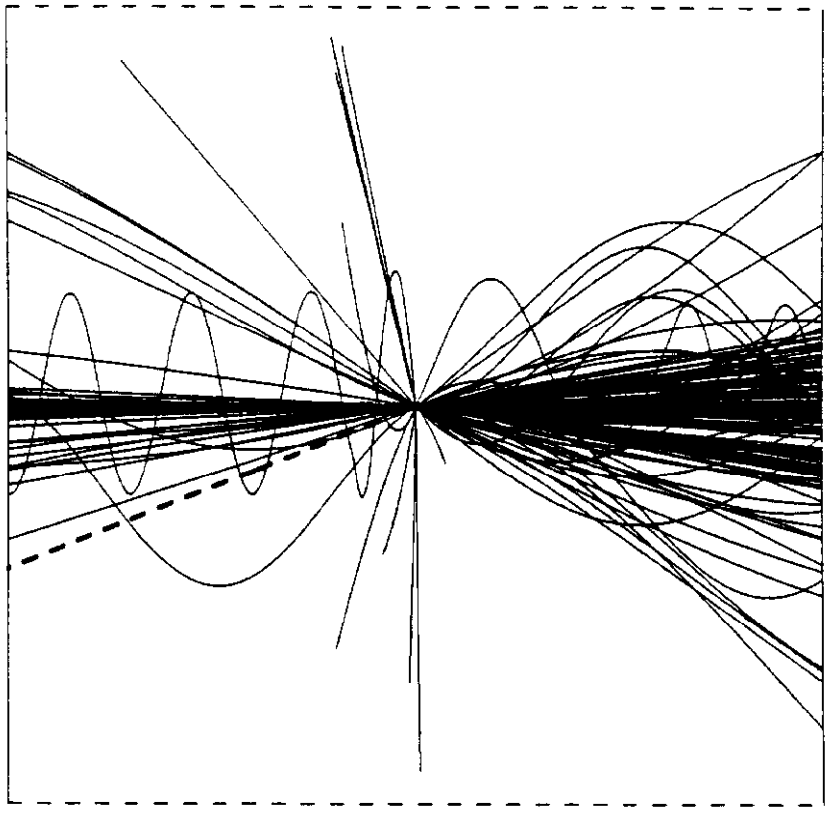

Figure 40 (a)

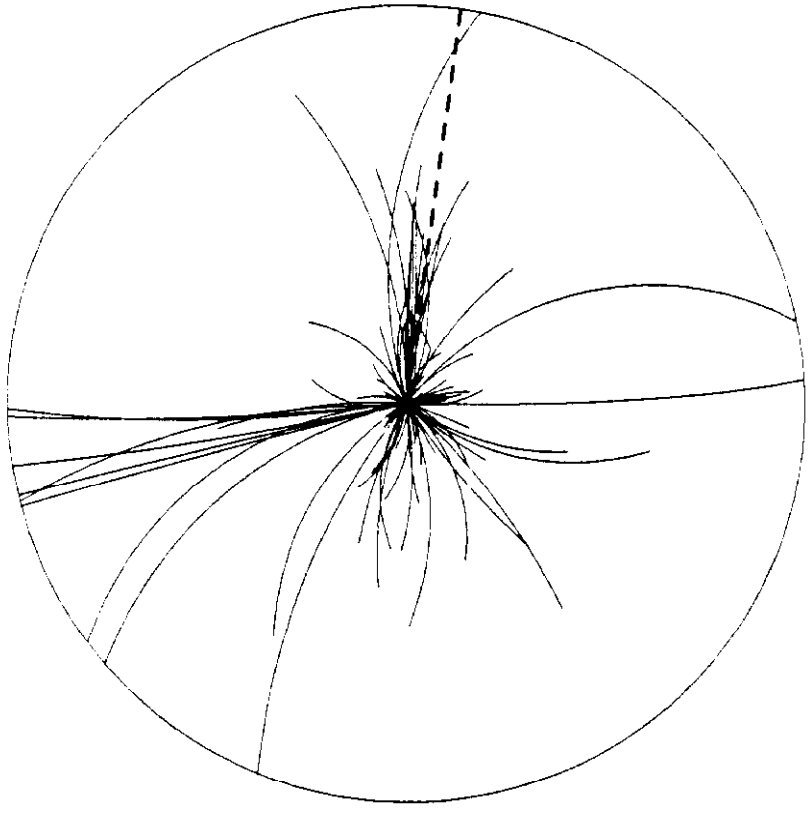

Figure 40 (b)

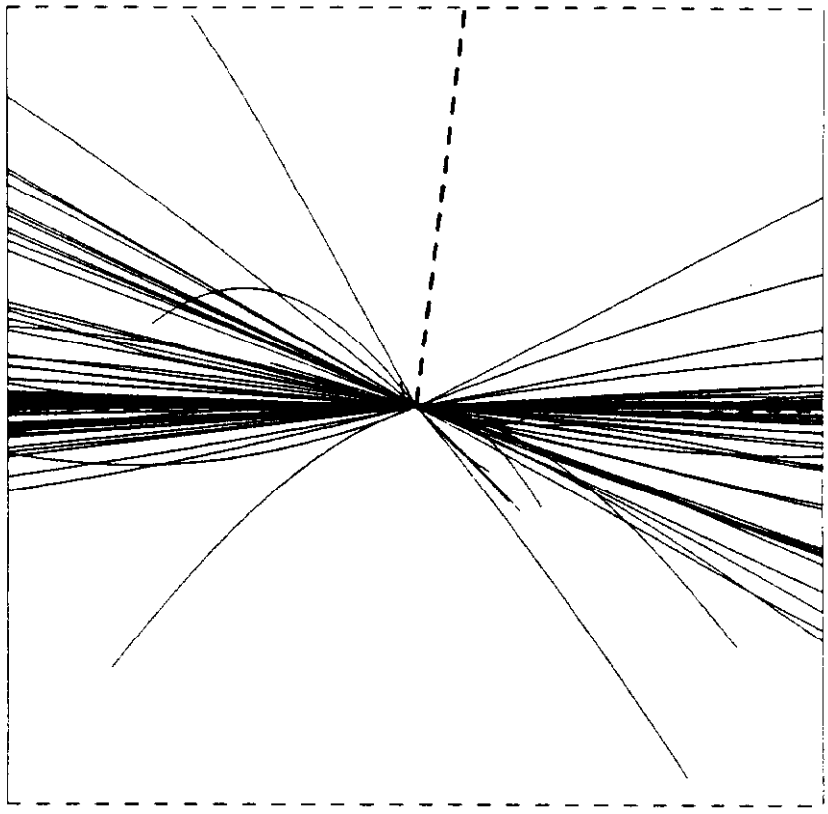

Figure 40 (c)

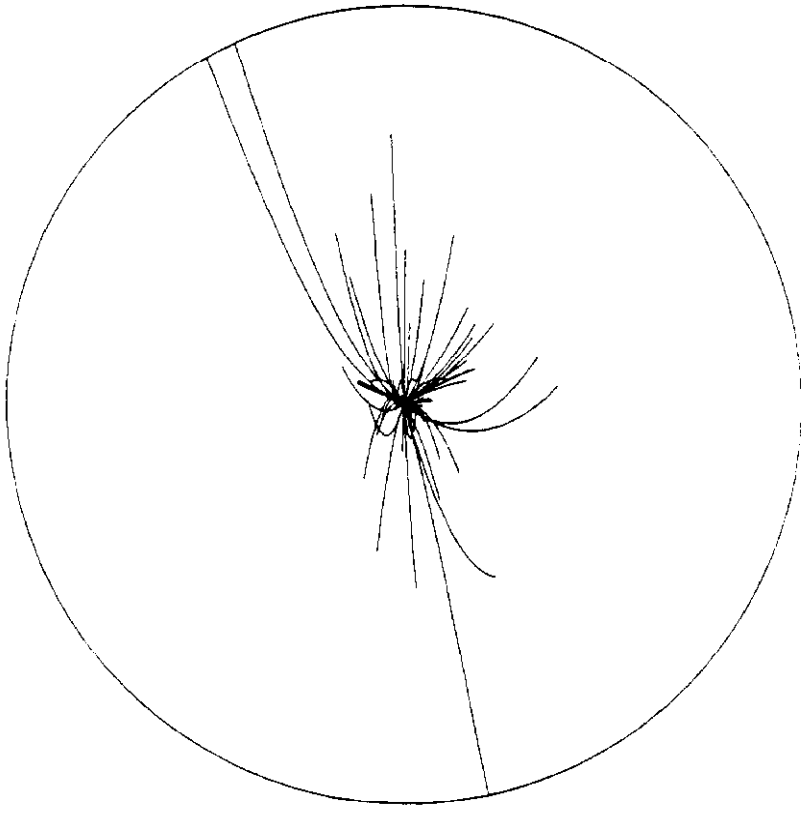

Figure 40 (d)

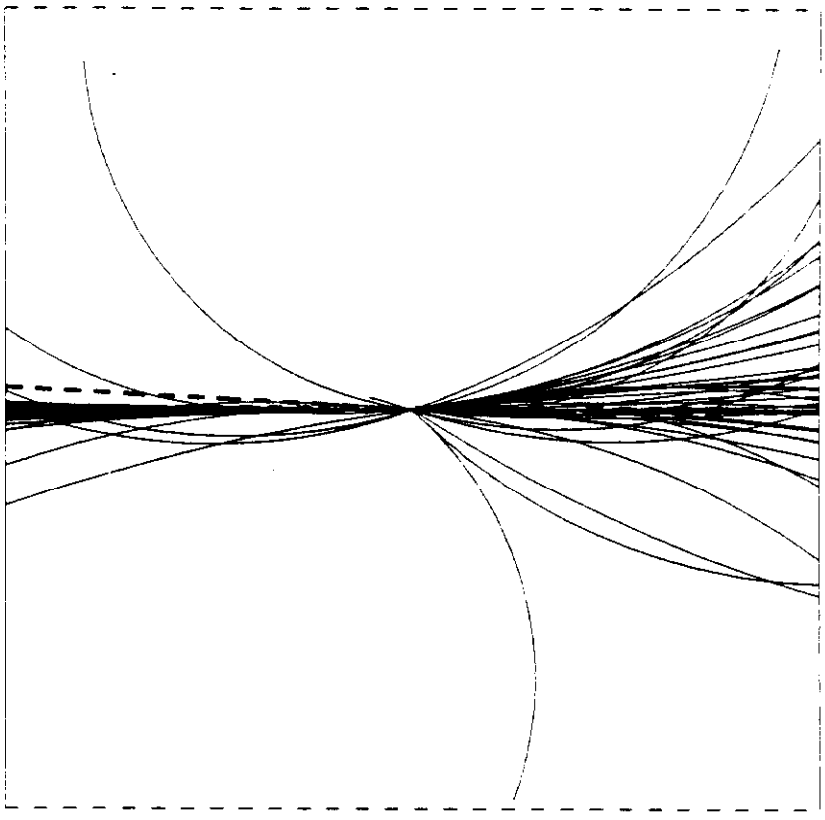

Figure 40 (e)

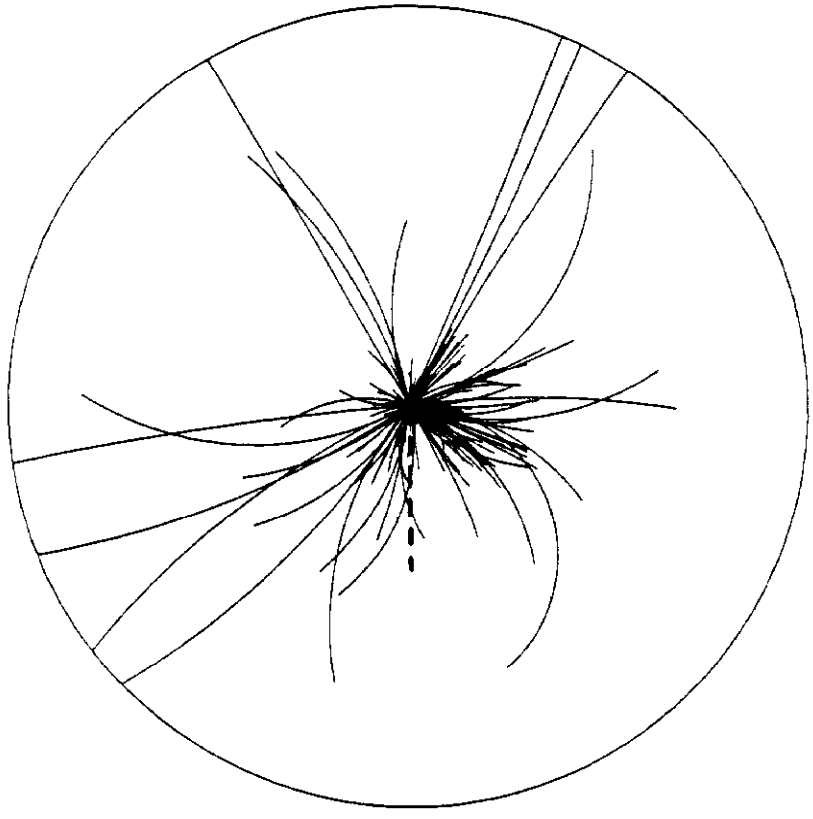

Figure 40 (f)

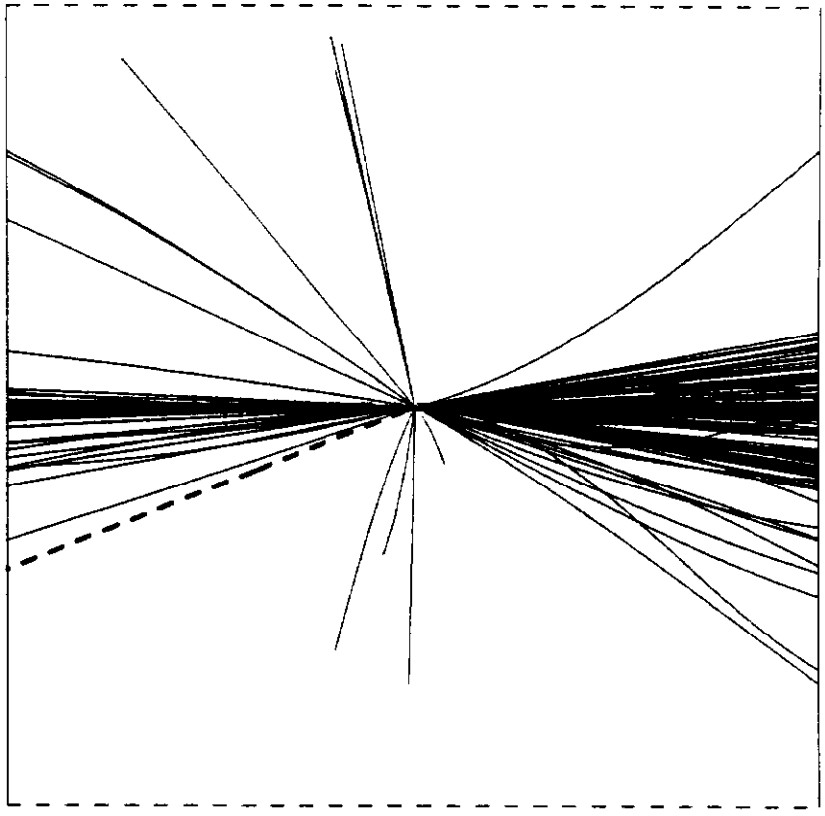

Figure 41 (a)

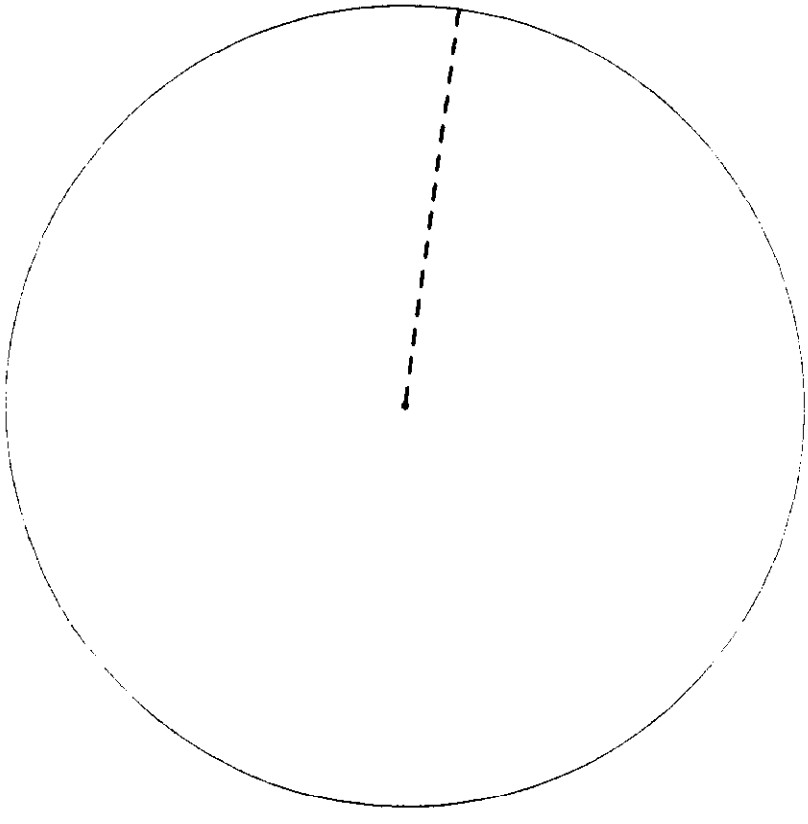

Figure 41 (b)

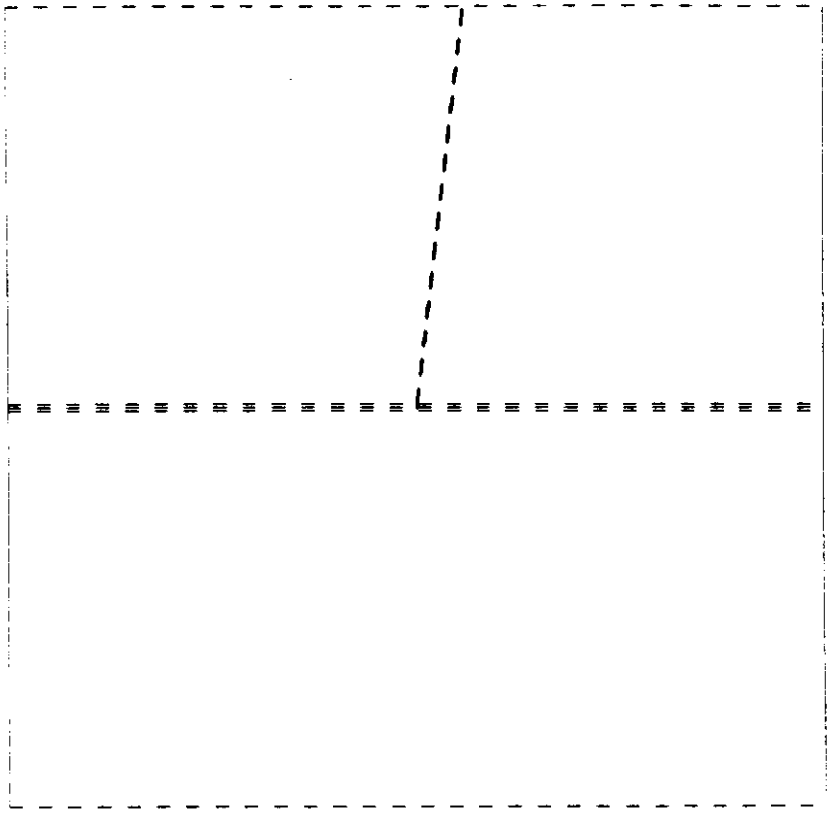

Figure 41 (c)

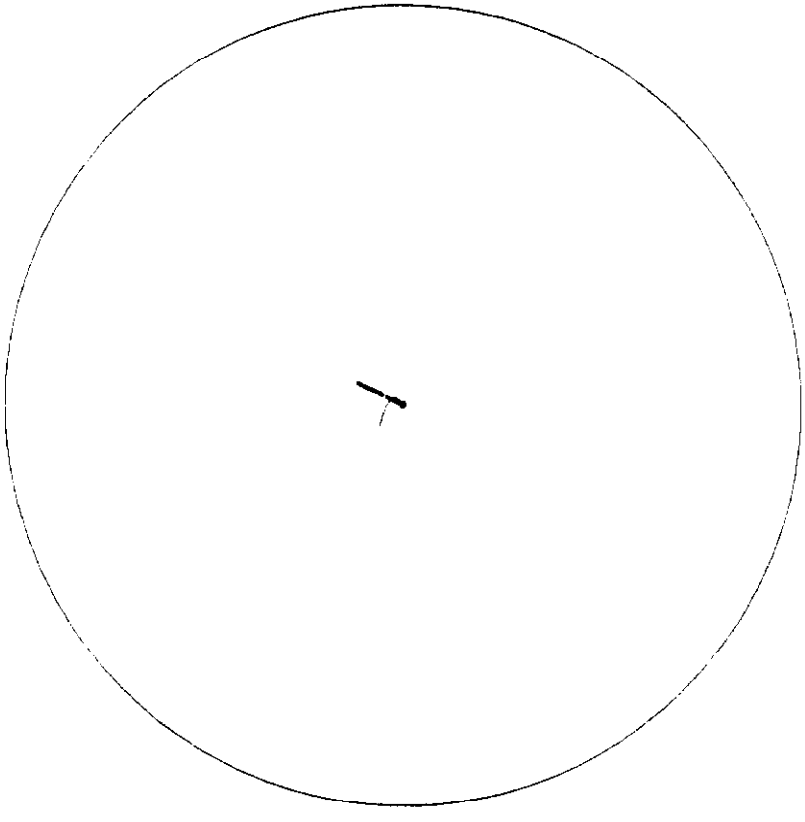

Figure 41 (d)

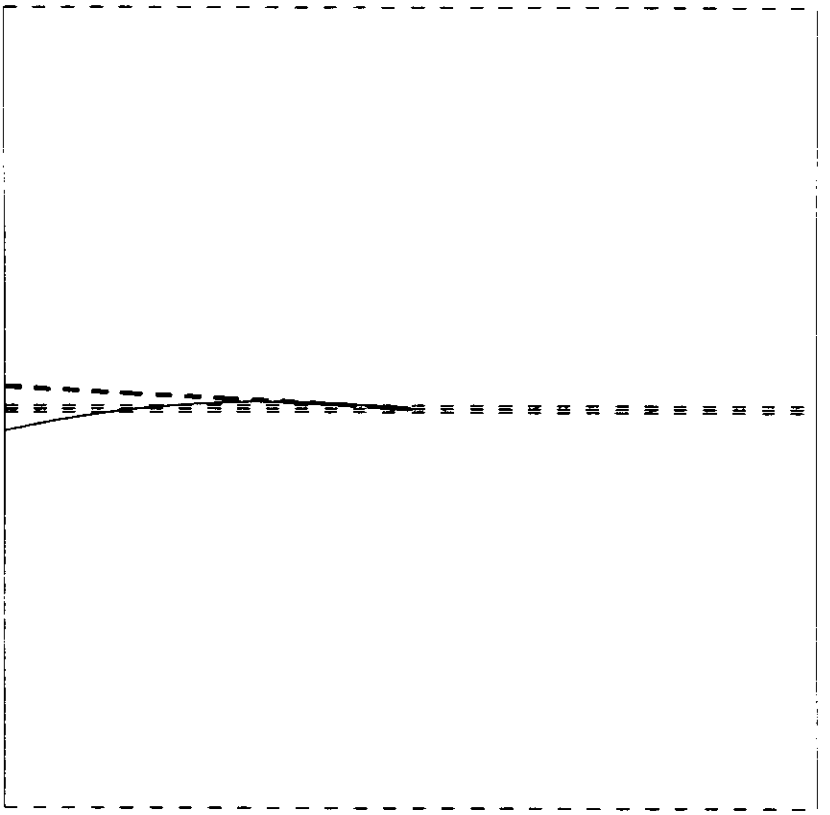

Figure 41 (e)

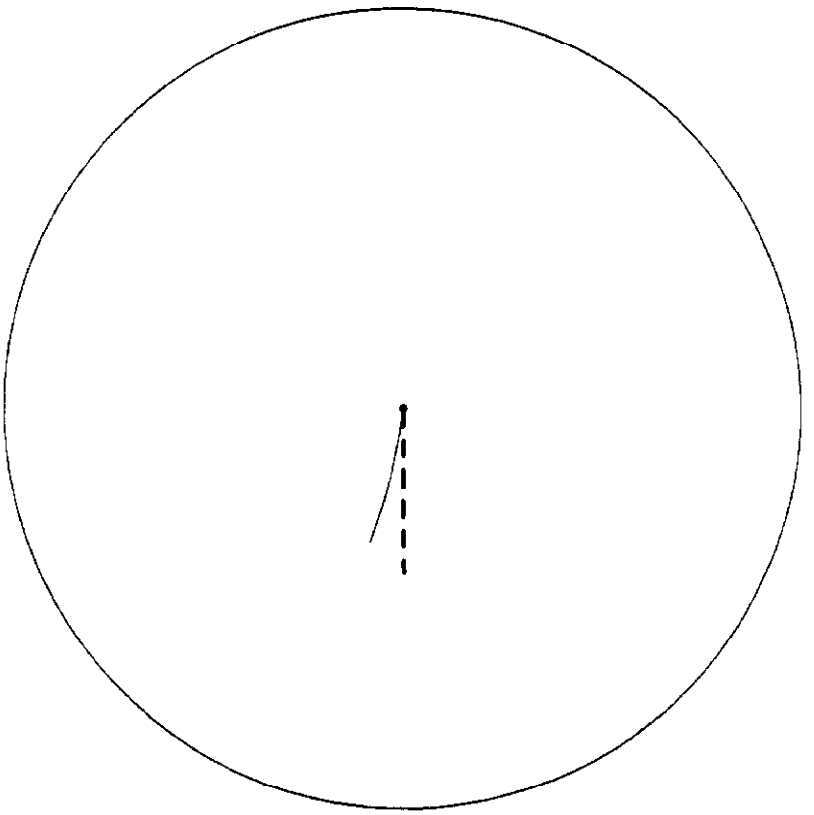

Figure 41 (f)

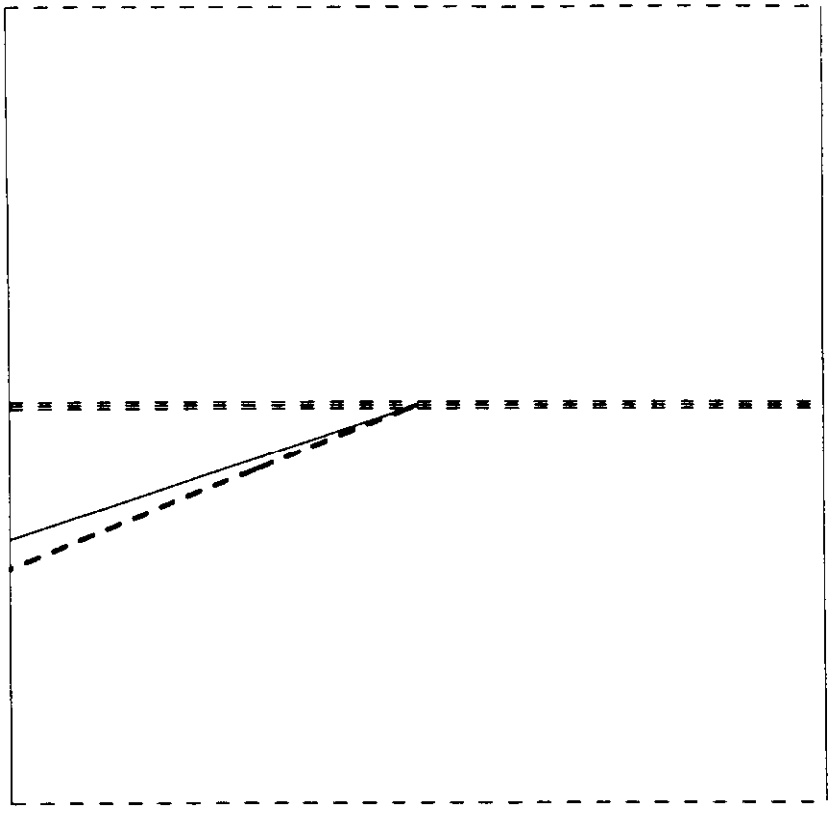

Pileup 5QCD•50GEV•HZZ800EE

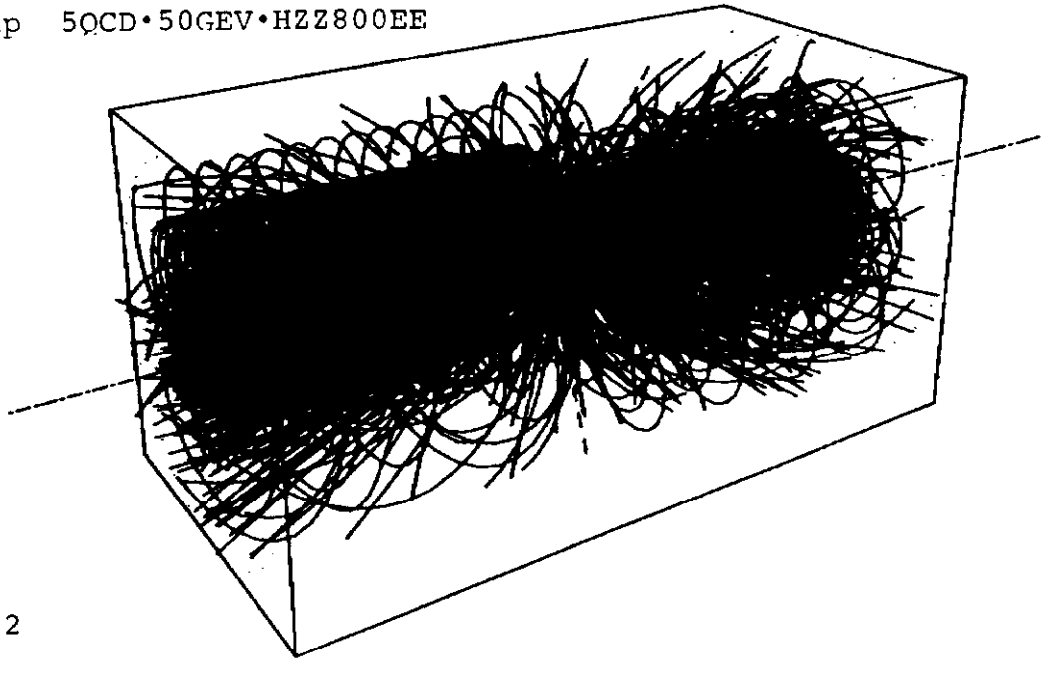

Figure 42

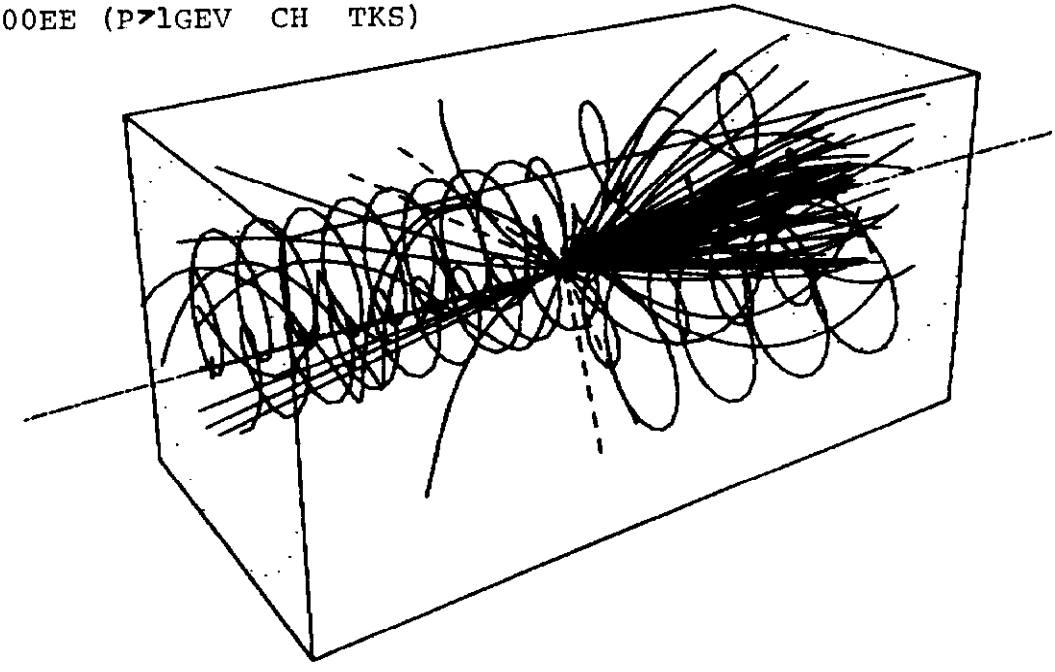

Figure 43

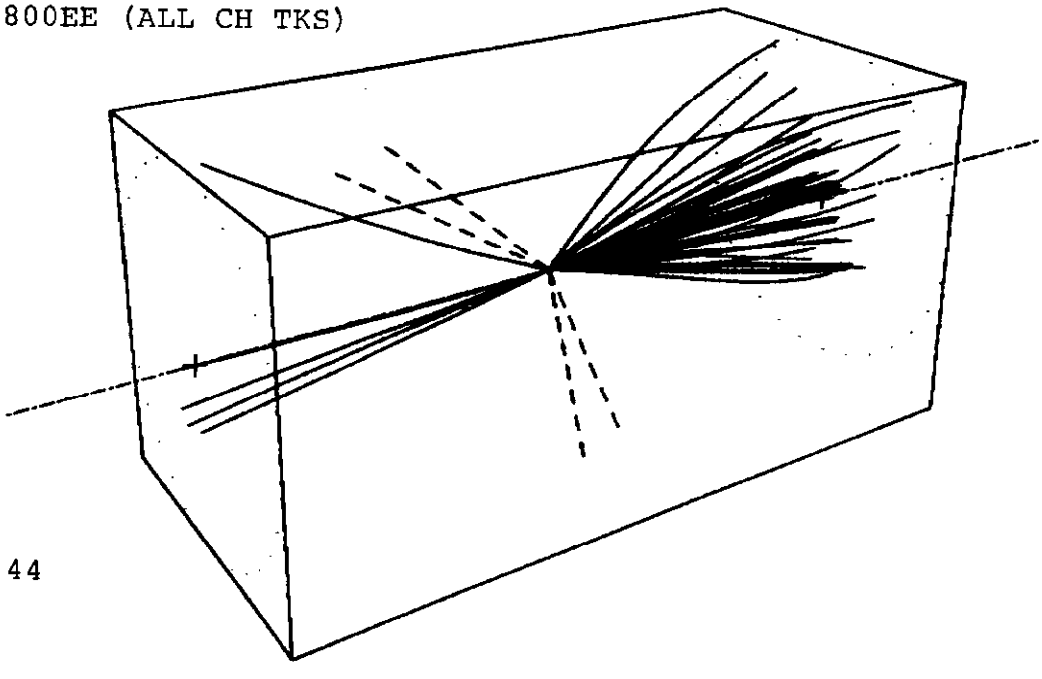

Figure 44

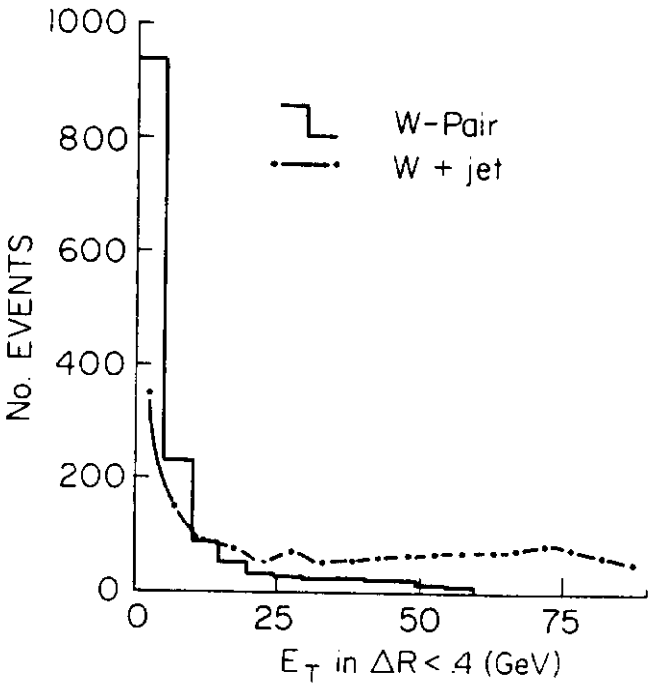

Figure 45

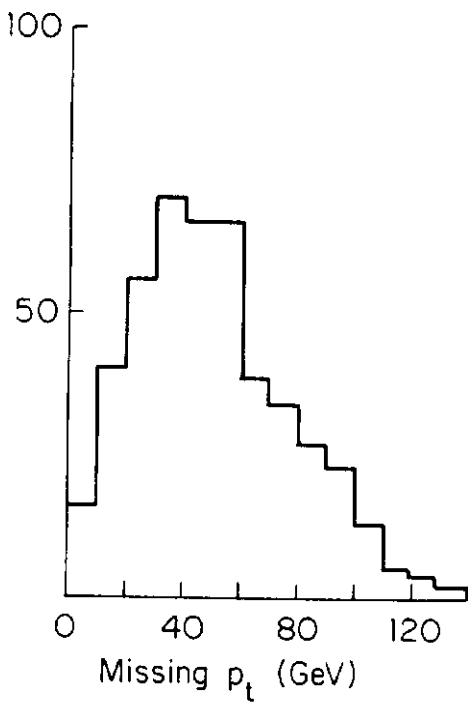

Figure 46

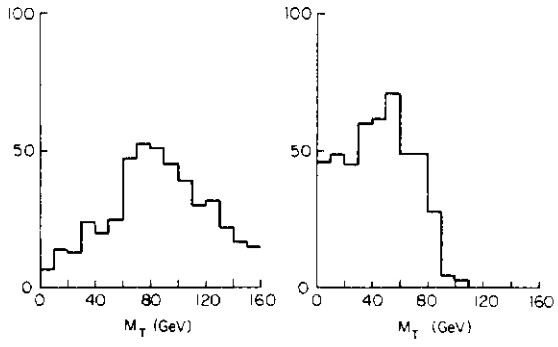

Figure 47

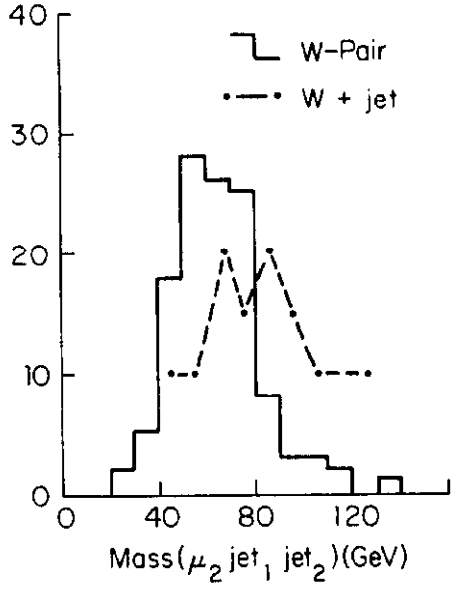

Figure 48

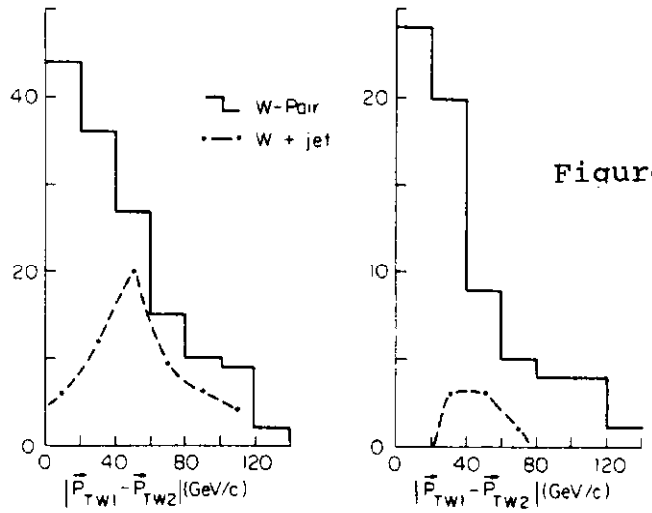

Figure 49

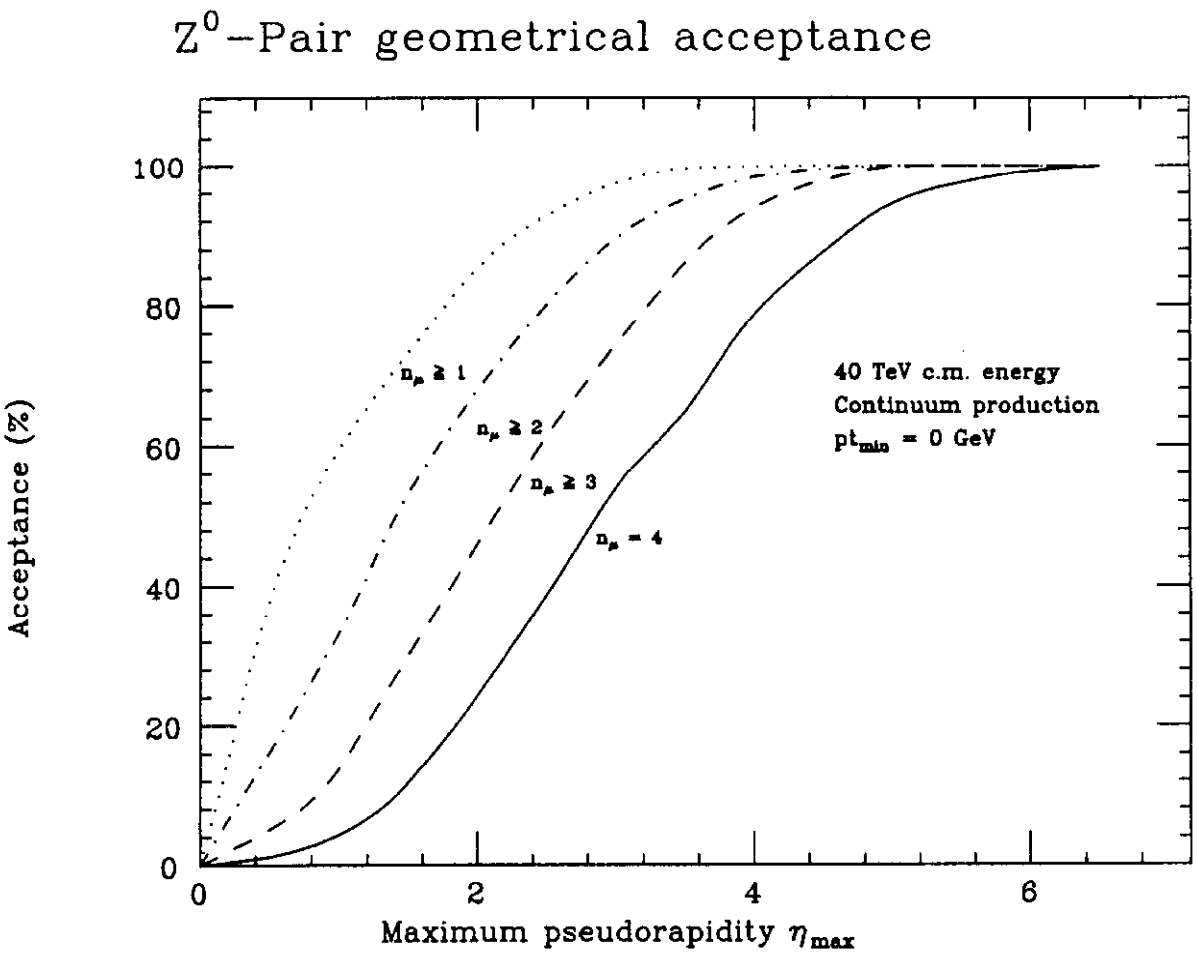

Figure 50 (a)

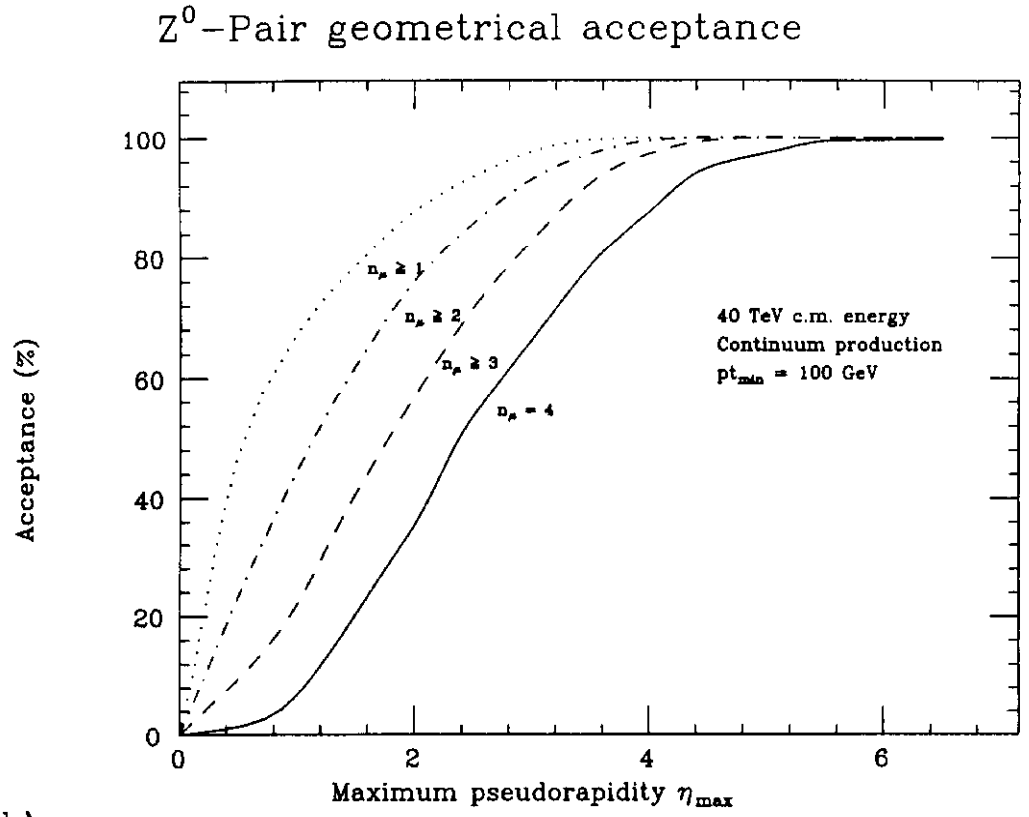

Figure 50 (b)

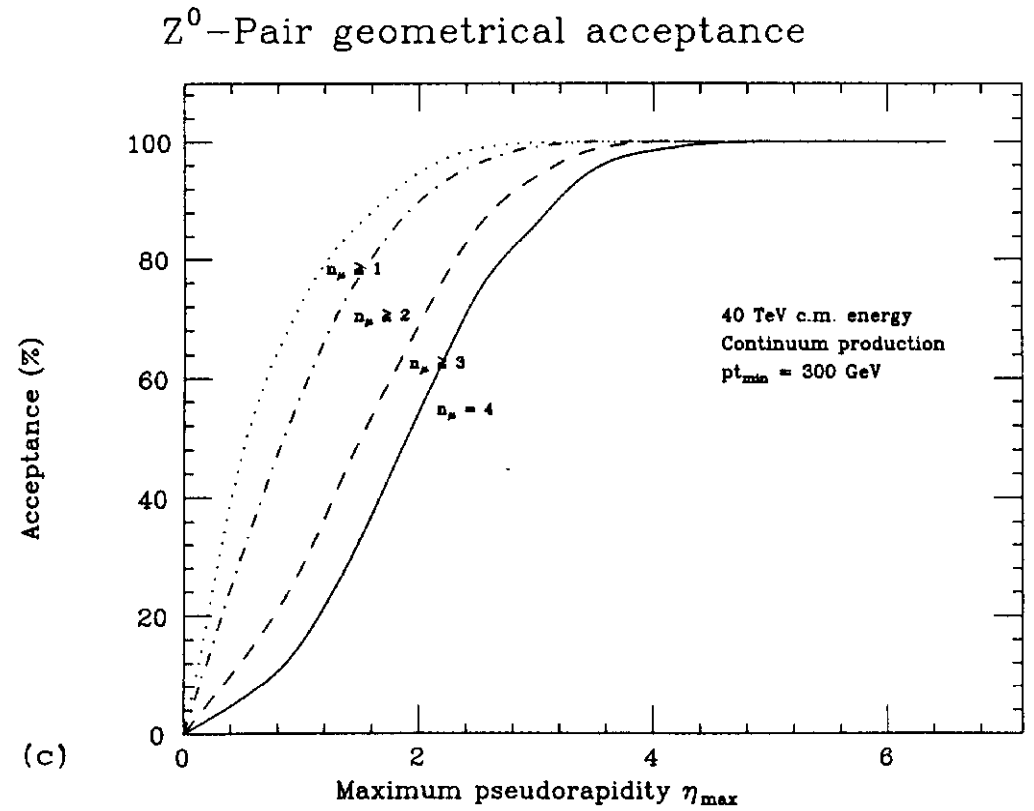

Figure 50 (c)

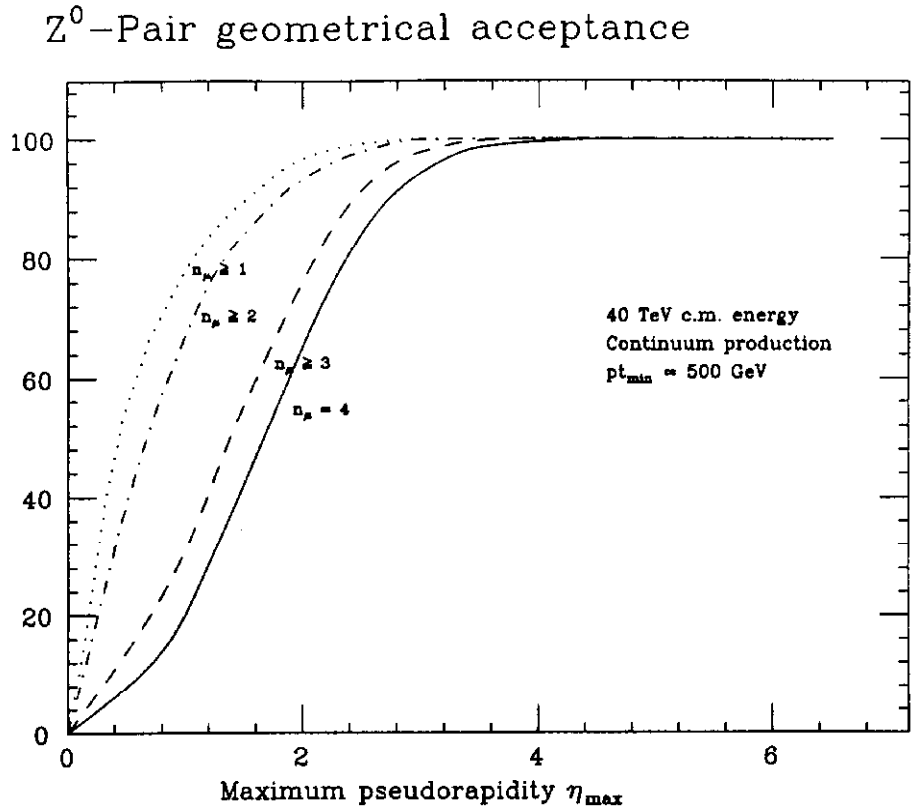

Figure 50 (d)

Figure 50 (d)

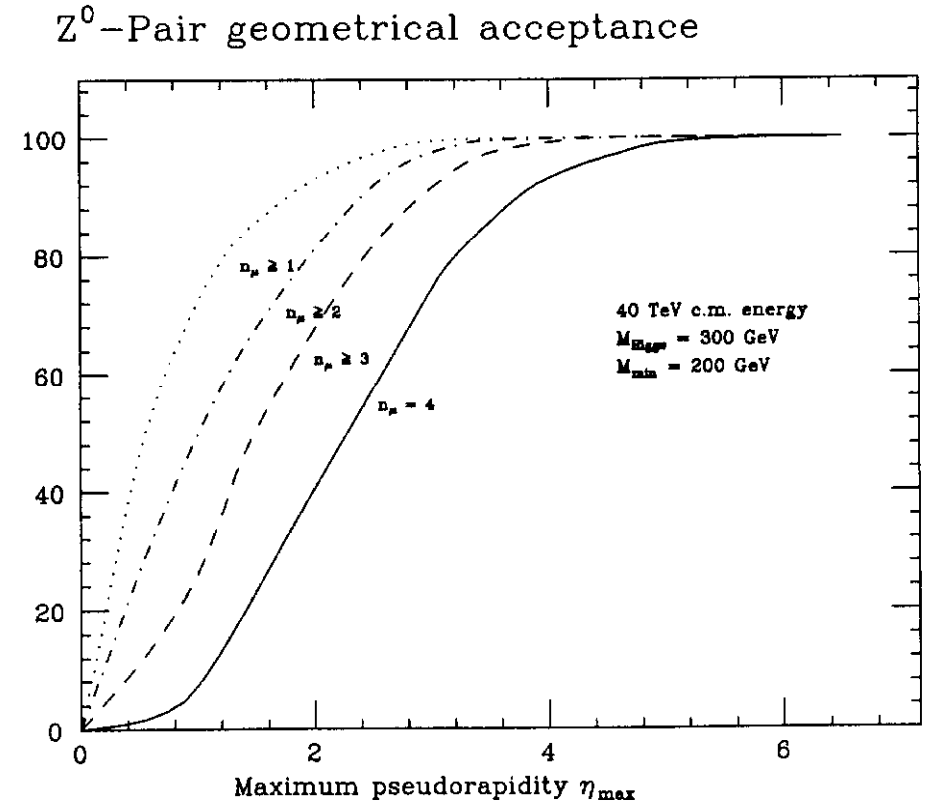

Figure 51 (a)

Figure 51 (a)

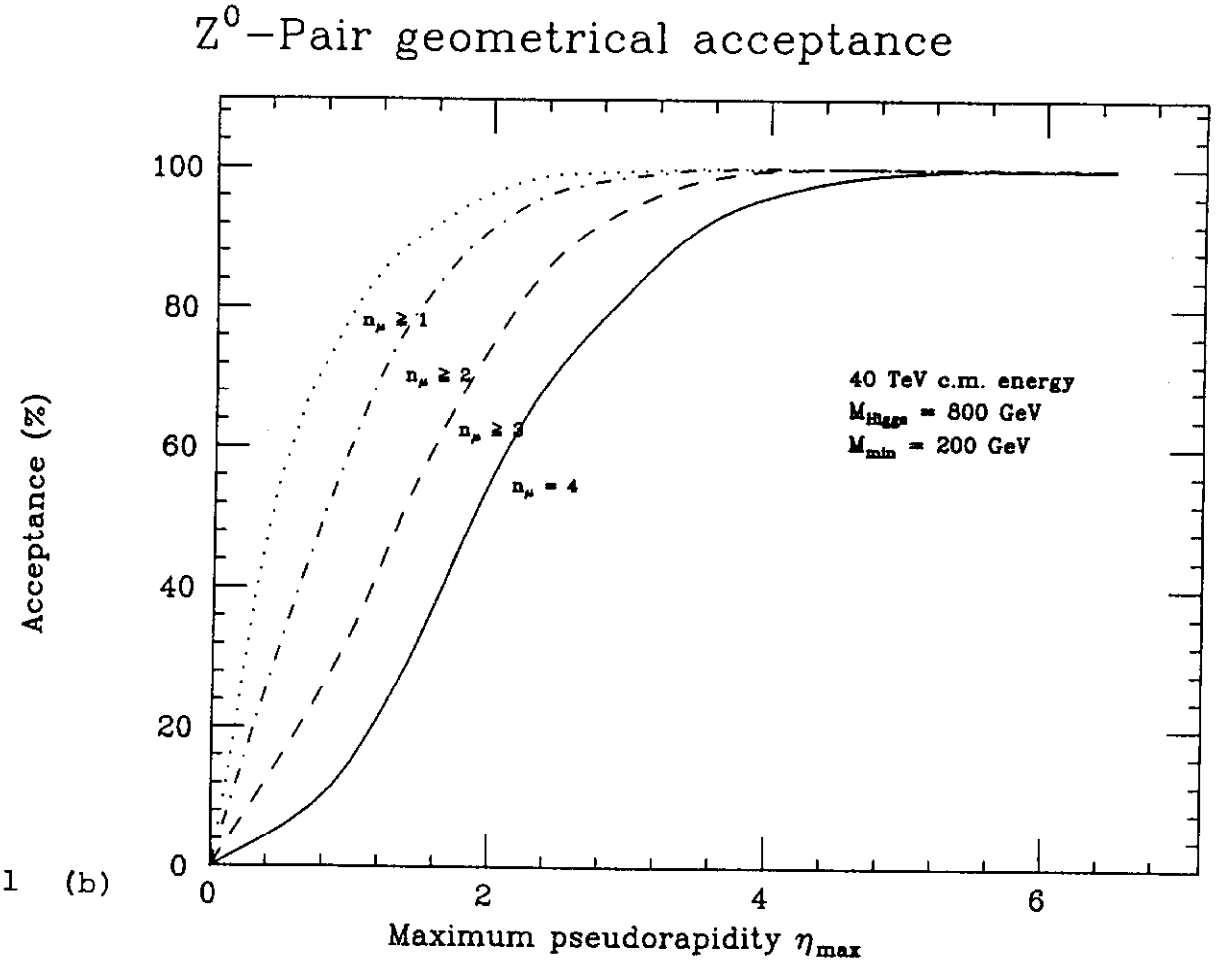

Figure 51 (b)

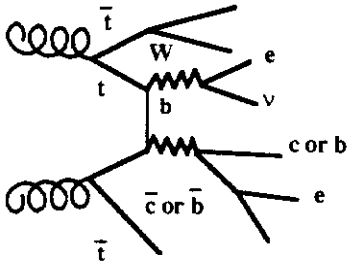

Figure 52

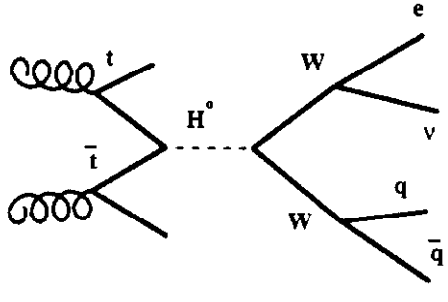

Figure 53

Figure 54

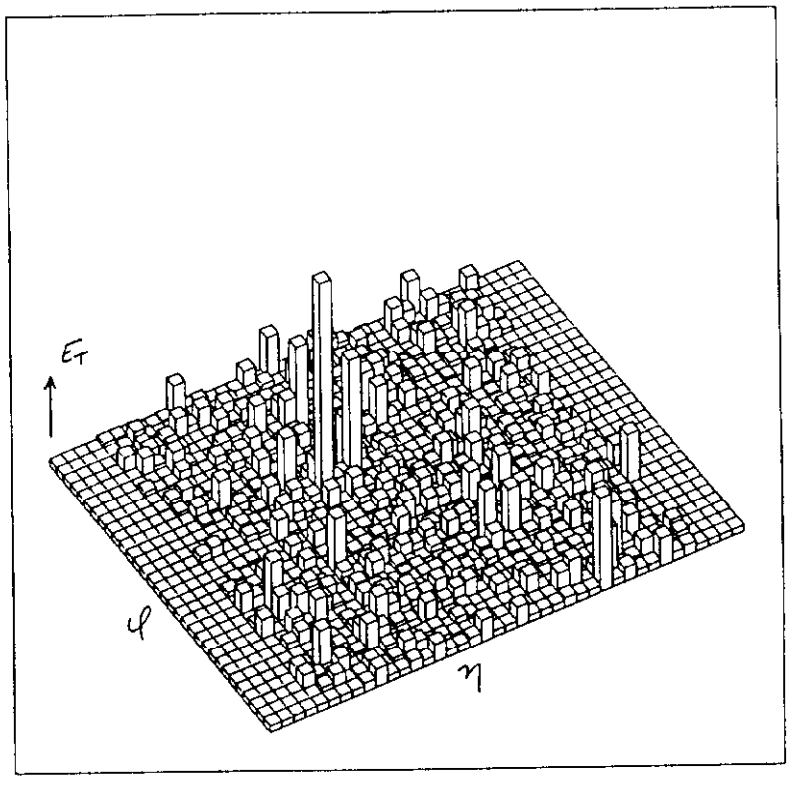

Figure 55

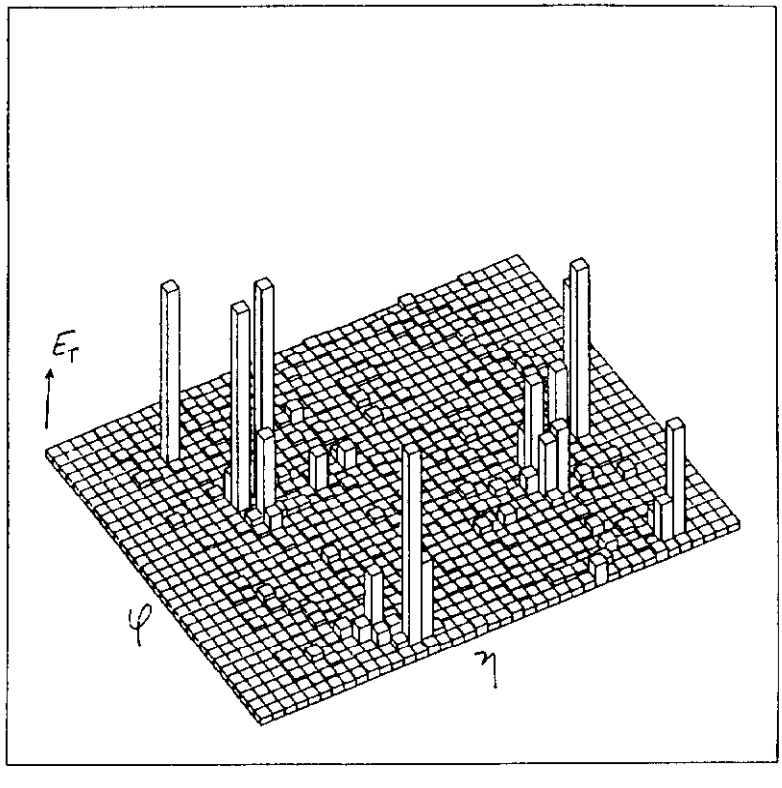

Figure 56